Generalized Zeno Effect and Entanglement Dynamics Induced by Fermion Counting

Elias Starchl,[1] Mark H. Fischer,[2] and Lukas M. Sieberer[1,*]

[1] *Institute for Theoretical Physics, University of Innsbruck, Innsbruck 6020, Austria*

[2] *Department of Physics, University of Zurich, Winterthurerstrasse 190, Zürich CH-8057, Switzerland*

(Received 19 June 2024; revised 12 February 2025; accepted 6 June 2025; published 2 July 2025)

We study a one-dimensional lattice system of free fermions subjected to a generalized measurement process: the system exchanges particles with its environment, but each fermion leaving or entering the system is counted. In contrast to the freezing of dynamics due to frequent measurements of lattice site occupation numbers, a high rate of fermion counts induces fast fluctuations in the state of the system. Still, through numerical simulations of quantum trajectories and an analytical approach based on replica Keldysh field theory, we find that instantaneous correlations and entanglement properties of free fermions subjected to fermion counting and local occupation measurements are strikingly similar. We explain this similarity through a generalized Zeno effect induced by fermion counting and a universal long-wavelength description in terms of a nonlinear sigma model. The physical requirements underlying this universal emergent behavior are conservation of the total number of particles in the system and its environment, and conservation of the purity of the state of the system by keeping a full record of all measurement outcomes. For both types of measurement processes, we present strong evidence against the existence of a critical phase with logarithmic entanglement and conformal invariance. Instead, we identify a finite critical range of length scales on which signatures of conformal invariance are observable. While area-law entanglement is established beyond a scale that is exponentially large in the measurement rate, the upper boundary of the critical range is only algebraically large and thus numerically accessible. Our finding that these properties do not rely on particle-number conservation has far-reaching implications for measurement-induced phenomena beyond noninteracting fermions, such as charge sharpening in random quantum circuits or generic interacting systems.

DOI: 10.1103/jppz-vdgn

I. INTRODUCTION

Frequent projective measurements that interrupt the otherwise continuous dynamics of a quantum system induce the quantum Zeno effect: the freezing of the evolution in an eigenstate of the measured observable [1]. For measurements of local observables in a spatially extended many-body system, these eigenstates exhibit area-law scaling of the entanglement entropy. The quantum Zeno effect thus stabilizes area-law entanglement even in systems that would in the absence of measurements continuously and unitarily evolve toward volume-law entanglement. Reducing the rate at which measurements are performed can lead to a novel type of dynamical phase transition between area-law and volume-law scaling of the entanglement entropy. Such measurement-induced phase transitions were first described in quantum circuits [2–25], but also occur in the continuous-time dynamics of fermionic [26–54], bosonic [55–59], and spin systems [60–66]. Experimental studies of measurement-induced phase transitions have been performed with trapped ions [67,68] and superconducting qubits [69–71]. While the freezing of continuous-time dynamics provides an intuitive explanation for area-law entanglement through repeated measurements, is it also a requirement? As we detail in the following, this question is of fundamental relevance for systems that are subjected to generalized measurements.

A generalized measurement is described by a collection of measurement operators $\hat{M}_n$, where the index n labels possible measurement outcomes [72]. The measurement operators obey the completeness relation $\sum_n \hat{M}_n^\dagger \hat{M}_n = 1$. If the state of a quantum system immediately before a generalized measurement performed at time t is $|\psi(t)\rangle$ then outcome n occurs with probability

*Contact author: lukas.sieberer@uibk.ac.at

Published by the American Physical Society under the terms of the Creative Commons Attribution 4.0 International license. Further distribution of this work must maintain attribution to the author(s) and the published article's title, journal citation, and DOI.

$p_n(t) = \langle\psi(t)|\hat{M}_n^\dagger \hat{M}_n|\psi(t)\rangle$, and the state of the system after the measurement is

$$|\psi(t+0^+)\rangle = \frac{1}{\sqrt{p_n(t)}}\hat{M}_n|\psi(t)\rangle. \quad (1)$$

Crucially, the measurement operators $\hat{M}_n$ need not be projectors. If they are not, performing a generalized measurement immediately after a measurement with outcome n does not generally yield the same result n. As such, repeated generalized measurements do not lead to a freezing of the dynamics.

Here, we describe a novel mechanism that stabilizes area-law entanglement through measurements, but does not require the freezing of the dynamics associated with the conventional Zeno effect. We consider a one-dimensional (1D) lattice model of free fermions subjected to monitored loss and gain, as illustrated in Fig. 1(a). That is, each lattice site is coupled to two reservoirs, acting as a drain and source of particles. The occupation of the reservoirs is monitored continuously, such that each fermion that leaves or enters the system is registered. This setup is analogous to photon counting in quantum optics [73,74]. There, a physical system such as an atom excited by a laser, or a leaky cavity, emits photons into the surrounding electromagnetic field. The electromagnetic field thus acts as an empty reservoir, and a photodetector continuously checks whether there is a photon present. Even though each site of the fermionic lattice system we consider is coupled to two reservoirs and can both "emit" and "absorb" fermions, the analogy to photon counting suggests that we refer to the monitored loss and gain of fermions as *fermion counting*.

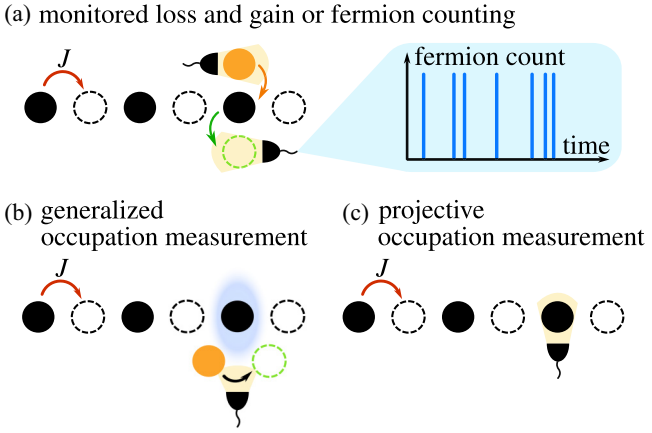


FIG. 1. The two generalized measurement processes we consider are (a) monitored loss and gain or fermion counting and (b) generalized occupation measurements. (a) Each site of the lattice (filled and open circles) with hopping amplitude J is coupled to two reservoirs acting as a drain (open green circle) and source (filled orange circle) of fermions, respectively. The occupations of the reservoirs are monitored continuously, such that each fermion leaving or entering the system is counted. (b) Each site is coupled to a source and drain in a way that tunneling of reservoir fermions from the source to the drain is possible only if the system site is occupied. The detection of tunneling events thus indicates the presence of fermions in the system. Details are provided in Sec. III and Appendices A and B. Generalized measurements in (a) and (b), which are implemented by coupling the system to auxiliary systems on which projective measurements are performed, should be contrasted with (c) projective measurements of occupation numbers performed directly on the system.

The process of fermion counting can be theoretically modeled as a continuous generalized measurement, where each measurement operator removes or adds a fermion at a particular lattice site. A high rate of fermion counts causes the number of fermions and thus the state of the system to fluctuate rapidly. At the same time, the local removal and addition of particles efficiently disentangles the many-body wave function similarly to generalized [29] or projective [42] measurements of local occupation numbers. These latter two types of measurements, which are illustrated in Figs. 1(b) and 1(c), conserve the total number of particles in the system, and induce a Zeno effect in the frequent-measurement limit.

In this work, we perform a comparative study of fermion counting and generalized measurements of local occupation numbers to obtain a comprehensive understanding of the similarities and differences between these scenarios. Despite their starkly different dynamics, both models exhibit almost identical steady-state correlations and entanglement properties. We trace this striking similarity back to a generalized Zeno effect induced by fermion counting. The key feature that the conventional and generalized Zeno effects have in common is the suppression of coherent dynamics, leading in turn to a suppression of the growth of entanglement.

More formally, we explain the near indistinguishability of the correlations and entanglement properties of the models through a common long-wavelength effective field theory. In particular, both models are described by a nonlinear sigma model (NLSM), which can be derived in the framework of replica Keldysh field theory [20,42,43,45]. The predictions from this analytical description are in good agreement with our numerical results and provide strong evidence that both types of measurements lead to area-law entanglement for any nonzero measurement rate γ.

Recent studies have obtained contradictory results concerning the existence of a measurement-induced entanglement transition in 1D free fermions with a conserved number of particles. Entanglement dynamics under continuous measurements of occupation numbers, described by either quantum state diffusion [75] or quantum jump trajectories [76] as considered in this work, was studied in Ref. [29]. For both types of dynamics, there is numerical evidence for a measurement-induced Kosterlitz-Thouless (KT) transition at a finite critical measurement rate γ_c, separating a critical phase with logarithmic growth of the

entanglement entropy as characteristic for a 1D conformal field theory (CFT) [77] from an area-law phase. These findings suggest that the precise way in which measurements are implemented might affect nonuniversal properties such as the value of the critical measurement rate, but not whether there is a transition or not. Therefore, one is led to assume that this question is decided by the emergent long-wavelength behavior, which is universal in the sense that it is determined solely by spatial dimensionality and symmetries. In turn, symmetries are reflected in conservation laws and in both quantum state diffusion and quantum jump trajectories, the number of particles is the only conserved quantity. The existence of a measurement-induced phase transition in 1D free fermions with particle-number conservation is corroborated by replica Keldysh theory for Dirac fermions with a linear dispersion relation [31].

However, based on the above assumption of universality, we should compare the results of Alberton *et al.* [29] and Buchhold *et al.* [31], who considered free fermions under continuous measurements of occupation numbers, to the findings of Poboiko *et al.* [42], who studied random projective measurements. Analytical and numerical results obtained in Ref. [42] indicate that there is no measurement-induced phase transition, in agreement with the numerical findings of Refs. [33,44]. Instead, for any finite measurement rate γ, the logarithmic growth of the entanglement entropy transitions into area-law behavior above an exponentially large scale $\ln(l_*) \sim \gamma^{-1}$ [42,52–54]. For small values of the measurement rate, for which the theory is expected to become quantitatively accurate, this scale is beyond numerically accessible system sizes.

Here, we show analytically and numerically that clear signatures of the crossover to area-law entanglement can be observed on much smaller scales, well within the reach of finite-size numerics. Approximately logarithmic growth of the entanglement entropy is restricted to a critical range of length scales, bounded from below by $l_0 \sim \gamma^{-1}$ and from above by $l_c \sim \gamma^{-2}$. Only within this critical range do we observe clear signatures of conformal invariance [29].

These results apply both to fermion counting and to generalized measurements of local occupation numbers. Thus, we show that particle-number conservation is, in fact, not a necessary precondition for the observed phenomenology of stationary correlations and entanglement, including the absence of a measurement-induced phase transition. As stated above, this phenomenology is described by a long-wavelength effective field theory in the form of an NLSM. We show that the two necessary requirements for the SU(R) symmetry underlying the NLSM to occur in free-fermionic systems are (i) the conservation of the total number of particles in the system and auxiliary reservoirs, as illustrated in Fig. 1, and (ii) the conservation of the purity of the state of the system. The purity is ensured by keeping a full record of the measurement outcomes. In particular, the SU(R) symmetry can be broken by inefficient detection, which can be theoretically modeled by averaging over a fraction of the measurement results [76]. Combining measurements that obey conditions (i) and (ii) with dynamics generated by a generic hopping Hamiltonian leads to an NLSM with target manifold SU(R). Note that if the hopping matrix has particle-hole symmetry—which is the case for the nearest-neighbor hopping with real hopping amplitudes we consider in this work—the target manifold is modified to SU($2R$)/Sp(R) [19,52,54]. However, both types of NLSMs have the same qualitative properties.

Our work thus clarifies the impact of particle-number conservation on the measurement-induced dynamics of pure states of 1D free-fermionic systems: there is no entanglement transition if the Hamiltonian conserves the number of particles, and measurements conserve the total number of particles in the system and auxiliary reservoirs that are required to implement the measurements. This includes the stronger condition that measurements conserve the number of particles in the system alone. In contrast, there can be a transition if these conditions are violated, as in the Majorana model of Ref. [45], where the Hamiltonian and also, depending on the choice of parameters, the measurement operators break particle-number conservation. We emphasize that these statements are specific to 1D systems: an entanglement transition has also been shown to occur in 2D free-fermionic systems when the number of particles is conserved [43,48].

While we focus here on free-fermionic systems, our finding that particle-number conservation is not fundamental for the observed entanglement properties has far-reaching implications beyond this class of models. For example, random quantum circuits with a conserved charge have been shown to exhibit a measurement-induced charge-sharpening transition that separates phases in which measurements can and cannot efficiently reveal the total charge of the system [17,18,21,68]. Very recently, charge sharpening has also been discussed for interacting fermions [53,54]. Our findings show that charge sharpening can occur even in the absence of charge conservation.

The rest of this paper is organized as follows. In Sec. II, we summarize our key results. The models we study are introduced in Sec. III. Then, in Sec. IV, we describe signatures of conventional and generalized Zeno effects for occupation measurements and fermion counting, respectively. An analytical description of our models in terms of a replica Keldysh field theory is introduced in Sec. V. We analyze the Gaussian field theory that applies in the weak-measurement limit in Sec. VI, and discuss the effect of fluctuations beyond Gaussian theory in Sec. VII. A detailed comparison between our analytical predictions and numerical results is provided in Sec. VIII, where we consider spatial correlations, measures of entanglement, and signatures of conformal invariance in the steady state.

Section IX contains our conclusions and an outlook on future research questions. Details of our analytical and numerical studies are described in several appendices.

II. KEY RESULTS

We have obtained the following results through analytical and numerical studies of free fermions on a 1D lattice subjected to fermion counting or generalized measurements of local lattice site occupation numbers.

Result 1. Frequent particle loss and gain suppress coherent dynamics and stabilize area-law entanglement via a generalized Zeno effect.

Before we explain the generalized Zeno effect, let us briefly recall the conventional Zeno effect for a single particle on a 1D lattice, subjected to repeated generalized measurements of lattice site occupation numbers, $\hat{M}_l = \hat{n}_l$. The first measurement collapses the initial wave function $|\psi\rangle$ of the particle to a state $|l_0\rangle$ that is localized on a single lattice site l_0, chosen from $l \in \{1, \ldots, L\}$ according to Born's rule with probability $p_l = \langle\psi|\hat{n}_l|\psi\rangle$. Subsequent measurements, performed at a rate γ, yield the same result l_0, since the probability distribution after the first collapse is $p_l = \delta_{l,l_0}$. Coherent hopping with amplitude $J \ll \gamma$ can induce transitions $|l_0\rangle \to |l_0 \pm 1\rangle$. However, these processes occur at second order in perturbation theory, in other words with a small rate $\nu = J^2/\gamma$. This suppression of coherent dynamics through frequent measurements is the essence of the conventional Zeno effect. The resultant slow dynamics is illustrated for a many-body system in Fig. 2(a).

To illustrate the generalized Zeno effect, we first consider a single fermionic lattice site with annihilation and creation operators $\hat{\psi}$ and $\hat{\psi}^\dagger$, respectively. Monitored loss and gain or fermion counting is described by generalized measurements performed at a rate γ and with measurement operators $\hat{M}_- = \hat{\psi}$ and $\hat{M}_+ = \hat{\psi}^\dagger$. The completeness relation $\hat{M}_-^\dagger \hat{M}_- + \hat{M}_+^\dagger \hat{M}_+ = 1$ follows from canonical anticommutation relations. Repeated measurements cause the occupation of the lattice site to fluctuate between 0 and 1, realizing a random telegraph process [78]. The autocorrelation function of the occupation number $\hat{n} = \hat{\psi}^\dagger \hat{\psi}$ decays exponentially with a rate of approximately γ. That is, the dynamics becomes faster for increasing measurement rate γ—the exact opposite of the freezing of the dynamics in the conventional Zeno effect.

In an extended lattice system with monitored loss and gain on each lattice site, the dynamics induced by measurements allows the system to ergodically explore all classical configurations of $N \in \{0, \ldots, L\}$ particles distributed on L lattice sites. Coherent hopping enables additional transitions between these configurations. Crucially,

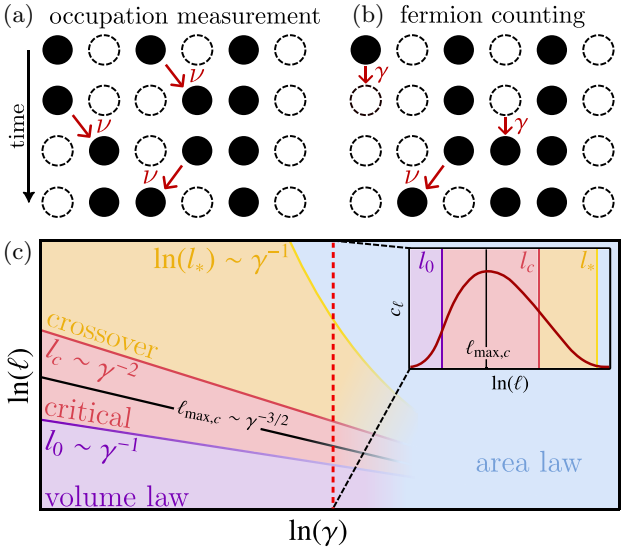


FIG. 2. (a) Zeno effect for fermions on a 1D lattice subjected to measurements of local occupation numbers. Frequent measurements freeze the system in a classical configuration with each lattice site either occupied or empty (filled and open circles). Incoherent hopping occurs at the slow rate $\nu = J^2/\gamma$. (b) Generalized Zeno effect induced by fermion counting. A high rate γ of fermion counts corresponds to fast transitions between classical configurations. As in the conventional Zeno effect, additional slow processes occur at rate ν. (c) Schematic finite-size phase diagram for fermion counting and occupation measurements. For low measurement rates, the entanglement exhibits volume-law scaling below $l_0 \sim \gamma^{-1}$ and grows logarithmically in the critical range between l_0 and $l_c \sim \gamma^{-2}$, before it slowly crosses over to area-law scaling, which is established beyond the exponentially large scale $\ln(l_*) \sim \gamma^{-1}$. Inset: the effective central charge c_ℓ has a maximum at $\ell_{\max,c} \sim \gamma^{-3/2}$.

in analogy to the conventional Zeno effect, these transitions are suppressed for $J \ll \gamma$ and occur with a slow rate $\nu = J^2/\gamma \ll \gamma$. Therefore, we refer to this phenomenon, which is illustrated in Fig. 2(b), as a generalized Zeno effect. The facts that the coherent dynamics is suppressed by frequent fermion counts and that the classical configurations, which dominate the dynamics for $J \ll \gamma$, have vanishing entanglement entropy rationalize the finding that fermion counting stabilizes area-law entanglement.

Result 2. The generalized and conventional Zeno effects induce almost identical correlations and entanglement properties.

Even though the dynamics are strikingly different for fermion counting and occupation measurements, both lead to equivalent behavior in various measures of correlations and entanglement in the steady state. This includes density-density correlations, the entanglement entropy, and the bipartite mutual information. We observe a qualitative difference only in higher-order correlations as quantified

through the tripartite mutual information, indicating that the tripartite mutual information probes properties that are not captured by the long-wavelength effective field theory, which is the same for both models, as described next.

Result 3. The similarity of correlations and entanglement properties can be explained in terms of a universal long-wavelength effective field theory.

Starting from a microscopic model of the fermionic lattice system shown in Fig. 1(a), with each site coherently coupled to particle reservoirs acting as a drain and source, a natural description of the dynamics of the system alone can be given in terms of a stochastic Schrödinger equation [76]. This equation describes the evolution of state $|\psi(t)\rangle$ of the system conditioned on the counting of fermions that are transferred between the system and reservoirs. For equal rates of fermion loss and gain, the same quantum trajectories $|\psi(t)\rangle$ are obtained from a description of fermion counting as generalized measurements that are performed at random times and with outcomes determined by Born's rule. This equivalence enables an analytical description of the system dynamics in terms of a replica Keldysh field theory [20,42,43,45,48,52–54], which we adopt to the case of generalized measurements.

The field theory approach gives access to two types of observables: (i) observables that are linear in the projector on the conditional state $\hat{\rho}(t) = |\psi(t)\rangle\langle\psi(t)|$, such as expectation values $\overline{\langle\hat{A}(t)\rangle}$ or temporal correlation functions $\overline{\langle\hat{A}(t)\hat{B}(t')\rangle}$, where the overbar denotes the average over trajectories; (ii) instantaneous observables that are nonlinear in $\hat{\rho}(t)$, such as connected equal-time correlation functions $\overline{\langle\hat{A}(t)\hat{B}(t)\rangle - \langle\hat{A}(t)\rangle\langle\hat{B}(t)\rangle}$ or the entanglement entropy. Observables of type (i) are encoded in the replica-symmetric sector of the theory, and observables of type (ii) in the replica-asymmetric or replicon sector.

Fermion counting leads to exponential decay of the density autocorrelation function, which is an observable of type (i). Instead, particle-number conservation in the model with occupation measurements leads to diffusive decay. Formally, this difference between exponential and algebraic decay is reflected in the replica-symmetric sector being massive and massless for fermion counting and occupation measurements, respectively. In contrast, the replicon sector is described in both cases by the same massless long-wavelength effective field theory that takes the form of an NLSM. While the Hamiltonian we consider obeys particle-hole symmetry, leading to an NLSM with target manifold $\mathrm{SU}(2R)/\mathrm{Sp}(R)$, the target manifold for the generic case is $\mathrm{SU}(R)$. Crucially, the qualitative behavior remains unchanged. This common long-wavelength effective field theory description analytically explains the numerically observed equivalence of correlations and entanglement properties. Importantly, the theory predicts that there is no measurement-induced entanglement transition in these models in one dimension. Instead, area-law entanglement is established for any nonzero measurement rate. Note, however, that a measurement-induced entanglement transition does occur in free-fermionic systems described by the same NLSM in higher spatial dimensions [43,48].

Result 4. Particle-number conservation is not necessary for the occurrence of the $\mathrm{SU}(R)$ symmetry underlying the NLSM, and thus the absence of an entanglement transition in one dimension.

A peculiar feature of measurement-induced phenomena is that both the dynamics and the observables of main interest are nonlinear in the quantum state of the system. This nonlinearity of the dynamics is due to the necessity to normalize the state after each measurement; the key nonlinear observable is the entanglement entropy. Nevertheless, it is possible to obtain a theoretical description that is linear in the state by introducing R replicas of the system [6,20]. Consequently, it is not sufficient to study the symmetries of the unitary time-evolution operator and measurement operators of a single realization of the system to fully understand relevant symmetries of the dynamics. Instead, one has to study symmetries of the dynamics of R replicas to obtain a comprehensive picture.

If the unitary dynamics and measurement operators of a single realization of the system of interest have the symmetry group G then the symmetry group of R replicas is $\mathrm{G}^R \rtimes S_R$, where S_R is the group of permutations of R replicas. Conservation of the number of particles corresponds to $\mathrm{G} = \mathrm{U}(1)$—for the moment, we disregard a possible additional particle-hole symmetry of the Hamiltonian—leading to the symmetry group $\mathrm{U}(1)^R \rtimes S_R$ for generic interacting fermions. This is enhanced to $\mathrm{U}(R)$ for free fermions, where it is possible to not only perform discrete permutations of replicas but even continuous rotations between them [10,19,31,42,45]. For example, the dynamics of R replicas of free fermions subjected to random projective measurements of lattice site occupation numbers studied in Ref. [42] is invariant under $\mathrm{U}(R)$ rotations. In a replica Keldysh field theory description of this model, the decomposition $\mathrm{U}(R) = \mathrm{U}(1) \rtimes \mathrm{SU}(R)$ has been found to emerge naturally: Goldstone modes associated with $\mathrm{U}(1)$ and $\mathrm{SU}(R)$ determine the long-wavelength behavior of the replica-symmetric and replicon sectors of the theory, respectively, and these sectors decouple for sufficiently rare measurements, $\gamma \ll J$. However, it has not been recognized before that in the above decomposition only the first factor, $\mathrm{U}(1)$, requires particle-number conservation; as we show, SU(R) symmetry is an exact property, realized on the microscopic level of the theory, even for fermion counting, where the number of particles is not conserved. Note, finally, that an additional particle-hole symmetry of the

hopping Hamiltonian can be incorporated into the field theory description by introducing a combined $2R$-dimensional particle-hole and replica space [54]. Then, the microscopic SU(R) symmetry is enhanced to SU($2R$), which becomes $\mathrm{U}(2R) = \mathrm{U}(1) \rtimes \mathrm{SU}(2R)$ for measurements that conserve the number of particles.

Our finding, that the SU(R) symmetry underlying the emergence of an NLSM at long wavelengths does not require particle-number conservation, indicates that phenomena that have so far been discussed for systems with particle-number conservation can, in fact, also occur when particle-number conservation is broken. An interesting example is provided by the charge-sharpening transition in random quantum circuits [17,18,21,68] and interacting fermionic systems [53,54]. We return to this point in Sec. IX below.

Result 5. The necessary conditions for SU(R) symmetry to occur are

(i) conservation of the total number of particles in the system and auxiliary reservoirs, and
(ii) preservation of the purity of the state.

The implementation of fermion counting illustrated in Fig. 1(a) relies on coupling each site of the fermionic lattice system to two auxiliary reservoirs, such that the total number of particles in the system and reservoirs is conserved. We show that, under this condition and the additional condition that all measurement outcomes are recorded such that the state of the system remains pure, the dynamics of R replicas features the SU(R) symmetry underlying both the SU($2R$)/Sp(R) and SU(R) NLSMs for hopping Hamiltonians with and without particle-hole symmetry, respectively. In contrast, the symmetry is broken for inefficient detection, meaning that some of the fermions that are transferred between the system and reservoirs remain undetected. These two conditions therefore provide a physical explanation for the observed phenomenology in terms of conservation laws, which complements the more heuristic reasoning in terms of the generalized Zeno effect. Furthermore, by identifying these conditions, we settle the question about the requirements for a measurement-induced entanglement transition to occur in 1D free fermions. Let us reiterate that in one spatial dimension, such a transition does not occur for particle-number-conserving models of random generalized [29] or projective measurements [42], or for fermion counting with a conserved total number of particles. Instead, such a transition does occur in the Majorana model of Ref. [45], where particle-number conservation is broken by the Hamiltonian that generates the unitary dynamics and also, depending on the choice of parameters, by the measurement operators. We find the long-wavelength effective replicon field theory to be identical for fermion counting as well as particle-number-conserving measurements of occupation numbers [42,43,48,52–54], but different for the Majorana model [45].

Result 6. Logarithmic growth of the entanglement entropy and signatures of conformal invariance are observable within a well-defined and finite critical range of length scales.

The renormalization-group (RG) flows of the SU($2R$)/Sp(R) and SU(R) NLSMs are qualitatively the same and indicate that area-law entanglement is established beyond a scale l_* that is exponentially large in γ^{-1}. However, RG-corrected Gaussian field theory predicts that, for small measurement rates γ, properties that are characteristic for a critical phase can be observed within a finite critical range of length scales between $l_0 \sim \gamma^{-1}$ and $l_c \sim \gamma^{-2}$, as illustrated in Fig. 2(c). These characteristics include logarithmic growth of the entanglement entropy and signatures of conformal invariance [29]. Beyond l_c, there is a wide crossover region that separates the critical range from the onset of area-law scaling. Since l_c is only algebraically large in γ, this scale is also numerically accessible for relatively small values of the measurement rate, even if area-law scaling beyond l_* is not observable.

To precisely characterize the behavior of the entanglement entropy, we introduce a scale-dependent effective central charge c_ℓ for a subsystem of size ℓ. On short scales $\ell \lesssim l_0 \sim \gamma^{-1}$, the effective central charge c_ℓ grows with ℓ, indicating volume-law scaling of the entanglement entropy; on an intermediate scale $\ell = \ell_{\mathrm{max},c} \sim \gamma^{-3/2}$, the central charge exhibits a maximum and thus becomes stationary, leading to logarithmic growth of the entanglement entropy; on large scales $\ell \gtrsim l_c \sim \gamma^{-2}$, the central charge decreases; and finally, beyond the exponentially large scale l_*, c_ℓ is expected to vanish, corresponding to area-law entanglement. The numerically observed behavior of the effective central charge, illustrated schematically in Fig. 2(c), is in good agreement with our analytical predictions.

Evidence for emergent conformal invariance is provided by the collapse of the mutual information as a function of the cross ratio with the form predicted by conformal field theory [29,79]. We perform a systematic numerical analysis of the mutual information for varying subsystem sizes, which reveals that this collapse occurs only for subsystem sizes within the critical range, corroborating the finding that conformal invariance is violated at both short and large scales.

The results described above apply equally to fermion counting and occupation measurements. Differences between the two types of generalized measurements and deviations from conformal invariance even within the critical range can be seen in the tripartite mutual information.

Our detailed analytical and numerical analysis of the crossover from the critical to the area-law phase corroborates and refines the conclusion of Ref. [42], that the evidence for an entanglement transition of free fermions presented in Ref. [29] describes, in fact, a finite-size crossover phenomenon.

III. MODELS AND TIME EVOLUTION

We consider two models of noninteracting fermions on a 1D lattice undergoing unitary time evolution interspersed with generalized measurements. In both models, the unitary dynamics is generated by the Hamiltonian

$$\hat{H} = -J \sum_{l=1}^{L} (\hat{\psi}_l^\dagger \hat{\psi}_{l+1} + \hat{\psi}_{l+1}^\dagger \hat{\psi}_l), \tag{2}$$

where $\hat{\psi}_l$ and $\hat{\psi}_l^\dagger$ are fermionic annihilation and creation operators, respectively, on lattice sites $l \in \{1, \ldots, L\}$ with periodic boundary conditions, $\hat{\psi}_{L+1} = \hat{\psi}_1$. The two models differ by the types of measurement processes, illustrated in Figs. 1(a) and (b), respectively: in the first model, we consider monitored loss and gain or fermion counting; in the second model, we consider measurements of local occupation numbers, $\hat{n}_l = \hat{\psi}_l^\dagger \hat{\psi}_l$. Our main focus lies on the first model, with the second serving as a reference. Entanglement dynamics under continuous and random measurements of local occupation numbers has been studied in Refs. [26,29], and under projective random measurements in Ref. [42].

In the following, we present two equivalent ways to describe quantum trajectories, that is, the evolution of the state vector of the fermionic many-body system, conditioned on a sequence of measurement outcomes. The first description in terms of a stochastic Schrödinger equation results naturally from microscopic physical models, such as implementing monitored loss and gain by coupling the system of interest to reservoirs, as illustrated in Fig. 1 [76]. In the second more formal description, generalized measurements are performed directly on the system at an externally imposed constant rate. This description has the technical advantage of lending itself naturally toward a reformulation as a replica Keldysh field theory, generalizing the construction of Ref. [42] for projective measurements. Crucially, the statistics of measurement times and outcomes, as well as the resulting quantum trajectory dynamics, are identical in both descriptions.

A. Stochastic Schrödinger equation

A minimal physical model for fermion counting consists of a quantum dot, meaning a single fermionic lattice site, tunnel coupled to two fermionic reservoirs. We further assume these reservoirs to be in thermodynamic equilibrium at a low temperature. The chemical potentials of the reservoirs are chosen such that fermions can tunnel from the quantum dot to the first reservoir, the drain, and from the second reservoir, the source, to the quantum dot, but the reverse processes are inhibited. We obtain a theoretical description of fermion counting by integrating the Schrödinger equation for the quantum dot and reservoirs in discrete time steps Δt using the Born and Markov approximations, in other words treating the coupling to the reservoirs perturbatively and assuming the reservoirs to have short correlation times as detailed in Appendix A. At each time step, the occupations of the drain and source are measured projectively. These measurements indirectly count the number of fermions leaving or entering the quantum dot: finding states of the drain and source to be occupied and empty, respectively, indicates that a fermion must have left or entered the quantum dot. A description of the dynamics of the quantum dot alone can be obtained by modeling the sequence of measurement results through appropriate stochastic processes. In the continuous-time limit $\Delta t \to \mathrm{d}t$ and generalizing the setup to L fermionic lattice sites, each in contact with its own drain and source as sketched in Fig. 1(a), we obtain a stochastic Schrödinger equation for state $|\psi(t)\rangle$ of the fermionic lattice system:

$$\mathrm{d}|\psi(t)\rangle = \Bigg(\Big\{ -\mathrm{i}\hat{H} - \sum_{\alpha=\pm} \sum_{l=1}^{L} [\hat{L}_{\alpha,l}^\dagger \hat{L}_{\alpha,l} - \tilde{p}_{\alpha,l}(t)] \Big\} \mathrm{d}t + \sum_{\alpha=\pm} \sum_{l=1}^{L} \left[\frac{\hat{L}_{\alpha,l}}{\sqrt{\tilde{p}_{\alpha,l}(t)}} - 1 \right] \mathrm{d}N_{\alpha,l}(t) \Bigg) |\psi(t)\rangle. \tag{3}$$

The first line describes deterministic dynamics, governed by Hamiltonian $\hat{H}$ in Eq. (2) and the jump operators

$$\hat{L}_{-,l} = \sqrt{\gamma_-/2}\, \hat{\psi}_l, \qquad \hat{L}_{+,l} = \sqrt{\gamma_+/2}\, \hat{\psi}_l^\dagger, \tag{4}$$

where the loss and gain rates γ_- and γ_+, respectively, are determined by microscopic parameters of the model, as specified in Appendix A. Nonnormalized probabilities are defined as

$$\tilde{p}_{\alpha,l}(t) = \langle \psi(t) | \hat{L}_{\alpha,l}^\dagger \hat{L}_{\alpha,l} | \psi(t) \rangle. \tag{5}$$

The second line of Eq. (3) incorporates the effect of measurements, where $\mathrm{d}N_{\alpha,l}(t) = 0, 1$ are stochastic increments. When $\mathrm{d}N_{\alpha,l}(t) = 0$, no jump occurs and the wave function evolves continuously. In contrast, $\mathrm{d}N_{\alpha,l}(t) = 1$ indicates a jump at time t and site l. For $\alpha = -$, this jump corresponds to the loss of a fermion; the jump describes the gain of a fermion for $\alpha = +$. After a jump, the state of the system is

$$|\psi(t + 0^+)\rangle = \frac{1}{\sqrt{\tilde{p}_{\alpha,l}(t)}} \hat{L}_{\alpha,l} |\psi(t)\rangle. \tag{6}$$

The stochastic increments $\mathrm{d}N_{\alpha,l}(t)$ obey a Poisson point process with mean $\overline{\mathrm{d}N_{\alpha,l}(t)} = 2\tilde{p}_{\alpha,l}(t)\mathrm{d}t$ [76]. For the case

of equal loss and gain rates, $\gamma = \gamma_- = \gamma_+$, the rate of jumps per lattice site is constant in time and given by

$$\frac{1}{L}\sum_{\alpha=\pm}\sum_{l=1}^{L}\overline{\frac{\mathrm{d}N_{\alpha,l}}{\mathrm{d}t}} = \frac{2}{L}\sum_{\alpha=\pm}\sum_{l=1}^{L}\tilde{p}_{\alpha,l}(t) = \gamma, \tag{7}$$

leading to an exponential distribution of waiting times between jumps. To integrate Eq. (3) numerically, we employ a higher-order quantum jump algorithm [80]. In this algorithm, waiting times are sampled from the exponential distribution, and the type of jump that occurs is chosen randomly according to the normalized probabilities given by

$$p_{-,l}(t) = \langle \hat{n}_l(t)\rangle/L, \qquad p_{+,l}(t) = (1 - \langle \hat{n}_l(t)\rangle)/L. \tag{8}$$

Between jumps, the system undergoes unitary time evolution described by Hamiltonian $\hat{H}$.

The occupation of a quantum dot can be measured through a modification of the above setup: instead of tunneling between the dot and reservoirs, we now consider direct tunneling from the source to the drain, with the tunneling amplitude proportional to the occupation number of the quantum dot [76,81]. Then, as described in Appendix A, the detection of fermions in the drain indirectly signals that the quantum dot is also occupied. In the resulting stochastic Schrödinger equation for the extended lattice system shown in Fig. 1(b), there is only a single type of jump operator at each site,

$$\hat{L}_l = \sqrt{\gamma}\hat{n}_l. \tag{9}$$

The rate of jumps per lattice site depends on the number of particles N,

$$\frac{1}{L}\sum_{l=1}^{L}\overline{\frac{\mathrm{d}N_l}{\mathrm{d}t}} = \frac{2\gamma N}{L}, \tag{10}$$

and, given that a jump occurs at time t, the lattice site l at which the jump operator (9) is applied is chosen with probability

$$p_l(t) = \langle \hat{n}_l(t)\rangle/N. \tag{11}$$

The key difference between fermion counting and occupation measurements is the conservation of the number of particles in the latter case. For fermion counting, each quantum jump decreases or increases the number of particles by one. Nevertheless, a meaningful quantitative comparison between the two models is enabled by choosing parameters such that the mean number of particles in the steady state and the rate of quantum jumps are the same. This is achieved by setting $\gamma = \gamma_- = \gamma_+$ and choosing the initial state as

$$|\psi_0\rangle = \prod_{l=1}^{L/2}\hat{\psi}^\dagger_{2l-1}|0\rangle, \tag{12}$$

which contains $N = L/2$ particles, corresponding to a fermion density of $n = N/L = 1/2$. Then, according to Eqs. (7) and (10), the rate of quantum jumps per lattice site is given by γ for both models. While we have obtained all of our numerical results for $n = 1/2$, we keep the explicit dependence on n in analytical expressions.

In solving Eq. (3) numerically, a great simplification results from the initial state (12) being Gaussian and the dynamics generated by the quadratic Hamiltonian (2) and the jump operators in Eqs. (4) and (9) preserving this property. Gaussian states are fully determined by the $L \times L$ single-particle density matrix

$$D_{l,l'}(t) = \langle\psi(t)|\hat{\psi}^\dagger_{l'}\hat{\psi}_l|\psi(t)\rangle. \tag{13}$$

A quantum jump at lattice site m as described by Eq. (6) modifies the single-particle density matrix as

$$D_{l,l'}(t+0^+) = \frac{\langle\psi(t)|\hat{L}^\dagger_{\alpha,m}\hat{\psi}^\dagger_{l'}\hat{\psi}_l\hat{L}_{\alpha,m}|\psi(t)\rangle}{\langle\psi(t)|\hat{L}^\dagger_{\alpha,m}\hat{L}_{\alpha,m}|\psi(t)\rangle}. \tag{14}$$

By using Wick's theorem, the expectation values on the right-hand side can be expressed in terms of $D_{l,l'}(t)$, which leads to a closed algorithm for the stochastic dynamics of the single-particle density matrix.

The stochastic Schrödinger equation (3) describes the evolution of the state vector $|\psi(t)\rangle$, conditioned on a sequence of measurement outcomes. Averaging over the stochastic increments $\mathrm{d}N_{\pm,l}(t)$ yields a quantum master equation in Lindblad form that describes the unconditional evolution of the density matrix $\overline{\hat{\rho}}(t) = \overline{|\psi(t)\rangle\langle\psi(t)|}$. In the unconditional dynamics, occupation measurements lead to dephasing between lattice sites, which in turn induces heating to infinite temperature in the steady state, $\overline{\hat{\rho}}_{\mathrm{ss}} = \hat{P}_N/\mathrm{tr}(\hat{P}_N)$, where $\hat{P}_N$ is the projector on the subspace with N particles. For fermion counting, the steady state is $\overline{\hat{\rho}}_{\mathrm{ss}} = \prod_{l=1}^{L}[1 + (\gamma_+ - \gamma_-)\hat{n}_l/(\gamma_+ + \gamma_-)]$, which reduces to $\overline{\hat{\rho}}_{\mathrm{ss}} = 1/2^L$ for our choice $\gamma_- = \gamma_+$ [82,83]. As a consequence, the unconditional steady state is completely featureless for both models, irrespective of the value of the jump rate γ. Consequently, observables that are linear in the state, such as expectation values $\overline{\langle\hat{A}(t)\rangle} = \mathrm{tr}[\hat{A}\overline{\hat{\rho}}(t)]$, do not exhibit any nontrivial effects of continuous monitoring. To see such effects, it is necessary to consider observables that are nonlinear in the projector on the conditional state $\hat{\rho}(t) = |\psi(t)\rangle\langle\psi(t)|$.

B. Interpretation as random generalized measurements

An alternative description of the dynamics under continuous monitoring that is equivalent to the stochastic Schrödinger equation (3) can be given by using the framework of generalized measurements introduced in Sec. I. Specifically, we consider unitary dynamics generated by Hamiltonian (2), interspersed with generalized measurements. The times at which measurements are performed and the measurement operators have to be chosen such that the effect of measurements on the quantum state described by Eq. (1) and the statistics of measurement times and outcomes reproduce the corresponding properties of quantum jumps in quantum trajectories described by the stochastic Schrödinger equation (3).

As explained above, for $\gamma = \gamma_- = \gamma_+$ and $N = L/2$, jumps occur at rate γ per lattice site. Therefore, the number of jumps during the evolution from time t_0 to t obeys a Poisson distribution with mean γLT, where $T = t - t_0$, and the times of individual jumps are distributed uniformly within the interval $[t_0, t]$. We choose the times at which measurements are performed accordingly.

Monitored loss and gain or fermion counting, as described by the jump operators in Eq. (4), corresponds to generalized measurements with the measurement operators

$$\hat{M}_{-,l} = \frac{1}{\sqrt{L}}\hat{\psi}_l, \qquad \hat{M}_{+,l} = \hat{M}_{-,l}^\dagger = \frac{1}{\sqrt{L}}\hat{\psi}_l^\dagger. \tag{15}$$

These measurement operators differ from the jump operators in Eq. (4) only through prefactors, which are chosen to obey the completeness relation $\sum_{\alpha=\pm}\sum_{l=1}^{L}\hat{M}_{\alpha,l}^\dagger\hat{M}_{\alpha,l} = 1$. As noted before, the completeness relation is a consequence of fermionic anticommutation relations. Since the measurement operators are proportional to the jump operators, the effect of generalized measurements and quantum jumps on the state, described by Eqs. (1) and (6), respectively, are the same. Furthermore, the probabilities $p_{\alpha,l} = \langle\hat{M}_{\alpha,l}^\dagger\hat{M}_{\alpha,l}\rangle$ of different measurement outcomes agree with the corresponding probabilities of the quantum jumps in Eq. (8).

The reformulation of the quantum trajectory dynamics with the jump operators in Eq. (9) as generalized measurements of occupation numbers relies on the fact that the dynamics is restricted to a subspace with a fixed number of particles N, which allows us to choose the measurement operators as

$$\hat{M}_l = \frac{1}{\sqrt{N}}\hat{n}_l. \tag{16}$$

These operators obey the completeness relation $\sum_{l=1}^{L}\hat{M}_l^\dagger\hat{M}_l = \hat{N}/N = 1$, where the last equality holds in the restriction to the relevant subspace in which the particle-number operator $\hat{N} = \sum_{l=1}^{L}\hat{n}_l$ reduces to the number N. Again, the measurement operators are proportional to the corresponding jump operators, implying that they induce the same change of the state, and the probabilities $p_l = \langle\hat{M}_l^\dagger\hat{M}_l\rangle$ of different measurement outcomes agree with the corresponding probabilities of the quantum jumps in Eq. (11). The rate of jumps given in Eq. (10) reduces to γ only for $N = L/2$. Nevertheless, we keep N unspecified in Eq. (16) for the sake of generality.

Note that in the reformulation of quantum jumps as generalized measurements, the lattice site index l is the *outcome* of a generalized measurement and, therefore, determined by the quantum state, and only the measurement times are imposed externally. In contrast, in the model considered in Ref. [42], both the measurement times and the lattice sites at which projective measurements of occupation numbers are performed are chosen independently from the state of the system. The measurement operators for such local projective measurements as illustrated in Fig. 1(c) are $\hat{M}_{0,l} = 1 - \hat{n}_l$ and $\hat{M}_{1,l} = \hat{n}_l$, and obey the local completeness relation $\hat{M}_{0,l} + \hat{M}_{1,l} = 1$, reflecting the fact that the measurement operators are projectors.

The physical difference between the generalized measurements of occupation numbers described by Eq. (16) and projective measurements is best understood by considering a single particle on a lattice in a state $|\psi\rangle$. Generalized occupation measurements amount to asking the question: "where is the particle?" The answer is a particular lattice site l, with probability $p_l = \langle\psi|\hat{n}_l|\psi\rangle$. In contrast, performing a projective measurement of $\hat{n}_l$ at a given lattice site l means asking the question: "is the particle at this site?" The answer is yes or no, with probabilities $p_1 = \langle\psi|\hat{n}_l|\psi\rangle$ and $p_0 = 1 - p_1$, respectively.

The fact that the lattice site l is the outcome of the measurement is crucial for generalized measurements of occupation numbers, for which the distribution of lattice sites in Eq. (11) is not uniform in space. In contrast, for fermion counting with probabilities given in Eq. (8), the marginal distribution $p_l(t) = p_{-,l}(t) + p_{+,l}(t) = 1/L$ is uniform.

We finish this discussion by noting that any generalized measurement on a given system can be implemented by coupling the system to auxiliary systems through unitary operations and performing a projective measurement on the auxiliary systems [72]. We describe how this is achieved for the measurement operators in Eqs. (15) and (16) in Appendix B. The proposed implementations utilize operations that are available on programmable quantum simulators of fermionic circuits [84–92].

IV. GENERALIZED ZENO EFFECT IN THE FREQUENT-MEASUREMENT LIMIT

While frequent generalized measurements of occupation numbers induce the conventional quantum Zeno effect,

fermion counting at high rates leads to a generalized Zeno effect. Importantly, both types of Zeno effects can be observed in the density autocorrelation function.

The simplest manifestation of the conventional quantum Zeno effect occurs in projective measurements: a single projective measurement causes the state of a quantum system to collapse to an eigenstate of the measured observable. Because of this initial collapse, repeated measurements yield the same result. If measurements are repeated at rate γ and in between measurements there is coherent evolution with a characteristic frequency J, then transitions to other eigenstates of the measured observable occur at the perturbatively small rate $\nu = J^2/\gamma$—this suppression of coherently induced transitions is the essence of the Zeno effect.

Generalized measurements of local occupation numbers are not projective measurements. However, the measurement operators (16) are proportional to the projection operators $\hat{n}_l$ and, therefore, repeated measurements still induce a quantum Zeno effect. Suppose that the system is prepared in a superposition of pointer states, in other words eigenstates of the measurement operators, which are classical configurations of N particles on L lattice sites. Then, repeated measurements gradually collapse this superposition to a single pointer state, randomly chosen according to Born's rule. The pointer states are thus fixed points of the measurement-only dynamics. Coherent hopping destabilizes these fixed points. However, they remain metastable on a time scale of about $1/\nu$ [93]. Since the pointer states are classical configurations, signatures of the Zeno effect induced by generalized measurements of local occupation numbers are both emergent classicality and the suppression of coherent dynamics. This is formalized in the mapping to the symmetric simple exclusion process [93–95].

The symmetric simple exclusion process is a classical stochastic process of N particles on a 1D lattice of size L. On each lattice site, there is at most one particle—in the present context, this is a consequence of the Pauli exclusion principle. Each particle has its own internal timer and waits for a random duration, drawn from an exponential distribution with a mean waiting time that is identical for all particles. After the waiting time has elapsed for a given particle, the particle attempts a jump. The process being symmetric means that the probabilities to jump to the left and to the right are the same; for a simple process, jumps are only to neighboring sites. If the target site is empty, the particle jumps there; otherwise, the particle stays at its current location. In both cases, the timer of the particle is restarted, and the particle waits for a random time before it attempts the next jump.

To observe emergent classicality and the suppression of coherent dynamics as described above, we consider the average over trajectories of the conditional density autocorrelation function in the steady state, which we define as

$$K(t-t') = 4[\overline{\langle \hat{n}_l(t)\rangle \langle \hat{n}_l(t')\rangle} - \overline{\langle \hat{n}_l(t)\rangle}\ \overline{\langle \hat{n}_l(t')\rangle}] = \overline{z_l(t) z_l(t')}. \tag{17}$$

In preparation for our discussion of the generalized Zeno effect below, we have introduced an alternative representation of the density autocorrelation function in terms of the variables $z_l(t) = 2\langle \hat{n}_l(t)\rangle - 1$, such that an occupied or empty site corresponds to $z_l(t) = +1$ or $z_l(t) = -1$, respectively, and we consider a system with average density $\overline{\langle \hat{n}_l(t)\rangle} = 1/2$.

Figure 3(a) shows the density autocorrelation function for generalized measurements of occupation numbers for a system of size $L = 100$. For large values of γ, the data agree well with numerical simulations of the symmetric simple exclusion process [96] with a jump rate of 2ν, where $\nu = J^2/\gamma$. In particular, the initial value

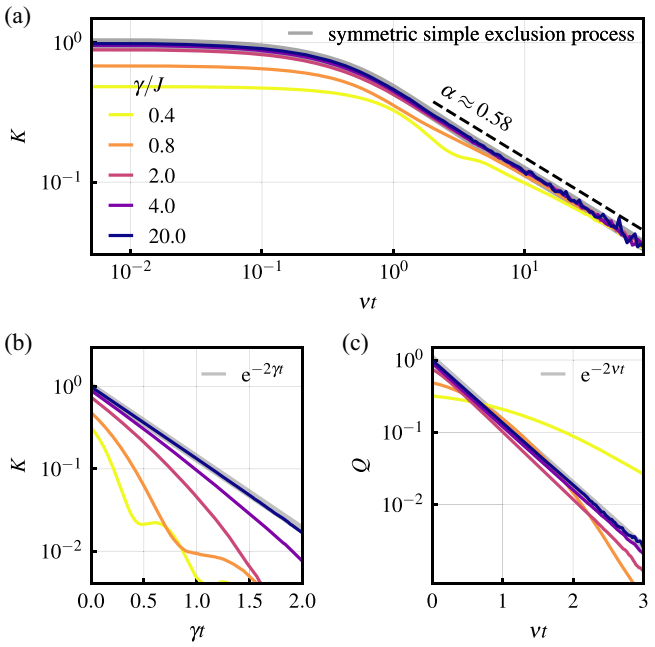


FIG. 3. (a) Density autocorrelation function (17) for occupation measurements. For $\gamma \gg J$, the dynamics agrees with a symmetric simple exclusion process. The Zeno effect is manifest in the collapse of the data after rescaling time with $\nu = J^2/\gamma$. Particle-number conservation causes algebraic decay $K(t) \sim t^{-\alpha}$ with $\alpha \approx 0.58$. (b) For fermion counting, the density autocorrelation function exhibits fast exponential decay, described by a random telegraph process. (c) The generalized Zeno effect is revealed by factoring out the telegraph process in Eq. (18). We observe a collapse of the telegraph-reduced autocorrelation function after rescaling time with ν. For the results shown in this figure, $L = 100$; in (a), the number of trajectories ranges from $N_{\text{traj}} = 10^4$ to $N_{\text{traj}} = 10^3$ for $\gamma = 0.4J$ to $\gamma = 20J$, and $N_{\text{traj}} = 10^6$ for the symmetric simple exclusion process; in (b) and (c), $N_{\text{traj}} = 5 \times 10^5$ to $N_{\text{traj}} = 5 \times 10^4$ for $\gamma = 0.4J$ to $\gamma = 20J$.

$K(0)$ approaches 1, which reflects the fact that individual trajectories become dominated by pointer states, in other words classical configurations with $z_l(t) = \pm 1$. The suppression of coherent dynamics is demonstrated by the collapse of the data after rescaling time with $\nu = J^2/\gamma$. Finally, particle-number conservation results in slow algebraic decay, $K(t) \sim t^{-\alpha}$. A fit to the data for $\gamma = 20J$ yields $\alpha \approx 0.58$, in reasonable agreement with the diffusive scaling with $\alpha = 1/2$ expected in larger systems [97]. To observe this slow decay, it is necessary to sample rare configurations with a strongly inhomogeneous distribution of particles, which require long times $t \sim O(L)$ to relax and contribute significantly to the algebraic tail of $K(t)$. Therefore, to obtain the data shown in Fig. 3(a), we have initialized each trajectory in a randomly chosen classical configuration with $N = L/2$ particles.

Monitored loss and gain or fermion counting can induce a generalized Zeno effect. As for the case of generalized measurements of occupation numbers, repeated application of the measurement operators (15) causes an initial superposition to collapse to a pointer state. However, the measurement operators (15) are not proportional to projection operators. Therefore, these operators do not stabilize pointer states, but rather induce transitions between pointer states. In spite of this qualitative difference, the dynamics in the frequent-measurement limit is again characterized by emergent classicality and the suppression of coherent evolution.

Figure 3(b) shows the density autocorrelation function for fermion counting. Again, $K(0) \to 1$ for increasing γ signals that the dynamics is dominated by classical configurations. Indeed, for $\gamma = 20J$, we observe good agreement with exponential decay with a rate of 2γ, corresponding to a classical random telegraph process [78]. That is, the occupation of each lattice site fluctuates between zero and one at a rate of about γ, akin to the signal produced by a telegraph. In stark contrast to the case of occupation measurements, here the measurement-only dynamics does not cause the evolution to freeze but rather to accelerate. To reveal the concomitant suppression of coherent dynamics, we consider the decay of density autocorrelations after factoring out the fast local telegraph process. This factorization can be achieved by noting that, for a single realization of the telegraph process on a lattice site l, the density autocorrelation function can be written as $z_l(t)z_l(t') = (-1)^{N_l(t,t')}$, where $N_l(t,t')$ is the fermion count at site l integrated from time t' to t. Put differently, each fermion count increases $N_l(t,t')$ by one and switches the sign of $z_l(t)$. Factoring out this classical contribution, we define the telegraph-reduced autocorrelation function as

$$Q(t-t') = \overline{z_l(t)(-1)^{N_l(t,t')}z_l(t')}. \tag{18}$$

By construction, $Q(t) = 1$ stays constant for measurement-only dynamics with $J = 0$. In contrast, a nonzero hopping amplitude causes $Q(t)$ to decay, with the decay rate providing a direct measure for the suppression of coherent dynamics for large values of γ. Indeed, a perturbative calculation presented in Appendix C and valid for $J \ll \gamma$ yields exponential decay, $Q(t) = \mathrm{e}^{-2\nu t}$, with a decay rate $\nu = J^2/\gamma$ that vanishes for $\gamma \to \infty$. We interpret this slowdown of coherent dynamics for high fermion count rates as a generalized quantum Zeno effect. The exponential rather than algebraic decay is due to the number of particles not being conserved.

Figure 3(c) shows numerical results for the telegraph-reduced autocorrelation function $Q(t)$. To demonstrate the suppression of coherent dynamics, we rescale time with $\nu = J^2/\gamma$. For increasing γ, the data agree with the analytically predicted behavior.

To reveal the generalized Zeno effect, in Eq. (18), we had to factor out the local telegraph process for each single trajectory before taking the average over trajectories. This indicates that the generalized Zeno effect is unique to conditional dynamics under continuous monitoring, and that the suppression of coherent dynamics with an emergent slow decay rate $\nu = J^2/\gamma$ cannot be seen in the unconditional dynamics. To provide supporting evidence for this conjecture, we consider the density autocorrelation function defined by

$$C_0(t-t') = \tfrac{1}{2}\overline{\langle\{\hat{n}_l(t), \hat{n}_l(t')\}\rangle} - \overline{\langle\hat{n}_l(t)\rangle}\,\overline{\langle\hat{n}_l(t')\rangle}. \tag{19}$$

Here, unconditional two-time averages are determined by the quantum regression theorem [73]. For example, for $t > t' > t_0$,

$$\overline{\langle\hat{n}_l(t)\hat{n}_l(t')\rangle} = \mathrm{tr}[\hat{n}_l \mathrm{e}^{\mathcal{L}(t-t')}\hat{n}_l \mathrm{e}^{\mathcal{L}(t'-t_0)}\hat{\rho}_0], \tag{20}$$

where $\hat{\rho}_0 = |\psi_0\rangle\langle\psi_0|$ is the projector on the initial state, and Liouvillian $\mathcal{L}$ is defined by

$$\mathcal{L}\hat{\rho} = -\mathrm{i}[\hat{H}, \hat{\rho}] + \sum_{\alpha=\pm}\sum_{l=1}^{L}(2\hat{L}_{\alpha,l}\hat{\rho}\hat{L}_{\alpha,l}^{\dagger} - \{\hat{L}_{\alpha,l}^{\dagger}\hat{L}_{\alpha,l}, \hat{\rho}\}). \tag{21}$$

The sum over α is absent for occupation measurements, which are described by a single type of jump operator. Let us anticipate that within the framework of replica Keldysh field theory introduced next, we find the unconditional density autocorrelation function for occupation measurements to be given by

$$C_0(t) \sim \frac{1}{8\sqrt{\pi\nu\,|t|}}. \tag{22}$$

That is, we also find slow, diffusive decay with a diffusion constant of about ν in the unconditional dynamics. For fermion counting, Liouvillian (21) is quadratic and the

unconditional autocorrelation function can be calculated exactly by elementary means. The exact result is reproduced by the replica Keldysh field theory approach introduced below, which yields

$$C_0(t) = \frac{1}{4}\mathrm{e}^{-2\gamma|t|}J_0(2J\,|t|)^2 \sim \frac{\mathrm{e}^{-2\gamma|t|}}{4\pi J\,|t|}\sin(2J\,|t| + \pi/4)^2, \tag{23}$$

where J_0 is the Bessel function of the first kind and the asymptotic form applies to $|t| \to \infty$. As for the conditional density correlation function (17), we obtain exponential decay with a rate of 2γ, and there is no indication of a suppression of coherent dynamics for $\gamma \gg J$.

Having established the suppression of coherent dynamics and emergent classicality in the conditional time evolution as common traits of the conventional and generalized Zeno effects, we now turn to the question of how these properties are reflected in correlations and entanglement in the steady state.

V. REPLICA KELDYSH FIELD THEORY

In Sec. III, we introduced two equivalent ways to describe the dynamics generated by continuous monitoring: in terms of a stochastic Schrödinger equation, and as random generalized measurements. We now focus on the latter formulation, which is a suitable starting point for making analytical progress using replica Keldysh field theory. To that end, we generalize the formalism introduced for projective measurements in Ref. [42] to the generalized measurements. Our presentation closely follows Ref. [42], but we highlight new aspects that are specific to our models. Already at this point, let us anticipate that considering generalized measurements described by Eqs. (15) and (16) instead of projective measurements of occupation numbers as in Ref. [42] results in a number of important conceptual, technical, and, ultimately, physical differences. (i) We have to account for the lattice site l being an outcome of a generalized measurement rather than selected randomly as for the projective measurements in Ref. [42]. (ii) The modified forms of interaction vertices in the measurement action necessitate a novel perturbative approach to preserve the causality structure of Keldysh field theory. (iii) The breaking of particle-number conservation due to monitored loss and gain or fermion counting is reflected in explicitly broken symmetries of the Keldysh action. We have already discussed the physical consequences of these broken symmetries in Sec. II. Below, we describe how they affect the long-wavelength effective field theory.

Recently, it has been pointed out that the long-wavelength effective field theory derived in Ref. [42] is modified if the Hamiltonian has particle-hole symmetry (PHS) [52]. This is the case, in particular, for the 1D lattice Hamiltonian (2) considered in Ref. [42] and our work: through a gauge transformation, $\hat{\psi}_l \mapsto \mathrm{i}^l\hat{\psi}_l$, the hopping amplitudes can be made purely imaginary; after this transformation, the hopping matrix, Eq. (47) below, obeys the PHS $H = -H^{\mathsf{T}}$. The PHS can be broken, for example, by adding next-nearest-neighbor hopping with real amplitudes. Crucially, the modifications of the field theory due to PHS do not lead to qualitatively different behavior. Therefore, we first present the theory for the technically simpler case of broken PHS, and we summarize changes due to PHS at the end [54].

A. Observables

As explained in Sec. III A, the unconditional steady state is completely featureless for both fermion counting and generalized occupation measurements for any value of the measurement rate γ. Therefore, to observe nontrivial effects of continuous monitoring, we have to consider observables that are nonlinear in the state, such that the averaging over trajectories does not simply amount to replacing the conditional by the unconditional state. As an important example, we study here the von Neumann entanglement entropy. For a pure state $\hat{\rho} = |\psi\rangle\langle\psi|$ and given a bipartition of the system into a subsystem A and its compliment B, the von Neumann entanglement entropy of subsystem A reads

$$S_A = -\overline{\mathrm{tr}[\hat{\rho}_A \ln(\hat{\rho}_A)]}, \tag{24}$$

where $\hat{\rho}_A = \mathrm{tr}_B(\hat{\rho})$ is the reduced density matrix of subsystem A. For Gaussian states, the entanglement entropy is related to the full counting statistics of the number of particles in subsystem A [98–102],

$$S_A = 2\sum_{k=1}^{\infty}\zeta(2k)C_A^{(2k)} = \frac{\pi^2}{3}C_A^{(2)} + \frac{\pi^4}{45}C_A^{(4)} + \cdots, \tag{25}$$

where $\zeta(k)$ denotes the Riemann zeta function and $C_A^{(k)}$ is the kth cumulant of the subsystem particle number $\hat{N}_A = \sum_{l\in A}\hat{n}_l$. In particular, the second cumulant is given by

$$C_A^{(2)} = \overline{\langle(\hat{N}_A - \langle\hat{N}_A\rangle)^2\rangle}. \tag{26}$$

The task at hand is therefore to calculate the average over trajectories of polynomials of quantum expectation values, which are taken in the pure conditional state. Since we are considering a quantum many-body system, we wish to perform this calculation within the framework of nonequilibrium quantum field theory. This will allow us to employ standard techniques to obtain an approximate solution in the long-wavelength limit.

B. Replica trick

Rewriting nonlinear observables such as the second cumulant (26) as functional integrals in the framework of

Keldysh field theory can be achieved by introducing copies or *replicas* of the system in two steps. First, we note that the average over trajectories of a product of k expectation values can be reformulated as a single expectation value that contains the average of k replicas of the density matrix. For example, for two operators $\hat{A}$ and $\hat{B}$, we can write

$$\begin{aligned}\overline{\langle\hat{A}(t)\rangle\langle\hat{B}(t)\rangle} &= \overline{\mathrm{tr}[A\hat{\rho}(t)]\,\mathrm{tr}[\hat{B}\hat{\rho}(t)]} \\ &= \mathrm{tr}\{(\hat{A}_1\otimes\hat{B}_2)\overline{[\hat{\rho}_1(t)\otimes\hat{\rho}_2(t)]}\}. \end{aligned} \tag{27}$$

In the last equality, we have introduced the replica index $r\in\{1,2\}$ to indicate on which copy of the system a particular operator is acting [103]. Generalizing Eq. (27), a product of k expectation values can be expressed in terms of the k-replica density matrix

$$\hat{\mu}_k(t) = \overline{\bigotimes_{r=1}^{k}\hat{\rho}_r(t)}. \tag{28}$$

In the formulation of our models in terms of random generalized measurements, the average over trajectories comprises three components. First, an average over the total number of measurements M. As explained in Sec. III B, the number of measurements M during the total evolution time $T=t-t_0$ obeys a Poisson distribution with mean γLT,

$$p_M(T) = \frac{1}{M!}(\gamma LT)^M \mathrm{e}^{-\gamma LT}. \tag{29}$$

Second, for each measurement labeled by $m\in\{1,\ldots,M\}$, the average in Eq. (28) contains an average over the measurement time t_m. The latter is uniformly distributed in the interval $t_m\in[t_0,t]$ of length $T=t-t_0$. Third, for each measurement, there is an average over measurement outcomes $\alpha_m\in\{+,-\}$ and $l_m\in\{1,\ldots,L\}$. The index α_m, which distinguishes the measurement operators in Eq. (15) for fermion counting, is absent for generalized occupation measurements with a single type of measurement operator given in Eq. (16). For measurements at times $\{t_m\}$, we denote the probability to obtain a sequence of measurement outcomes $\{\alpha_m,l_m\}$ by $p_{\{\alpha_m,l_m\}}(\{t_m\})$. The average in Eq. (28) is thus

$$\hat{\mu}_k(t) = \sum_{\{\alpha_m,l_m,t_m\}} p_{\{\alpha_m,l_m\}}(\{t_m\})\bigotimes_{r=1}^{k}\hat{\rho}_r(t), \tag{30}$$

where the symbolic sum includes the average over both the Poisson distribution of the number of measurements M and the uniform distributions of measurement times $\{t_m\}$, as well as a summation over measurement outcomes $\{\alpha_m,l_m\}$,

$$\sum_{\{\alpha_m,l_m,t_m\}} = \sum_{M=0}^{\infty} p_M(T)\prod_{m=1}^{M}\sum_{\alpha_m=\pm}\sum_{l_m=1}^{L}\int_{t_0}^{t}\frac{\mathrm{d}t_m}{T}. \tag{31}$$

The probability $p_{\{\alpha_m,l_m\}}(\{t_m\})$ of a sequence of measurement results $\{\alpha_m,l_m\}$ can be expressed in terms of the nonnormalized density matrix for a single copy of the system. If we omit the normalization factor in Eq. (1), the state of the system after a time t can be written as

$$\hat{D}(t) = \hat{V}(t)\hat{\rho}_0\hat{V}(t)^\dagger \tag{32}$$

with the initial state $\hat{\rho}_0=|\psi_0\rangle\langle\psi_0|$ and

$$\hat{V}(t) = \hat{U}(t-t_M)\hat{M}_{\alpha_M,l_M}\hat{U}(t_M-t_{M-1})\cdots\hat{M}_{\alpha_1,l_1}\hat{U}(t_1-t_0). \tag{33}$$

In $\hat{V}(t)$, unitary evolution $\hat{U}(t)=\mathrm{e}^{-\mathrm{i}\hat{H}t}$ is interspersed with quantum jumps $\hat{M}_{\alpha_m,l_m}$ at times t_m. We leave the dependence of $\hat{V}(t)$ on the sequence of measurement outcomes and times $\{\alpha_m,l_m,t_m\}$ implicit. The normalized density matrix is obtained by reinstating the factors $p_{\alpha_m,l_m}(t)$ in Eq. (1),

$$\hat{\rho}(t) = \frac{1}{\prod_{m=1}^{M}p_{\alpha_m,l_m}(t_m)}\hat{D}(t). \tag{34}$$

Finally, using the fact that $\mathrm{tr}[\hat{\rho}(t)]=1$, we obtain the probability of the entire sequence of measurement outcomes, $p_{\{\alpha_m,l_m\}}(\{t_m\})$, given by the product of probabilities of individual measurement outcomes, $p_{\alpha_m,l_m}(t_m)$, as

$$p_{\{\alpha_m,l_m\}}(\{t_m\}) = \prod_{m=1}^{M}p_{\alpha_m,l_m}(t_m) = \mathrm{tr}[\hat{D}(t)]. \tag{35}$$

Recall the discussion in Sec. III B that treating generalized occupation measurements requires us to consider the site indices l_m as measurement outcomes. Their distribution is contained in the factors $p_{\alpha_m,l_m}(t_m)$. In contrast, the projective measurements studied in Ref. [42] are assumed to be distributed uniformly in space, and the uniform probability $1/L$ is combined with the summation over l_m in Eq. (31). Inserting the above expression for $p_{\{\alpha_m,l_m\}}(\{t_m\})$ into Eq. (30), we obtain

$$\hat{\mu}_k(t) = \sum_{\{\alpha_m,l_m,t_m\}}\left[\bigotimes_{r=1}^{k}\hat{D}_r(t)\right]\Big/\mathrm{tr}[\hat{D}(t)]^{k-1}. \tag{36}$$

The denominator in Eq. (36) obstructs the application of the usual Keldysh construction to obtain a functional integral representation of the time evolution of the k-replica

density matrix. We can get rid of this denominator by using the replica trick, which amounts here to first introducing additional replicas with indices $r \in \{k+1,\dots,R\}$ and then taking the replica limit $R \to 1$ [6,20,42,45]:

$$\hat{\mu}_k(t) = \lim_{R\to 1} \sum_{\{\alpha_m,l_m,t_m\}} \mathrm{tr}_{r=k+1,\dots,R}\left[\bigotimes_{r=1}^{R} \hat{D}_r(t)\right]. \tag{37}$$

We note that the replica limit $R \to 1$, which is required to reproduce the probability according to Born's rule given in Eq. (35), is different from the usual replica limit $R \to 0$ in the theory of disordered systems.

We can now obtain averages over trajectories of nonlinear observables such as the cumulant, Eq. (26), by calculating expectation values that are linear in the nonnormalized density matrix of R replicas of the original system and taking the replica limit $R \to 1$ in the end. Note that the way in which we have introduced replicas in Eq. (27) allows us to obtain *equal-time* correlations of conditional expectation values $\langle \hat{A}(t)\rangle$ and $\langle \hat{B}(t)\rangle$. However, unconditional averages, such as the autocorrelation function (19), can also be obtained for operators $\hat{A}(t)$ and $\hat{B}(t')$ at different times $t \neq t'$. A convenient way to generate different forms of expectation values is by introducing source terms in the R-replica Keldysh partition function,

$$Z_R(t) = \sum_{\{\alpha_m,l_m,t_m\}} \mathrm{tr}\left[\bigotimes_{r=1}^{R} \hat{D}_r(t)\right]. \tag{38}$$

By construction, the R-replica Keldysh partition function is normalized such that $Z_R(t) \to 1$ for $R \to 1$. Below, we derive a functional integral representation of $Z_R(t)$, where source fields can be introduced as required at a later stage. Before that, however, we discuss symmetries of the R-fold replicated dynamics.

C. Symmetries in the operator formalism

The long-wavelength behavior of our models is dominated by strong fluctuations of soft modes, which are related to symmetries of the dynamics. Therefore, a prerequisite for deriving a long-wavelength effective theory is to identify the relevant symmetries. This analysis provides important insights into the consequences of particle-number conservation for generalized occupation measurements. As explained at the beginning of Sec. V, we consider here the case of broken PHS. Modifications due to PHS will be discussed below.

In the Keldysh partition function (38) time evolution is described by the R-fold replication of operator $\hat{V}(t)$ defined in Eq. (33), $\prod_{r=1}^{R} \hat{V}_r(t)$. Indeed, both $\prod_{r=1}^{R} \hat{V}_r(t)$ and $\prod_{r=1}^{R} \hat{V}_r(t)^\dagger$ appear in Eq. (38), acting on the initial density matrix $\hat{\rho}_{R,0} = \bigotimes_{r=1}^{R} \hat{\rho}_{0,r}$ from the left- and right-hand sides, respectively. This can be expressed in terms of a superoperator $\mathcal{V}(t)$ defined by

$$\mathcal{V}(t)\hat{\rho} = \left(\prod_{r=1}^{R} \hat{V}_r(t)\right)\hat{\rho}\left(\prod_{r=1}^{R} \hat{V}_r(t)^\dagger\right), \tag{39}$$

which allows us to write Eq. (38) in the form

$$Z_R(t) = \sum_{\{\alpha_m,l_m,t_m\}} \mathrm{tr}[\mathcal{V}(t)\hat{\rho}_{R,0}]. \tag{40}$$

For a superoperator such as $\mathcal{V}(t)$, one distinguishes between weak and strong symmetries [104,105]: the unitary operator $\hat{G}$ is a weak symmetry if $\mathcal{V}(t)$ is invariant under the simultaneous transformation with $\hat{G}$ and $\hat{G}^\dagger$ from the left- and right-hand sides, respectively. That is, defining the superoperator $\mathcal{G}$ as this simultaneous transformation, $\mathcal{G}\hat{\rho} = \hat{G}\hat{\rho}\hat{G}^\dagger$, the weak symmetry condition reads $[\mathcal{V}(t),\mathcal{G}] = 0$. In contrast, $\hat{G}$ is a strong symmetry if $\mathcal{V}(t)$ is invariant under independent transformations on the left- and right-hand sides. Defining $\mathcal{G}_+\hat{\rho} = \hat{G}\hat{\rho}$ and $\mathcal{G}_-\hat{\rho} = \hat{\rho}\hat{G}^\dagger$, the strong symmetry condition can be stated equivalently as $[\mathcal{V}(t),\mathcal{G}_+] = 0$ or $[\mathcal{V}(t),\mathcal{G}_-] = 0$. In turn, these relations are equivalent to $[\prod_{r=1}^{R} \hat{V}_r(t),\hat{G}] = 0$. For strong symmetries $\hat{G}$ forming a group G, the full symmetry group of superoperator $\mathcal{V}(t)$ is therefore $\mathrm{G}\times\mathrm{G}$. In contrast, the full symmetry group is only G if the transformations $\hat{G} \in \mathrm{G}$ are weak symmetries. Since $\mathcal{G} = \mathcal{G}_+\mathcal{G}_-$, the strong symmetry condition implies the weak symmetry condition.

By construction, the replicated time-evolution operator, $\prod_{r=1}^{R} \hat{V}_r(t)$, is invariant under permutations of replicas, which form the symmetric group S_R. Therefore, $\mathcal{V}(t)$ has a strong S_R symmetry. This discrete symmetry does not give rise to soft modes. However, in the models we study, the discrete S_R symmetry is enhanced to a continuous symmetry: $\mathrm{SU}(R)$ for fermion counting, and $\mathrm{U}(R) = \mathrm{U}(1) \rtimes \mathrm{SU}(R)$ for occupation measurements. As detailed in Appendix E, this symmetry enhancement is specific to coherent dynamics and measurements that preserve Gaussianity of the time-evolved state. Furthermore, there are two requirements for such a symmetry enhancement to occur. (i) The number of particles has to be conserved by the coherent dynamics; measurements are allowed to change the number of particles by integer values, but they have to keep the system in a state with a well-defined number of particles. This is the case, in particular, for the measurement operators in Eqs. (15) and (16), which change the number of particles by $\Delta N = \pm 1$ and $\Delta N = 0$, respectively. For the Majorana model of Ref. [45], this condition is not met. (ii) The outcomes of all measurements have to be recorded. The symmetry is broken, in particular, for inefficient detection, which is commonly modeled by averaging over a fraction of the measurement outcomes [76].

These two requirements, combined with the symmetry under permutations of replicas that is built into the formalism, imply that the R-fold replicated state of the system is at all times a Slater determinant with a well-defined number N of particles in each replica,

$$|\psi_{R,N}\rangle = \prod_{r=1}^{R}\prod_{n=1}^{N}\sum_{l=1}^{L}\psi_{l,n}\hat{\psi}^{\dagger}_{r,l}|0\rangle. \tag{41}$$

Here, the ψ_n are N orthonormal single-particle states with amplitude $\psi_{l,n}$ on lattice site l. The fermionic field operators $\hat{\psi}_{r,l}$ act in the Hilbert space of R replicas of the original lattice system. Furthermore, the R-replica vacuum state obeys $\hat{\psi}_{r,l}|0\rangle = 0$.

Because of the symmetry under permutations of replicas, each single-particle state ψ_n is occupied in all replicas. Furthermore, fermionic statistics imply that each state ψ_n remains fully occupied after a single-particle transformation that corresponds to a change of basis in replica space but not in the Hilbert space of individual replicas. Therefore, each unitary transformation that describes such a change of basis leaves the above Slater determinant invariant up to a phase factor. Such transformations can be written as

$$\hat{G}_{\Phi} = \mathrm{e}^{\mathrm{i}\hat{\Phi}/2}, \qquad \hat{\Phi} = \sum_{r,r'=1}^{R}\sum_{l=1}^{L}\hat{\psi}^{\dagger}_{r,l}\Phi_{r,r'}\hat{\psi}_{r',l}, \tag{42}$$

where Φ is an Hermitian $R\times R$ matrix. Below, we also require the action of $\hat{G}_{\Phi}$ on fermionic field operators, which is given by

$$\hat{G}^{\dagger}_{\Phi}\hat{\psi}_{r,l}\hat{G}_{\Phi} = \sum_{r'=1}^{R}(G_{\Phi})_{r,r'}\hat{\psi}_{r',l}, \qquad G_{\Phi} = \mathrm{e}^{\mathrm{i}\Phi/2}. \tag{43}$$

The replicated time-evolution operator maps Slater determinants as in Eq. (41) to states of the same form but with a number of particles that, depending on measurement outcomes, can differ from N by an integer ΔN. As we show in Appendix E, applying the transformation defined in Eq. (42) to the replicated time-evolution operator yields

$$\hat{G}^{\dagger}_{\Phi}\left(\prod_{r=1}^{R}\hat{V}_r(t)\right)\hat{G}_{\Phi} = \mathrm{e}^{-\mathrm{i}\Delta N\,\mathrm{tr}_R(\Phi)/2}. \tag{44}$$

We thus see that $\hat{G}_{\Phi}$ commutes with the replicated time-evolution operator and is thus a strong symmetry of superoperator $\mathcal{V}(t)$ if $\Delta N = 0$. This is the case for occupation measurements. But, also for fermion counting where $\Delta N \neq 0$, we obtain a strong symmetry by imposing the constraint $\mathrm{tr}_R(\Phi) = 0$. In the former case, unconstrained $R\times R$ matrices Φ generate the group $\mathrm{U}(R)$; in the latter case, the condition $\mathrm{tr}_R(\Phi) = 0$ restricts the symmetry group to $\mathrm{SU}(R)$. However, note that the phase factor appearing in Eq. (44) is canceled when $\hat{G}_{\Phi}$ is applied to both the replicated time-evolution operator and its Hermitian conjugate appearing in $\mathcal{V}(t)$. Therefore, $\hat{G}_{\Phi}$ with unrestricted Φ is a weak symmetry for both occupation measurements and fermion counting.

As we show below in a formulation of the dynamics as a Keldysh field theory, the strong $\mathrm{SU}(R)$ symmetry that is common to both fermion counting and occupation measurements underlies the long-wavelength description in terms of an NLSM. However, before turning to the field-theory approach, let us provide a physical explanation of the $\mathrm{SU}(R)$ symmetry in terms of conservation of the total number of particles. We first note that conservation of the number of particles in each of the R replicas is associated with R strong symmetries of the form given in Eq. (42) with $\Phi_{r,r'} = \phi\delta_{r,r_0}\delta_{r',r_0}$ for $r_0 \in \{1,\ldots,R\}$. Evidently, these rotations with $\mathrm{tr}_R(\Phi) = \phi$ are not contained in the group $\mathrm{SU}(R)$ characterized by $\mathrm{tr}_R(\Phi) = 0$. This observation reaffirms that the $\mathrm{SU}(R)$ symmetry does not require particle-number conservation within the system. However, it is interesting to note that the implementations of fermion counting described in Appendices A and B require coupling the fermionic lattice system to auxiliary reservoirs in such a way that the total number of particles in the system and reservoirs is conserved. Indeed, the conservation of matter in a closed system implies that the implementation of any measurement that obeys condition (i) above requires coupling the system to reservoirs to compensate the change of the number of particles in the system. Therefore, we can regard conservation of the total number of particles as the physical reason for the occurrence of the $\mathrm{SU}(R)$ symmetry. However, an important caveat is formulated above in condition (ii): averaging over measurement outcomes corresponds to a loss of information that is reflected in the state of the system becoming mixed rather than pure as in Eq. (41). Then, as detailed in Appendix E, the $\mathrm{SU}(R)$ symmetry is broken, even though the total number of particles is still conserved.

D. Replica Keldysh action

In Keldysh field theory [106–109], the R-replica Keldysh partition function (38) is expressed as a functional integral over two independent sets of Grassmann fields $\psi_{k,r,l}(t)$ and $\psi^{*}_{k,r,l}(t)$ with Keldysh index k and replica index r, which we collect into $2R$-component vectors denoted by $\psi_l(t)$ and $\psi^{*}_l(t)$. Time evolution of the nonnormalized density matrix (32) is visualized as proceeding along two branches: the forward branch described by $\hat{V}(t)$ acting on $\hat{\rho}_0$ from the left, and the backward branch described by $\hat{V}(t)^{\dagger}$ acting on $\hat{\rho}_0$ from the right. Replacing operators on the forward and backward branches by fields with Keldysh

indices $k = +$ and $k = -$, respectively, we obtain

$$Z_R(t) = \int \mathrm{D}[\psi^*, \psi] \mathrm{e}^{\mathrm{i}\psi^\dagger G_0^{-1}\psi} \times \sum_{\{\alpha_m, l_m, t_m\}} \prod_{r=1}^{R} M_{+,r,\alpha_m,l_m}(t_m) M^\dagger_{-,r,\alpha_m,l_m}(t_m). \quad (45)$$

We omit the matrix element of the initial state $\hat{\rho}_0$, which fixes the number of particles for occupation measurements but is otherwise irrelevant in the steady state. The latter can be described by taking the limit $t_0 \to -\infty$. Unitary evolution contained in $\hat{V}(t)$, Eq. (33), gives rise to the quadratic Keldysh action, where we use a shorthand notation leaving the integration over time and summation over lattice sites implicit,

$$\psi^\dagger G_0^{-1} \psi = \int_{t_0}^{t} \mathrm{d}t' \sum_{l,l'=1}^{L} \psi_l^*(t') G^{-1}_{0,l,l'} \psi_{l'}(t'). \quad (46)$$

The inverse Green function reads $G_0^{-1} = (\mathrm{i}\partial_t - H)\sigma_z$, where σ_z is a Pauli matrix in Keldysh space and matrix H describes hopping according to Eq. (2),

$$H_{l,l'} = -J(\delta_{l+1,l'} + \delta_{l,l'+1}). \quad (47)$$

To further simplify the notation, we have omitted the identity 1_R in replica space in the definition of the inverse Green function. In the limit $t_0 \to -\infty$, Green's function should be augmented by an infinitesimal regularization term, fixing the correct causality properties and particle number [42]. We omit this term, anticipating that Green's function will be dressed due to measurements.

According to the rule formulated above for replacing operators by fields, the measurement operators for monitored loss and gain or fermion counting, Eq. (15), are represented by

$$M_{\pm,r,-,l}(t) = M^\dagger_{\pm,r,+,l}(t) = \pm\frac{1}{\sqrt{L}}\psi_{\pm,r,l}(t), \qquad M_{\pm,r,+,l}(t) = M^\dagger_{\pm,r,-,l}(t) = \pm\frac{1}{\sqrt{L}}\psi^*_{\pm,r,l}(t), \quad (48)$$

where we include the minus sign acquired by Grassmann fields on the backward branch [109]. For the measurement operators describing generalized measurements of occupation numbers, Eq. (16), we obtain

$$M_{\pm,r,l}(t) = M^\dagger_{\pm,r,l}(t) = \frac{1}{\sqrt{N}}\psi^*_{\pm,r,l}(t)\psi_{\pm,r,l}(t). \quad (49)$$

Inserting the explicit expression, Eq. (31), for the average over the number of measurements as well as the measurement times and outcomes into the functional integral representation of the R-replica Keldysh partition function in Eq. (45), we find that each factor in the product over measurements labeled by m is identical. We may thus omit the label m to obtain

$$Z_R(t) = \int \mathrm{D}[\psi^*, \psi] \mathrm{e}^{\mathrm{i}\psi^\dagger G_0^{-1}\psi} \sum_{M=0}^{\infty} \frac{\mathrm{e}^{-\gamma L T}}{M!} \times \left[\gamma L \sum_{\alpha=\pm}\sum_{l=1}^{L}\int_{t_0}^{t}\mathrm{d}t \prod_{r=1}^{R} M_{+,r,\alpha,l}(t) M^\dagger_{-,r,\alpha,l}(t)\right]^M. \quad (50)$$

When we now perform the sum over the number of measurements M, the expression in the second line of Eq. (50) is exponentiated. This leads to $Z_R(t) = \int \mathrm{D}[\psi^*, \psi] \mathrm{e}^{\mathrm{i}S[\psi^*,\psi]}$, where the action reads

$$S[\psi^*, \psi] = \int_{t_0}^{t} \mathrm{d}t' \sum_{l,l'=1}^{L} \psi_l^* G^{-1}_{0,l,l'} \psi_{l'} + \gamma \int \mathrm{d}^2\mathbf{x}\, \mathcal{L}_M[\psi_l^*, \psi_l]. \quad (51)$$

Here and occasionally in the following, we abbreviate expressions by omitting field indices and time arguments. Furthermore, we abbreviate integration over space and time as $\int \mathrm{d}^2\mathbf{x} = \sum_{l=1}^{L}\int_{t_0}^{t}\mathrm{d}t'$. The Lagrangian density due to random generalized measurements reads

$$\mathrm{i}\mathcal{L}_M[\psi^*, \psi] = \frac{1}{L^{R-1}} \sum_{\alpha=\pm}\prod_{r=1}^{R} V_\alpha[\psi_r^*, \psi_r] - 1, \quad (52)$$

where the prefactor L^{1-R} vanishes in the replica limit and will be omitted in the following. The last term in the measurement Lagrangian stems from the factor $\mathrm{e}^{-\gamma LT}$ in Eq. (50), where we have used the fact that $LT = \int \mathrm{d}^2\mathbf{x}\, 1$. For fermion counting, the vertices in the measurement Lagrangian are given by

$$V_-[\psi^*, \psi] = -\psi_+\psi_-^*, \qquad V_+[\psi^*, \psi] = -\psi_+^*\psi_-. \quad (53)$$

The product over replicas in Eq. (52) thus yields an interaction vertex containing $2R$ fermionic fields. For occupation measurements, there is a single vertex that depends explicitly on the fermion density $n = N/L$,

$$V[\psi^*, \psi] = \frac{1}{n}\psi_+^*\psi_+\psi_-^*\psi_-. \quad (54)$$

In this case, the product over replicas in Eq. (52) yields an interaction vertex containing $4R$ fermionic fields [110].

The replica Keldysh construction we have presented above provides an exact reformulation of the dynamics under continuous monitoring as a field theory. To

make further progress, we now have to introduce suitable approximations. The first step is to identify the relevant degrees of freedom, which dominate correlations and—via Eq. (25)—the dynamics of entanglement at long wavelengths. For generalized measurements of occupation numbers, we expect that the relevant slow modes are the same as for the case of projective measurements, that is, fermionic bilinears that we collect in the matrix $\mathcal{G}_l(t) = -\mathrm{i}\psi_l(t)\psi_l^*(t)$ [42]. As we will see comparing with our numerical results, this turns out to also be the correct choice for fermion counting.

Specifically, we want $\langle \mathcal{G}_l(t)\rangle$ to represent the fermionic Green function at equal positions and in the symmetrized limit of equal time arguments of the fields $\psi_l(t)$ and $\psi_l^*(t)$,

$$\langle \mathcal{G}_l(t)\rangle = -\frac{\mathrm{i}}{2}[\langle \psi_l(t)\psi_l^*(t+0^+)\rangle + \langle \psi_l(t)\psi_l^*(t-0^+)\rangle]. \tag{55}$$

Two technical issues arise: (i) in the construction of the Keldysh field integral, which is based on a discretization of time, products of field operators $\hat{n}_l = \hat{\psi}_l^\dagger \hat{\psi}_l$, as occur in the measurement operators for occupation measurements in Eq. (16), are replaced by fields that are a discrete time step apart; (ii) the discrete-time Green function at equal discrete times differs from the symmetrized limit of equal time arguments in the continuous-time formulation [107], and we want $\langle \mathcal{G}_l(t)\rangle$ to represent the latter. These discrepancies can be resolved by using the regularization procedure detailed in Appendix D.

The measurement operators for fermion counting are linear in fermionic field operators. Therefore, in this case the issues described above do not arise, and the vertices in Eq. (53) are not affected by the regularization. After a Larkin-Ovchinnikov rotation [106,107],

$$\psi_{1,2} = \frac{1}{\sqrt{2}}(\psi_+ \pm \psi_-), \qquad \psi_{1,2}^* = \frac{1}{\sqrt{2}}(\psi_+^* \mp \psi_-^*), \tag{56}$$

these vertices take the form

$$V_\pm[\psi^*,\psi] = -\tfrac{1}{2}[\psi_1^*\psi_1 - \psi_2^*\psi_2 \mp (\psi_1^*\psi_2 - \psi_2^*\psi_1)]. \tag{57}$$

In contrast, we obtain a modified vertex for generalized measurements of occupation numbers through the regularization,

$$V[\psi^*,\psi] = \frac{1}{n}\left[\frac{1}{4} + \frac{1}{2}\psi^\dagger\sigma_x\psi - \psi_1^*\psi_1\psi_2^*\psi_2\right] = \frac{1}{4n}\mathrm{e}^{2\psi^\dagger\sigma_x\psi}. \tag{58}$$

Up to the prefactor $1/n$, the regularized vertex is identical to one of the regularized vertices for projective occupation measurements of Ref. [42].

The vertices in Eqs. (57) and (58) contain the term $\psi_2^*\psi_1$, which would correspond to an anti-Keldysh component of the self-energy, and thus violates the familiar causality structure of fermionic Keldysh field theory [107,111]. For fermion counting and in the replica limit $R \to 1$, this term cancels in the sum over α in Eq. (52). A similar cancelation occurs for projective measurements of occupation numbers [42]. However, this is not the case for generalized occupation measurements. In Appendix D, we discuss how the appearance of an anti-Keldysh component can be reconciled with the normalization of the Keldysh partition function in the replica limit, $Z_R(t) \to 1$ for $R \to 1$. The violation of the usual causality structure is only due to the part of the Lagrangian for occupation measurements that is quadratic in fermionic fields,

$$\mathrm{i}\mathcal{L}_{M,Q}[\psi^*,\psi] = \frac{1}{2^{2R-1}n^R}\sum_{r=1}^{R}(\psi_{1,r}^*\psi_{2,r} + \psi_{2,r}^*\psi_{1,r}), \tag{59}$$

which we therefore separate from the nonquadratic part, $\mathcal{L}_{M,NQ} = \mathcal{L}_M - \mathcal{L}_{M,Q}$. To preserve the usual structure of the Keldysh formalism, we treat $\mathcal{L}_{M,Q}$ perturbatively, so that the self-energy, which nonperturbatively dresses Green's function, is fully determined by $\mathcal{L}_{M,NQ}$. For brevity, we drop the subscript NQ in the following. We anticipate that the theory we develop in the following applies in the limit $\gamma \ll J$. Therefore, treating $\mathcal{L}_{M,Q}$ perturbatively is justified within the scope of validity of our theory.

With these precautions, we introduce Hermitian $2R \times 2R$ matrix fields $\mathcal{G}$ and Σ, corresponding to the equal-time fermionic Green function and the self-energy, by means of a generalized Hubbard-Stratonovich transformation [42]. Specifically, we include the factor

$$1 = \int \mathrm{D}[\mathcal{G},\Sigma]\mathrm{e}^{-\epsilon\,\mathrm{Tr}(\Sigma^2)/2 - \mathrm{i}\,\mathrm{Tr}(\mathcal{G}\Sigma) - \psi^\dagger\Sigma\psi} \tag{60}$$

into the functional integral over ψ and ψ^*. The trace $\mathrm{Tr}(\cdot)$ acts in Keldysh, replica, lattice, and time spaces, with the matrices $\mathcal{G}$ and Σ being diagonal in lattice and time spaces. Convergence of the integration over $\mathcal{G}$ and Σ is ensured by the term proportional to ϵ. We omit this term in the following, with the understanding that the limit $\epsilon \to 0$ has to be taken at the end of the calculation. In this limit, the integral over Σ reduces to a delta functional fixing $\mathcal{G} = -\mathrm{i}\psi\psi^\dagger$ [42]. Using this relation, decoupling the measurement Lagrangian simultaneously in all possible slow channels is achieved by taking the average of $\mathcal{L}_M$ with respect to the Gaussian action $\psi^\dagger\mathcal{G}^{-1}\psi$ [42]. For fermion counting, this is done most conveniently with the form of the vertices given in Eq. (53), and the result can be expressed as a trace tr_K in Keldysh space and a determinant

$\det_R$ in replica space,

$$\mathrm{i}\mathcal{L}_M[\mathcal{G}] = \sum_{\alpha=\pm} \det_R[\mathrm{tr}_K(\tau_\alpha \mathcal{G})] - 1, \tag{61}$$

where $\tau_\pm = (\mathrm{i}\sigma_z \pm \sigma_y)/2$ and the σ_i are the Pauli matrices. The Lagrangian for occupation measurements contains a determinant $\det(\cdot)$ and a trace $\mathrm{tr}(\cdot)$ in both Keldysh and replica spaces:

$$\mathrm{i}\mathcal{L}_M[\mathcal{G}] = \frac{1}{n^R} \det\left(\frac{1}{2} - \mathrm{i}\sigma_x \mathcal{G}\right) + \frac{\mathrm{i}}{2^{2R-1} n^R} \mathrm{tr}(\sigma_x \mathcal{G}) - 1. \tag{62}$$

This form of the measurement Lagrangian is similar to that for projective measurements [42]: the latter does not contain the prefactor $1/n^R$ and the two types of projection operators, $\hat{n}_l$ and $1 - \hat{n}_l$, result in two determinant contributions with opposite signs of the term containing $\mathcal{G}$, in contrast to our model with only one determinant term. The trace in Eq. (62) stems from the subtraction of $\mathcal{L}_{M,Q}$, Eq. (59), and ensures that $\mathcal{L}_M$ does not contain terms that are linear in $\mathcal{G}$.

After decoupling the measurement Lagrangian, the action is quadratic in the fermionic fields ψ and ψ^*, which can thus be integrated out, leading to

$$S[\mathcal{G}, \Sigma] = S_0[\mathcal{G}, \Sigma] + \gamma \int \mathrm{d}^2\mathbf{x}\, \mathcal{L}_M[\mathcal{G}_l], \tag{63}$$

where

$$\mathrm{i}S_0[\mathcal{G}, \Sigma] = \mathrm{Tr}\{\ln[G_0^{-1} + \mathrm{i}(\Sigma + A)] - \mathrm{i}\mathcal{G}\Sigma\}. \tag{64}$$

In the basis of fields introduced in the Larkin-Ovchinnikov rotation (56), the bare Green function is proportional to the identity in both Keldysh and replica spaces, $G_0^{-1} = \mathrm{i}\partial_t - H$. Matrix A results from expressing the quadratic part of the measurement action, Eq. (59), as

$$\mathrm{i}\gamma \int \mathrm{d}^2\mathbf{x}\, \mathcal{L}_{M,Q}[\psi_l^*, \psi_l] = -\psi^\dagger A \psi, \tag{65}$$

where $A = 0$ for fermion counting and, for occupation measurements,

$$A = -\frac{\gamma}{2^{2R-1} n^R} \sigma_x. \tag{66}$$

As anticipated, we treat $A \sim \gamma$ perturbatively. To first order in A, action (64) reads

$$\mathrm{i}S_0[\mathcal{G}, \Sigma] = \mathrm{Tr}[\ln(G^{-1}) + \mathrm{i}(GA - \mathcal{G}\Sigma)], \tag{67}$$

where the dressed Green function is given by

$$G^{-1} = G_0^{-1} + \mathrm{i}\Sigma. \tag{68}$$

E. Symmetries in the functional integral formalism

We have already provided a preliminary discussion of symmetries in Sec. V C. The symmetries of superoperator $\mathcal{V}(t)$ discussed there are directly related to symmetries of the Keldysh action. To establish this connection, we start from the Keldysh partition function as written in Eq. (40). Using Eq. (44), the Keldysh partition function can be expressed as

$$Z_R(t) = \sum_{\{\alpha_m, l_m, t_m\}} \mathrm{e}^{\mathrm{i}\Delta N \,\mathrm{tr}_R(\Phi_+ - \Phi_-)/2} \times \mathrm{tr}\left[\left(\prod_{r=1}^{R} \hat{G}^\dagger_{\Phi_+} \hat{V}_r(t) \hat{G}_{\Phi_+}\right) \hat{\rho}_{R,0} \left(\prod_{r=1}^{R} \hat{G}^\dagger_{\Phi_-} \hat{V}_r(t)^\dagger \hat{G}_{\Phi_-}\right)\right]. \tag{69}$$

The phase factor in the first line evaluates to unity if one of the following three conditions is met: (i) $\Phi_+ = \Phi_-$, corresponding to the weak $\mathrm{U}(R)$ symmetry of $\mathcal{V}(t)$ as discussed in Sec. V C; (ii) $\mathrm{tr}_R(\Phi_\pm) = 0$, corresponding to the strong $\mathrm{SU}(R)$ symmetry for fermion counting; (iii) $\Delta N = 0$, corresponding to the strong $\mathrm{U}(R)$ symmetry for occupation measurements. Then, the operators $\hat{G}^\dagger_{\Phi_+}$ and $\hat{G}^\dagger_{\Phi_-}$ can be pulled through $\hat{V}_r(t)$ and $\hat{V}_r(t)^\dagger$, respectively, by transforming all field operators that appear in $\hat{V}_r(t)$ and $\hat{V}_r(t)^\dagger$ according to Eq. (43). Using the resulting expression as the starting point for the construction of the Keldysh functional integral representation as in Eq. (45), we find the same action as in Eq. (51), but with transformed fields. Leaving matrix multiplication in replica space and the lattice site index implicit, the transformations of the fields are

$$\psi_\pm \mapsto G_{\Phi_\pm} \psi_\pm, \qquad \psi_\pm^\dagger \mapsto \psi_\pm^\dagger G^\dagger_{\Phi_\pm}. \tag{70}$$

We thus see that the weak symmetry of $\mathcal{V}(t)$ corresponds to the symmetry of the Keldysh action under identical transformations of fields on the forward and backward branches. In contrast, the strong symmetry of $\mathcal{V}(t)$ for $\Delta N = 0$ or $\mathrm{tr}_R(\Phi) = 0$ is reflected in the symmetry of the Keldysh action under independent transformations on the forward and backward branches [109].

Having established the field transformations corresponding to the symmetries of superoperator $\mathcal{V}(t)$ in the basis of fields defined on the forward and backward branches, we wish to find the corresponding transformations of the fields introduced in the Larkin-Ovchinnikov rotation (56). To that end, we define symmetric and antisymmetric combinations of the matrices $\Phi_\pm$ as

$$\bar{\Phi} = \tfrac{1}{2}(\Phi_+ + \Phi_-), \qquad \Phi = \tfrac{1}{2}(\Phi_+ - \Phi_-). \tag{71}$$

Then, for $\psi = (\psi_1, \psi_2)^\intercal$, Eq. (70) becomes

$$\psi \mapsto \mathrm{e}^{\mathrm{i}(\bar{\Phi} + \Phi\sigma_x)/2} \psi. \tag{72}$$

The weak symmetry of $\mathcal{V}(t)$ under $\hat{G}_\Phi$ is described by $\bar{\Phi} = \Phi_+ = \Phi_-$ and $\Phi = 0$. This symmetry of superoperator $\mathcal{V}(t)$ implies the symmetry of the Keldysh action under $\psi \mapsto \mathcal{R}_{\bar{\Phi}}\psi$ with $\mathcal{R}_{\bar{\Phi}} = e^{i\bar{\Phi}/2}$. The strong symmetry of $\mathcal{V}(t)$ corresponds to arbitrary choices of $\Phi_\pm$ and thus $\bar{\Phi}$ and Φ. A particular choice is given by setting $\bar{\Phi} = 0$ and $\Phi = \Phi_+ = -\Phi_-$, which implies the symmetry of the Keldysh action under $\mathcal{R}_\Phi = e^{i\Phi\sigma_x/2}$. For fermion counting, this is a symmetry only for $\mathrm{tr}_R(\Phi) = 0$.

We next examine how these symmetries are realized in the Keldysh action after performing the generalized Hubbard-Stratonovich transformation, meaning for action (67) and the measurement Lagrangians given in Eqs. (61) and (62) in terms of the matrix fields $\mathcal{G}$ and Σ. Rotations of the fermionic fields described by $\psi \mapsto \mathcal{R}\psi$ and $\psi^\dagger \mapsto \psi^\dagger\mathcal{R}^{-1}$ act on the matrix fields as $\mathcal{G} \mapsto \mathcal{R}\mathcal{G}\mathcal{R}^{-1}$ and $\Sigma \mapsto \mathcal{R}\Sigma\mathcal{R}^{-1}$. In the Larkin-Ovchinnikov basis (56) the bare Green function G_0 is diagonal in Keldysh and replica spaces and, therefore, the symmetries of the Keldysh action are determined by the symmetries of the measurement Lagrangian and of matrix A appearing in action (67), which vanishes for fermion counting and is given in Eq. (66) for occupation measurements. Interestingly, the symmetries are different for $R = 1$ and $R > 1$, corresponding to the unconditional evolution of observables that are linear in the system state and to the conditional evolution of nonlinear observables, respectively.

We consider first the case $R = 1$. Then, $\mathcal{R}_{\bar{\Phi}} = e^{i\bar{\Phi}/2}$ reduces to a phase factor and does not yield a nontrivial transformation of $\mathcal{G}$ and Σ. For fermion counting, the condition $\mathrm{tr}_R(\Phi) = 0$ implies for $R = 1$ that $\mathcal{R}_\Phi = 1$ also acts trivially. Nevertheless, the measurement Lagrangian for fermion counting, Eq. (61), which for $R = 1$ is given by

$$i\mathcal{L}_M[\mathcal{G}] = i\,\mathrm{tr}_K(\sigma_z\mathcal{G}) - 1, \tag{73}$$

admits a nontrivial symmetry transformation of the from $\mathcal{R}_\zeta = e^{i\zeta\sigma_z/2}$ with $\zeta \in \mathbb{R}$. An inverse Larkin-Ovchinnikov rotation (56) shows that $\mathcal{R}_\zeta = e^{i\zeta\sigma_z/2}$ mixes fields on the forward and backward branches, and is thus not captured by Eq. (70). For occupation measurements, Lagrangian (62) simplifies for $R = 1$ to

$$i\mathcal{L}_M[\mathcal{G}] = \frac{1}{n}\left[\frac{1}{4} + \det{}_K(\mathcal{G})\right] - 1, \tag{74}$$

which is invariant under arbitrary rotations $\mathcal{R} \in \mathrm{U}(2)$. However, matrix A in Eq. (66) appearing in action (67) is proportional to σ_x, thus reducing the symmetries of the action to rotations of the form $\mathcal{R}_\phi = e^{i\phi\sigma_x/2}$, where we have set $\Phi = \phi \in \mathbb{R}$ for $R = 1$. Note that $\mathcal{R}_\phi$ corresponds to phase rotations with opposite signs on the forward and backward branches of the Keldysh contour. The symmetry of the Keldysh action under this type of rotation is associated with particle-number conservation [108,112].

We now turn to the case $R > 1$. Then, $\mathcal{R}_{\bar{\Phi}}$ and $\mathcal{R}_\Phi$ are nontrivial symmetry transformations for both fermion counting and occupation measurements—with the additional constraint that $\mathrm{tr}_R(\Phi) = 0$ in the former case. Here, we have deduced these symmetries of the Keldysh action from symmetries of the time-evolution superoperator $\mathcal{V}(t)$. We explicitly show that $\mathcal{R}_\Phi$ is a symmetry of the measurement Lagrangian for fermion counting, Eq. (61), in Appendix E. For the case of occupation measurements, this follows directly from inspection of Eqs. (62) and (67) with Eq. (66).

F. Saddle-point manifold

The field integral over $\mathcal{G}$ and Σ is dominated by the spatially homogeneous and time-independent saddle points of the Keldysh action. Because of the symmetries of the Keldysh action discussed in the previous section, there is, in fact, a manifold of saddle points. To establish the manifold, it is sufficient to find one particular saddle point. The full manifold is then obtained by applying all rotations that are symmetries of the action to the particular saddle point.

We consider first the variation of the action with respect to Σ, which yields the saddle-point equation

$$\mathcal{G} = \int_{-\pi}^{\pi}\frac{dq}{2\pi}\int_{-\infty}^{\infty}\frac{d\omega}{2\pi}\frac{1}{\omega - \xi_q + i\Sigma}, \tag{75}$$

where $\xi_q = -2J\cos(q)$ is the dispersion relation of Hamiltonian (2). We omit a contribution to the saddle point of $\mathcal{G}$ that contains A. Since $\Sigma \sim \gamma$ at the saddle point, as shown below, such a contribution would lead to terms of second order in γ when we insert $\mathcal{G}$ into action (67). In accordance with Eq. (55), the integration over frequencies in Eq. (75) has to be regularized by introducing a factor $(e^{i\omega t} + e^{-i\omega t})/2$, where the limit $t \to 0^+$ is taken after the integration. By writing $\Sigma = \mathcal{V}\lambda\mathcal{V}^{-1}$, where λ is a diagonal matrix, we thus find that [42]

$$\mathcal{G} = -iQ/2, \qquad Q = \mathrm{sgn}[\mathrm{Re}(\Sigma)] = \mathcal{V}\,\mathrm{sgn}[\mathrm{Re}(\lambda)]\mathcal{V}^{-1}. \tag{76}$$

Note that matrix Q obeys the nonlinear constraint $Q^2 = 1$.

To simplify the analysis of the saddle-point equation that follows from the variation of the action with respect to $\mathcal{G}$, we use the fact that—as explained above—to establish the full manifold of saddle points, it is sufficient to find one particular saddle point. We thus focus on replica-symmetric saddle points, $Q = Q_0 \otimes 1_R$. Equation (55) suggests that a particular solution of the saddle-point equation for $\mathcal{G}$ is given by the symmetrized equal-time limit of Green's function, which, as discussed in Appendix D, is fully determined by fermionic anticommutation relations and the distribution function $\langle\hat{n}_l\rangle_{\mathrm{ss}} = n$ in the steady state. This particular solution is obtained from Eq. (76) by setting

$\Sigma \propto \Lambda$, leading to $Q_0 = \Lambda$, where

$$\Lambda = \begin{pmatrix} 1 & 2(1-2n) \\ 0 & -1 \end{pmatrix}. \tag{77}$$

For $n = 1/2$, we thus find that $\Lambda = \sigma_z$ for fermion counting. The variation of the action with respect to $\mathcal{G}$ can be obtained conveniently by inserting $\mathcal{G} = -\mathrm{i}(Q_0 + \delta Q_\mathcal{G})/2$ into the measurement Lagrangian and performing an expansion in $\delta Q_\mathcal{G}$, as detailed in Appendix F. Accounting for the symmetries of the Keldysh action discussed in Sec. V E, we then obtain the manifold of saddle points for fermion counting:

$$\Sigma = \gamma Q/2^{R-1}, \qquad Q = \mathcal{R}_\Phi \sigma_z \mathcal{R}_\Phi^{-1}. \tag{78}$$

The symmetry transformations $\mathcal{R}_\zeta$ and $\mathcal{R}_{\bar{\Phi}}$ do not rotate the saddle point, and therefore do not further enlarge the saddle-point manifold. Note that the relation between Σ and Q is consistent with the definition of Q in Eq. (76). For occupation measurements, we find that

$$\Sigma = \gamma Q/(2n), \qquad Q = \mathcal{R}_\Phi \mathcal{R}_\phi \Lambda \mathcal{R}_\phi^{-1} \mathcal{R}_\Phi^{-1}. \tag{79}$$

Here and in the following, we set $\mathrm{tr}_R(\Phi) = 0$ for both fermion counting and occupation measurements. Therefore, to account for all relevant symmetries, we have to include the factor $\mathcal{R}_\phi$ in Eq. (79). Furthermore, we omit a shift of the saddle point that vanishes in the replica limit $R \to 1$ and is given explicitly in Appendix F.

Each particular saddle point in the manifold spontaneously breaks the symmetries of the Keldysh action under $\mathcal{R}_\Phi$ and, for occupation measurements, also $\mathcal{R}_\phi$. This gives rise to Goldstone modes. The Goldstone mode associated with $\mathcal{R}_\phi$ leads to the slow algebraic decay of the unconditional density autocorrelation function for occupation measurements, Eq. (22). In contrast, for fermion counting, there are no Goldstone modes in the replica limit $R \to 1$ that describes the unconditional dynamics—by definition, the traceless $R \times R$ matrix Φ reduces to $\Phi = 0$ in this case. The absence of Goldstone modes is reflected in the exponential decay of the autocorrelation function in Eq. (23). However, as we discuss below, the Goldstone mode associated with $\mathcal{R}_\Phi$ is described by the same long-wavelength effective theory for both fermion counting and occupation measurements, leading to almost identical correlations and entanglement properties in the steady state.

VI. GAUSSIAN THEORY

Having identified the saddle-point manifold, first important insights can be obtained from considering quadratic fluctuations of $\mathcal{G}$ and Σ around a particular saddle point. A convenient expansion point is given by $Q = \Lambda$, where $n = 1/2$ such that $\Lambda = \sigma_z$ for fermion counting. Expanding the action in fluctuations to quadratic order leads to a Gaussian functional integral, which can be evaluated explicitly to obtain expressions for correlation functions and the entanglement entropy [106]. The Gaussian approximation, which we detail in the following, is controlled for $\gamma \ll J$ and valid up to intermediate length scales. On larger scales, strong fluctuations of Goldstone modes invalidate the expansion to quadratic order. These fluctuations are described by an NLSM, which we discuss in the next section, Sec. VII.

A. Expansion in fluctuations

Arbitrary fluctuations around the saddle point $Q = \Lambda$ can be parametrized as

$$\mathcal{G} = -\mathrm{i}(\Lambda + \delta Q_\mathcal{G})/2, \qquad \Sigma = \gamma(\Lambda + \delta Q_\Sigma)/(2n), \tag{80}$$

with Hermitian $2R \times 2R$ matrices $\delta Q_\mathcal{G}$ and δQ_Σ. For simplicity, we set $R = 1$ in all numerical factors. Then, the expansion point for Σ lies within the manifold for both fermion counting, Eq. (78), and occupation measurements, Eq. (79), when we set $n = 1/2$ for fermion counting. As detailed in Appendix F, the Keldysh action vanishes to zeroth order in fluctuations, and there are no contributions to first order for an expansion around a saddle point. At second order, we find that

$$S^{(2)} = S_0^{(2)} + \gamma \int \mathrm{d}^2\mathbf{x}\, \mathcal{L}_M^{(2)}, \tag{81}$$

where [42]

$$\begin{aligned} \mathrm{i}S_0^{(2)} = {} & \frac{1}{(4\tau_0)^2} \int \mathrm{d}^2\mathbf{x}\, \mathrm{d}^2\mathbf{x}'\, \mathcal{B}_{l-l'}(t-t') \\ & \times \mathrm{tr}[\delta Q_{\Sigma,l}(t)(1+\Lambda)\delta Q_{\Sigma,l'}(t')(1-\Lambda)] \\ & - \frac{1}{4\tau_0} \int \mathrm{d}^2\mathbf{x}\, \mathrm{tr}[\delta Q_{\Sigma,l}(t)\delta Q_{\mathcal{G},l}(t)] \end{aligned} \tag{82}$$

with the mean free time $\tau_0 = n/\gamma$ and the block of the diffusion ladder $\mathcal{B}_{l-l'}(t-t')$, which, in momentum and frequency space, reads

$$\mathcal{B}_q(\omega) = \{(\mathrm{i}\omega - 1/\tau_0)^2 + [4J\sin(q/2)]^2\}^{-1/2}. \tag{83}$$

The expansion of the measurement Lagrangian is carried out in Appendix F. There are in general two contributions,

$$\mathcal{L}_M^{(2)} = \mathcal{L}_M^{(2,1)} + \mathcal{L}_M^{(2,2)}. \tag{84}$$

For fermion counting, the first contribution contains the trace of a square and the second contribution the square

of a trace:

$$\begin{aligned} \mathrm{i}\gamma\mathcal{L}_M^{(2,1)} &= -\frac{1}{16\tau_0}\,\mathrm{tr}[(\sigma_z\delta Q_{\mathcal{G}})^2 - (\sigma_y\delta Q_{\mathcal{G}})^2], \\ \mathrm{i}\gamma\mathcal{L}_M^{(2,2)} &= \frac{1}{16\tau_0}[\mathrm{tr}(\sigma_z\delta Q_{\mathcal{G}})^2 - \mathrm{tr}(\sigma_y\delta Q_{\mathcal{G}})^2]. \end{aligned} \tag{85}$$

Similarly, for generalized occupation measurements, we find that

$$\begin{aligned} \mathrm{i}\gamma\mathcal{L}_M^{(2,1)} &= -\frac{1}{32n\tau_0}\,\mathrm{tr}\{[(\Lambda-\sigma_x)\delta Q_{\mathcal{G}}]^2\}, \\ \mathrm{i}\gamma\mathcal{L}_M^{(2,2)} &= \frac{1}{32n\tau_0}\,\mathrm{tr}[(\Lambda-\sigma_x)\delta Q_{\mathcal{G}}]^2. \end{aligned} \tag{86}$$

At this point, it is useful to decompose the fluctuation matrices into longitudinal or replica-symmetric and transversal or replicon modes according to

$$\delta Q = \delta Q^{\parallel}\otimes 1_R + \delta Q^{\perp}, \tag{87}$$

where, by construction, $\delta Q^{\parallel} = (1/R)\,\mathrm{tr}_R(\delta Q)$ and $\delta Q^{\perp} = \delta Q - \delta Q^{\parallel}\otimes 1_R$. These modes are orthogonal,

$$\mathrm{tr}_R[(\delta Q^{\parallel}\otimes 1_R)\delta Q^{\perp}] = 0, \tag{88}$$

and, therefore, the theory splits into two sectors, $Z_R = Z_R^{\parallel}Z_R^{\perp}$. The replica-symmetric and replicon sectors respectively describe unconditional and conditional correlation functions.

B. Density correlations

We consider two types of connected density correlation function: the unconditional dynamics is described by

$$C_{0,l,l'}(t,t') = \tfrac{1}{2}\overline{\langle\{\hat{n}_l(t),\hat{n}_{l'}(t')\}\rangle} - \overline{\langle\hat{n}_l(t)\rangle}\;\overline{\langle\hat{n}_{l'}(t')\rangle}, \tag{89}$$

which reduces to Eq. (19) for $l = l'$, and equal-time correlations under conditional dynamics are captured by

$$C_{l,l'}(t) = \tfrac{1}{2}\overline{\langle\{\hat{n}_l(t),\hat{n}_{l'}(t)\}\rangle} - \overline{\langle\hat{n}_l(t)\rangle\langle\hat{n}_{l'}(t)\rangle}. \tag{90}$$

A unified description of both types of correlation function can be obtained in replica Keldysh field theory by considering

$$C_{r,r',l,l'}(t,t') = \langle\delta\rho_{r,l}(t)\delta\rho_{r',l'}(t')\rangle, \tag{91}$$

where r and r' are replica indices and the density fluctuations are related to the fluctuation matrix $\delta Q_{\mathcal{G}}$ by [42]

$$\delta\rho_{r,l}(t) = -\tfrac{1}{4}\,\mathrm{tr}_K[\sigma_x\delta Q_{\mathcal{G},r,r,l}(t)]. \tag{92}$$

In particular, replica-diagonal and replica-off-diagonal components determine the unconditional and conditional density correlation functions as

$$C_{0,l,l'}(t,t') = C_{r,r,l,l'}(t,t'), \tag{93}$$

$$C_{l,l'}(t) = C_{r,r,l,l'}(t,t) - C_{r,r',l,l'}(t,t). \tag{94}$$

Because of the symmetry under permutations of replicas, the result does not depend on the choice of $r \neq r'$. It is worthwhile to recall that the formalism is constructed to enable the computation of conditional averages as in Eqs. (27) and (90) at equal times. While Eq. (91) can be evaluated at arbitrary times t and t', only $t = t'$ has a clear physical meaning for $r \neq r'$.

The correlation function (91) can be evaluated by introducing sources that couple to density fluctuations, that is, by adding to the action a contribution

$$\mathrm{i}S_\xi = \mathrm{i}\int \mathrm{d}^2\mathbf{x}\sum_{r=1}^{R}\xi_{r,l}(t)\delta\rho_{r,l}(t), \tag{95}$$

and taking derivatives with respect to the sources after performing the Gaussian integral over $\delta Q_{\mathcal{G}}$ and δQ_Σ. To that end, an explicit parametrization of the Hermitian matrices $\delta Q_{\mathcal{G}}$ and δQ_Σ has to be chosen. It is convenient to expand the fluctuation matrices in a basis of Pauli matrices in Keldysh space. Replica-symmetric fluctuations $\delta Q^{\parallel}$ are fully determined by the scalar coefficients in this expansion. For replicon modes $\delta Q^{\perp}$, the coefficients themselves are traceless Hermitian $R\times R$ matrices, which can be parametrized by decomposing them into their real and imaginary parts, taking into account the restrictions imposed by tracelessness and Hermiticity.

We consider correlations in the steady state, which are invariant under translations in both space and time, such that $C_{0,l,l'}(t,t') = C_{0,l-l'}(t-t')$, whereas $C_{l,l'}(t) = C_{l-l'}$ becomes independent of t. For fermion counting, we then find the unconditional correlation function

$$C_{0,l}(t) = \tfrac{1}{4}\mathrm{e}^{-|t|/\tau_0}J_l(2J\,|t|)^2, \tag{96}$$

which reduces to Eq. (23) for $l = 0$. By taking the derivative with respect to time of Eq. (89) and using the explicit representation of two-time averages in Eq. (20), it is straightforward to check that this is, in fact, the exact result [82,83].

For generalized occupation measurements, we obtain

$$C_{0,l}(t) \sim n(1-n)\frac{\mathrm{e}^{-l^2/(4\nu|t|)}}{\sqrt{4\pi\,\nu\,|t|}} \tag{97}$$

with $\nu = 2nJ^2/\gamma$. This result is valid in the limit of large distances $l \gg l_0$, where the mean free path is given by

$$l_0 = \sqrt{2}Jn/\gamma, \tag{98}$$

or at long times $t \gg \tau_0$. Equation (97) agrees with the corresponding result for random projective measurements obtained in Ref. [42] when we set $n = 1/2$ in the expression for v but not in the prefactor of the correlation function. For $l = 0$ and $n = 1/2$, we recover Eq. (22). From the structure of the measurement-induced interaction vertices, it follows that the asymptotic behavior described by Eq. (97) obtained in the Gaussian approximation is actually exact [42].

In contrast to the completely different unconditional correlation functions, Eqs. (96) and (97), we find the conditional density correlation function in the steady state and for $n = 1/2$ to be identical for fermion counting and both generalized and projective measurements of occupation numbers [42]. This will be justified further in Sec. VII below where, instead of considering arbitrary Gaussian fluctuations as in Eq. (80), we focus on fluctuations of massless Goldstone modes, which obey the same long-wavelength effective theory in all three models.

To calculate the conditional correlation function, one has to take the boundary condition induced by stopping the measurement process at a finite time t into account [42]. For projective measurements of occupation numbers, this leads to the correlation function in momentum space, C_q, being expressed in terms of the solution of an integral equation that depends on a single parameter, $u = 2l_0 \sin(q/2)$. However, one obtains approximately the same result for the correlation function by omitting the boundary condition and instead rescaling u by a factor of 2, which yields [42]

$$C_q \approx n(1-n)\tilde{c}(ql_0), \tag{99}$$

where

$$\tilde{c}(u) = \frac{2}{\pi}\int_0^\infty \mathrm{d}v\, \frac{\mathrm{Re}[b(2u,v)] - |b(2u,v)|^2}{1 - \mathrm{Re}[b(2u,v)]} \tag{100}$$

and

$$b(u,v) = [(1-\mathrm{i}v)^2 + 2u^2]^{-1/2}. \tag{101}$$

For $n = 1/2$, we also find the same expressions for fermion counting and for generalized occupation measurements; for generalized occupation measurements with $n \neq 1/2$, Eq. (100) is modified, with $f = 1 - 2n$, as

$$\tilde{c}(u) = \frac{4n}{\pi}\int_0^\infty \mathrm{d}v\, \frac{2n\,\mathrm{Re}[b(2u,v)] - |b(2u,v)|^2}{4n^2\{1 - \mathrm{Re}[b(2u,v)]\} - f\ |b(2u,v)|^2}. \tag{102}$$

According to Eq. (99), l_0 is the only length scale that determines the behavior of spatial correlations. Taking the inverse Fourier transform of Eq. (99), one finds algebraic decay on scales $l \gg l_0$ [42],

$$C_l \sim -n(1-n)\frac{2l_0}{\pi l^2}. \tag{103}$$

From the conditional density correlation function, the second cumulant (26) of the subsystem number of particles follows as

$$C_A^{(2)} = \sum_{l,l' \in A} C_{l-l'}, \tag{104}$$

which allows us to calculate the entanglement entropy to leading order in the cumulant expansion (25). The algebraic decay of C_l, Eq. (103), leads to logarithmic growth of the entanglement entropy of a subsystem of length ℓ [42],

$$S_\ell \sim \frac{4\pi}{3} n(1-n) l_0 \ln(\ell/l_0). \tag{105}$$

Algebraic decay of spatial correlations and logarithmic growth of the entanglement entropy are characteristic for a critical phase with conformal invariance [29]. However, strong fluctuations of Goldstone modes that are not captured by the Gaussian approximation lead to a substantial renormalization of the effective measurement rate, which invalidates the Gaussian approximation at large scales. To treat this effect properly, we now turn to an NLSM for fluctuations of Goldstone modes within the saddle-point manifold.

VII. EFFECTIVE FIELD THEORY IN THE RARE-MEASUREMENT LIMIT

Going beyond the Gaussian approximation, we generalize Eq. (80) to incorporate nonlinear fluctuations around the saddle point Λ [42]:

$$\mathcal{G} = -\mathrm{i}Q/2, \qquad \Sigma = \gamma Q/(2n), \qquad Q = \mathcal{R}\Lambda\mathcal{R}^{-1}, \tag{106}$$

again with the understanding that $n = 1/2$ and thus $\Lambda = \sigma_z$ for fermion counting. There is a subgroup $\mathrm{U}(R) \times \mathrm{U}(R)$ of rotations $\mathcal{R}$ that leave the saddle point Λ invariant. Therefore, nontrivial rotations of the saddle point form the symmetric space $\mathrm{U}(2R)/\mathrm{U}(R) \times \mathrm{U}(R)$. We parametrize these rotations as

$$Q = \mathcal{R}_\Phi \mathcal{R}_\Theta Q_0 \mathcal{R}_\Theta^{-1}\mathcal{R}_\Phi^{-1} \tag{107}$$

with

$$\mathcal{R}_\Phi = \mathrm{e}^{\mathrm{i}\Phi\sigma_x/2}, \qquad \mathcal{R}_\Theta = \mathrm{e}^{\mathrm{i}\Theta\sigma_y/2}, \tag{108}$$

where Φ and Θ are traceless Hermitian matrices in replica space. Furthermore,

$$Q_0 = \mathcal{R}_\phi \mathcal{R}_\theta \Lambda \mathcal{R}_\theta^{-1} \mathcal{R}_\phi^{-1}, \tag{109}$$

where $\mathcal{R}_\phi$ and $\mathcal{R}_\theta$ describe replica-symmetric rotations by the angles ϕ and θ,

$$\mathcal{R}_\phi = \mathrm{e}^{\mathrm{i}\phi\sigma_x/2}, \qquad \mathcal{R}_\theta = \mathrm{e}^{\mathrm{i}\theta\sigma_y/2}. \tag{110}$$

This parametrization is chosen such that the symmetries of the action, identified in Sec. V E, appear explicitly as factors in the rotations $\mathcal{R}$. In particular, for fermion counting, the only symmetry is given by $\mathcal{R}_\Phi$, whereas for occupation measurements, $\mathcal{R}_\phi$ is also a symmetry. Considering now matrices Φ and Θ and angles ϕ and θ that vary slowly in space and time, an effective long-wavelength field theory, given by an NLSM for the massless Goldstone modes associated with the broken symmetries of the action, is obtained by integrating out massive modes in the Gaussian approximation. Technical details of this procedure are presented in Appendix G.

A. Replica-symmetric sector

We first consider the replica-symmetric sector of the theory, where we can set $R = 1$ and which describes fluctuations of the modes ϕ and θ. For fermion counting, both modes are massive and an expansion to second order yields the Lagrangian

$$\mathrm{i}\mathcal{L}[Q_0] = -\frac{\mathrm{i}}{2}\theta\partial_t\phi - \frac{\nu}{4}[(\partial_x\phi)^2 + (\partial_x\theta)^2] - \frac{\gamma}{2}(\theta^2 + \phi^2). \tag{111}$$

To describe long-wavelength fluctuations, we have taken a spatial continuum limit, in which the lattice site index l is replaced by a continuous position variable x, and we have performed an expansion in spatial and temporal derivatives as detailed in Appendix G. As an artifact of the gradient expansion, the diffusion coefficient $\nu = J^2/\gamma$, which does not occur in the exact correlation function, Eq. (96), appears in Eq. (111).

For occupation measurements, ϕ is massless, but we can still expand the Lagrangian in θ. We obtain

$$\begin{aligned}\mathrm{i}\mathcal{L}[Q_0] = &-\frac{\mathrm{i}}{4}(2 + f\,\theta)\theta\partial_t\phi \\ &- \frac{\nu}{4}\{[1 - f^2 + 2f\,\theta - (1 - f^2)\theta^2](\partial_x\phi)^2 \\ &- \mathrm{i}2f\,(f\, - \theta)(\partial_x\phi)(\partial_x\theta) + (1 + f^2)(\partial_x\theta)^2\}\end{aligned} \tag{112}$$

with $f\, = 1 - 2n$. Recall that we have expanded the action to first order in γ, both in Eq. (67) and in the regularization described in Appendix D. At this order of approximation, the expected mass term of for θ does not occur in Eq. (112).

B. Replicon sector

We now turn to the replicon sector. For both fermion counting and occupation measurements, the traceless Hermitian matrices Φ are Goldstone modes. These modes parametrize the group SU(R) as $U = \mathrm{e}^{\mathrm{i}\Phi}$. Integration over the massive modes Θ yields an NLSM with Lagrangian given by

$$\mathrm{i}\mathcal{L}[\Phi] = -\frac{g[Q_0]}{2}\,\mathrm{tr}_R\left(\frac{1}{v[Q_0]}\partial_t U^\dagger \partial_t U + v[Q_0]\partial_x U^\dagger \partial_x U\right). \tag{113}$$

For fermion counting and occupation measurements, the velocity $v[Q_0]$ and coupling constant $g[Q_0]$ are respectively

$$\begin{aligned} v[Q_0] &= (2l_0/\tau_0)\sqrt{\rho_0(1-\rho_0)}, \quad & g[Q_0] &= l_0\sqrt{\rho_0(1-\rho_0)}, \\ v[Q_0] &= (l_0/\tau_0)\sqrt{2(1-\rho_0)}, & g[Q_0] &= l_0\rho_0\sqrt{2(1-\rho_0)}. \end{aligned} \tag{114}$$

A coupling between the replica-symmetric and replicon sectors of the theory is established through the dependence of these quantities on

$$\rho_0 = \tfrac{1}{4}\,\mathrm{tr}_K(1 - Q_0\sigma_x). \tag{115}$$

However, to leading order in $\gamma \ll J$, we can neglect fluctuations in the replica-symmetric sector and set $Q_0 = \Lambda$ such that $\rho_0 = n$. This leads to

$$v_0 = v[\Lambda] = \frac{l_0}{\tau_0}\sqrt{2(1-n)}, \quad g_0 = g[\Lambda] = l_0 n\sqrt{2(1-n)}, \tag{116}$$

where $n = 1/2$ for fermion counting. Indeed, for $n = 1/2$, the velocity v_0 and the coupling constant g_0 and, therefore, the NLSM Lagrangian in Eq. (113), are identical to the corresponding expressions for projective measurements of occupation numbers [42]. Therefore, we can expect the same quantitative behavior of correlations and entanglement in the conditional dynamics for all three types of measurements: fermion counting and random generalized as well as projective measurements of occupation numbers.

As indicated at the beginning of Sec. V, so far, we have not taken the PHS of Hamiltonian (2) into account. PHS does not affect the theory on the Gaussian level. However, PHS does modify the target manifold of the NLSM. The target manifold can be determined even without constructing the NLSM explicitly. Key steps of this analysis are summarized in Appendix H. Focusing on the replicon sector of the theory, we find that the target manifold of the NLSM for a Hamiltonian with PHS is SU($2R$)/Sp(R). This applies to fermion counting as well as for generalized

occupation measurements, and is in agreement with other models with a conserved number of particles [52,54]. Crucially, the SU($2R$)/Sp(R) and SU(R) NLSMs for Hamiltonians with and without PHS, respectively, lead to the same qualitative behavior of entanglement and correlations on large scales. This behavior is determined by the RG flow of the coupling constant g_0. To one-loop order, the RG flow is given by [54,113–115]

$$g = g_0 - \frac{1}{4\pi\beta}\ln(l/l_0), \tag{117}$$

where $\beta = 1/2$ and $\beta = 1$ for intact and broken PHSs, respectively. In both cases, and for any value of the bare coupling g_0, the flow reaches the strong-coupling regime $g \lesssim 1$ at the exponentially large scale

$$l_* = l_0 \mathrm{e}^{4\pi\beta g_0}, \tag{118}$$

indicating that a frequent-measurement phase with area-law entanglement is established in the thermodynamic limit. Note that the RG flow is qualitatively different in spatial dimensions $d > 1$. In this case, there is a critical point at a finite value of g, separating an area-law phase with the entanglement entropy S_ℓ scaling with the subsystem sizes ℓ as $S_\ell \sim \ell^{d-1}$, from a phase with $S_\ell \sim \ell^{d-1}\ln(\ell)$ [43,48].

Numerically observing emergent area-law behavior due to the renormalization of g on exponentially large scales is challenging. However, as we show in the following, the renormalization of g leaves clear fingerprints on much shorter scales.

VIII. CORRELATIONS AND ENTANGLEMENT IN THE STEADY STATE

We now compare analytical predictions from replica Keldysh field theory to numerical results obtained from the quantum jump algorithm outlined in Sec. III A. In contrast to Sec. IV, where we studied time-dependent correlations, here we focus on equal-time correlations and entanglement in the steady state. Studying carefully the crossover to area-law entanglement on large scales, we reconcile numerical observations of algebraic correlations, logarithmic growth of the entanglement entropy, and the conformal invariance characteristic of a critical phase [29], with the absence of a measurement-induced phase transition in the thermodynamic limit. Crucially, clear numerical signatures of the absence of a critical phase in the thermodynamic limit are visible on length scales much shorter than the exponentially large scale l_* in Eq. (118), and these signatures can be readily explained by the theory introduced above. We first investigate algebraic scaling of the connected density correlation function, then focus on the entanglement entropy and the effective central charge, and finally we study the bipartite and tripartite mutual information.

A. Connected density correlation function

In the steady state, the conditional density correlation function (90) becomes time independent and translationally invariant, $C_{l,l'}(t) = C_{l-l'}$. Using Wick's theorem, the density correlation function can be expressed in terms of the single-particle density matrix D defined in Eq. (13):

$$C_{l-l'} = \overline{\langle \hat{n}_l \hat{n}_{l'} \rangle} - \overline{\langle \hat{n}_l \rangle \langle \hat{n}_{l'} \rangle} = \frac{\delta_{l,l'}}{2} - \overline{\left| D_{l,l'} \right|^2}. \tag{119}$$

As explained in Sec. III A, the quantum jump algorithm gives direct access to the single-particle density matrix. Here and in the following, we set $\overline{\langle \hat{n}_l \rangle} = n = 1/2$, as in our numerical studies. Furthermore, for all numerical results, the overbar indicates averaging over both trajectories and position.

1. Analytical predictions

As explained in Sec. VI B, on the Gaussian level the connected density correlation is identical for fermion counting and random generalized as well as projective measurements of occupation numbers. In momentum space, it is given by Eq. (99). To incorporate the renormalization of $l_0 = 2g_0$, we expand the Gaussian result for low momenta and replace g_0 by its renormalized value g, Eq. (117), where we identify $l = 1/q$ with the external momentum of the correlation function that cuts off the RG flow in the infrared [42]. We thus obtain the rescaled correlation function

$$\frac{C_q}{g_0 q} \approx 1 - 2ql_0 + \frac{1}{4\pi\beta g_0}\ln(ql_0). \tag{120}$$

For $q \to 0$, the logarithmic renormalization dominates, pushing $C_q/(g_0 q)$ to small values, while $C_q/(g_0 q) \to 1$ for $q \to 0$ in Gaussian theory. The momentum scale at which the logarithm starts to dominate marks the beginning of the crossover from Gaussian behavior—with algebraic correlations, Eq. (103), and logarithmic growth of the entanglement entropy, Eq. (105)—to the emergent frequent-measurement regime. We identify this crossover scale with the maximum of the rescaled correlation function at $q_c = (4\pi\beta l_0^2)^{-1} \sim \gamma^2$. Associated with this momentum scale is a crossover length scale $l_c \sim \gamma^{-2}$. Importantly, the crossover scale l_c is only algebraically large in γ and, therefore, numerically accessible.

2. Numerics

Figure 4 shows the density correlation function (119) as a function of the chord length $\tilde{\ell} = (L/\pi)\sin(\pi\ell/L)$, which accounts for the finite system size and periodic boundary conditions, for both fermion counting (solid lines) and generalized occupation measurements (dashed lines). The quantitative agreement between both models despite their

fundamentally different dynamics is remarkable. For comparison, we show the Gaussian result, obtained by numerically taking the inverse Fourier transform of Eq. (99) (black dashed line). The Gaussian result transitions from slow decay at short distances $\tilde{l} \ll l_0$ to algebraic scaling $C_l \sim \tilde{l}^{-2}$ on large scales $\tilde{l} \gg l_0$. For small values of γ, the numerical data follow the Gaussian result up to intermediate scales. However, in accord with the renormalized correlation function (120), the decay of the correlation function visibly becomes faster than algebraic beyond a crossover scale l_c. To quantify the deviation from the Gaussian prediction, we define l_c as the scale beyond which the numerical data deviate from a line $\sim \tilde{l}^{-2}$, put tangentially to the data, by more than 10%. As shown in the inset of Fig. 4, the crossover scale exhibits the scaling $l_c \sim \gamma^{-2}$, confirming our expectation based on replica Keldysh field theory. The critical range of algebraic behavior of spatial correlations is thus bounded from below by l_0 and from above by l_c, as sketched in Fig. 2(c).

B. Entanglement entropy

We now turn to the von Neumann entanglement entropy S_ℓ, Eq. (24), of a subsystem A consisting of ℓ contiguous lattice sites. The RG flow of the NLSM indicates that area-law scaling of the entanglement entropy is established beyond the exponentially large scale l_* in Eq. (118). However, logarithmic growth of S_ℓ as characteristic for a 1D conformal field theory with central charge c [79,116],

$$S_\ell \sim \frac{c}{3} \ln(\ell), \tag{121}$$

can be observed within the critical range $\ell \in [l_0, l_c]$.

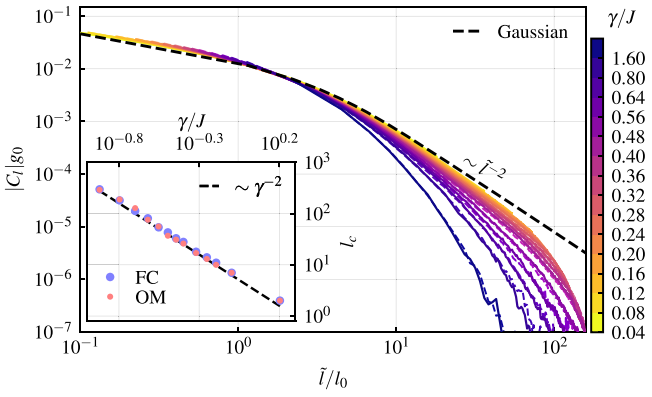


FIG. 4. Rescaled density correlation function for fermion counting (solid lines) and generalized occupation measurements (colored dashed lines) for various monitoring rates γ. For $\gamma \ll J$, the data approach the prediction from the Gaussian theory (black dashed line) with an algebraic scaling $\sim \tilde{l}^{-2}$ for $\tilde{l}/l_0 \gg 1$. Inset: upper boundary of the critical range l_c for fermion counting (FC; blue circles) and occupation measurements (OMs; red circles), agreeing well with the analytical prediction $l_c \sim \gamma^{-2}$ (black dashed line). The system size is $L = 1000$ and data are averaged over $N_{\text{traj}} = 160$ trajectories for this and all subsequent figures.

1. Analytical predictions

Gaussian theory predicts logarithmic growth of the entanglement entropy (105), with a central charge given by $2\pi g_0$. To quantify the agreement of our numerical results with this prediction, we find it useful to introduce an effective scale-dependent central charge c_ℓ. Equation (121) suggests defining c_ℓ as the derivative of S_ℓ with respect to $\ln(\ell)$. However, since ℓ is an integer, we define c_ℓ as the discrete difference,

$$c_\ell = 3\frac{S_{\ell'} - S_\ell}{\ln(\ell'/\ell)}, \tag{122}$$

where ℓ' should be chosen such that $\ell'/\ell = \mathrm{e}^\epsilon$ with $\epsilon \ll 1$. For logarithmic growth of the entanglement entropy as in Eq. (121), this definition yields $c_\ell = c$; volume-law scaling results in $c_\ell \sim \ell$, while area-law behavior leads to $c_\ell = 0$.

To obtain an analytical prediction for c_ℓ, we extend the Gaussian result (105) by including higher orders in an asymptotic expansion in $\ell \gg l_0 \gg 1$ and incorporating the renormalization of g_0, Eq. (117). This can be achieved by expressing the entanglement entropy S_ℓ using the cumulant expansion, Eq. (104), and Eq. (25) as

$$S_\ell = \frac{2\pi}{3}\int_0^\infty \frac{\mathrm{d}q}{q^2} C_q[1 - \cos(q\ell)] \tag{123}$$

and expanding the Gaussian result for C_q, Eq. (99), to third order in ql_0. We thus obtain

$$\frac{S_\ell}{2\pi g_0/3} \sim \ln\left(\frac{\ell}{l_0}\right) + s_0 + \frac{7l_0^2}{\ell^2} - \frac{1}{8\pi\beta g_0}\ln\left(\frac{\ell}{l_0}\right)^2, \tag{124}$$

where s_0 is a constant that does not depend on ℓ. The first three terms on the right-hand side describe the asymptotic behavior of S_ℓ predicted by Gaussian theory, with the leading contribution reproducing the CFT form (121) with a central charge $c = 2\pi g_0$. Renormalization effects are contained in the last term. The effective central charge, Eq. (122), is then

$$\frac{c_\ell}{2\pi g_0} \sim 1 - \frac{14l_0^2}{\ell^2} - \frac{1}{4\pi\beta g_0}\ln\left(\frac{\ell}{l_0}\right). \tag{125}$$

As explained above, $c_\ell \to 2\pi g_0$ for $\ell \gg l_0$ would correspond to logarithmic growth of the entanglement entropy. However, the last term in Eq. (125), which is due to the

renormalization of g_0, causes the value of c_ℓ to decrease with ℓ. Consequently, c_ℓ is never constant, but only takes a maximum at

$$\ell_{\max,c} \sim 2\sqrt{14\pi\beta} l_0^{3/2}. \tag{126}$$

The scaling $\ell_{\max,c} \sim l_0^{3/2} \sim \gamma^{-3/2}$ implies that the maximum of the effective central charge $c_{\max}$ is within the critical range, which is bounded from below by $l_0 \sim \gamma^{-1}$ and from above by the crossover scale $l_c \sim \gamma^{-2}$. In the vicinity of the maximum, the entanglement entropy again obeys the CFT form (121), but with $c = c_{\max} < 2\pi g_0$ approaching the Gaussian result $c = 2\pi g_0$ only for $\gamma \ll J$. It is worthwhile to reiterate that while Gaussian theory predicts unbounded logarithmic growth of the entanglement entropy on scales $\ell \gtrsim l_0$ and with $c = 2\pi g_0$, the renormalization of g_0 results in the range of logarithmic growth being restricted to $\ell \lesssim l_c$, and with a reduced value of the effective central charge $c_{\max} < 2\pi g_0$.

2. Numerics

To confirm these predictions, we have determined the entanglement entropy and effective central charge numerically. For a subsystem A of size ℓ, the entanglement entropy (24) can be obtained from the eigenvalues λ_l of the reduced single-particle density matrix $D_A = (D)_{l,l' \in A}$ as [117]

$$S_\ell = -\sum_{l=1}^{\ell} \overline{[\lambda_l \ln(\lambda_l) + (1-\lambda_l)\ln(1-\lambda_l)]}, \tag{127}$$

where the overbar again denotes an average over both trajectories and position.

Figure 5 shows the entanglement entropy for $\ell \in \{1, \ldots, L/2\}$ for fermion counting (solid lines) and generalized occupation measurements (dashed lines). Qualitatively, these results appear to support the existence of an entanglement transition between a critical phase with logarithmic growth of the entanglement entropy and an area-law phase for larger values of γ. However, an analysis of the effective central charge c_ℓ reveals clear evidence for an area-law phase for all values of γ, as predicted analytically.

To account for the finite system size and periodic boundary conditions imposed in our numerical studies, we rewrite the definition of the effective scale-dependent central charge, Eq. (122), in terms of chord lengths,

$$c_\ell = 3\frac{S_{\ell'} - S_\ell}{\ln(\tilde{\ell}'/\tilde{\ell})}. \tag{128}$$

Ideally, the ratio $\tilde{\ell}'/\tilde{\ell}$ should be close to one and not depend on ℓ. In practice, due to ℓ being an integer, these conditions cannot be met uniformly over the entire range of

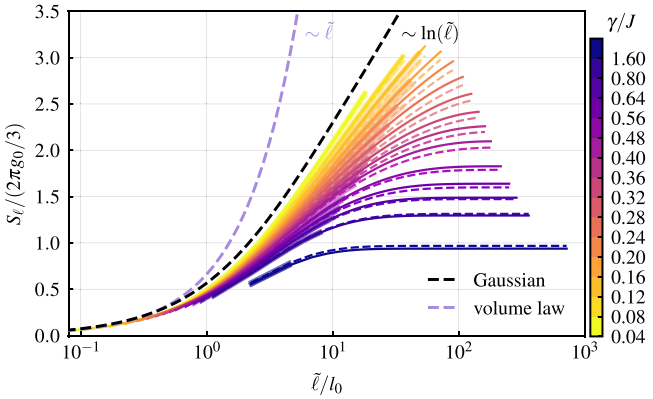


FIG. 5. Rescaled entanglement entropy for fermion counting (solid lines) and generalized occupation measurements (colored dashed lines) for a subsystem of size ℓ of a system with periodic boundary conditions (see the inset). Thicker lines indicate the extent of the critical range $\tilde{\ell} \in [l_0, l_c]$. The critical range is analogously indicated in the figures below. For $\gamma \ll J$, the numerical data approach the Gaussian result obtained by inserting Eq. (99) into Eq. (123) (black dashed line), which grows logarithmically $\sim \ln(\tilde{\ell})$ for $\tilde{\ell} \gg l_0$. Volume-law scaling with $S_\ell \sim \ell$ can be observed at $\tilde{\ell} \lesssim l_0$ (purple dashed line).

values from $\ell = 1$ to $\ell = L/2$. To calculate c_ℓ numerically, we have chosen N_ℓ values ℓ_i with $\ell_1 = 1$ and $\ell_{N_\ell} = L/2$ such that $\tilde{\ell}'/\tilde{\ell} = \tilde{\ell}_{i+1}/\tilde{\ell}_i = \mathrm{e}^{\epsilon_i}$ is approximately constant. For $N_\ell = 66$, we obtain $\epsilon_i < 0.1$ for $i > 10$, ensuring that corrections to the value of c_ℓ obtained in the limit $\epsilon_i \to 0$ are small.

Figure 6 shows the effective central charge for fermion counting (solid lines) and generalized occupation measurements (colored dashed lines). As anticipated in Fig. 2(c), c_ℓ first grows with ℓ, then reaches a maximum $c_{\max}$ at a scale $\ell_{\max,c}$, and eventually starts to decrease, indicating the crossover to the area-law regime. The lower inset shows that the position of the maximum scales as $\ell_{\max,c} \sim \gamma^{-3/2}$, in good agreement with Eq. (126) and within the critical range between $l_0 \sim \gamma^{-1}$ and $l_c \sim \gamma^{-2}$. This finding demonstrates that the logarithmic growth of the entanglement entropy observed in Fig. 5 for small values of γ and for $\ell \to L/2$ is due to l_c becoming larger than $L/2$, and that the apparent transition from a critical phase to an area-law phase at larger γ is, in fact, due to l_c dropping below $L/2$.

Another signature of an apparent KT transition is a discontinuous jump of the central charge at a finite critical value γ_c [29]. As we discuss in Sec. VIII C next, it is the maximum value $c_{\max}$ of c_ℓ that yields best agreement with CFT predictions within the critical range. The dependence of this maximum value on γ is shown in the upper inset in Fig. 6, where we observe good agreement with the prediction obtained by inserting Eq. (126) into Eq. (125). In particular, the maximum value $c_{\max}$ varies smoothly with γ, providing further evidence for the absence of a KT transition at a finite γ_c.

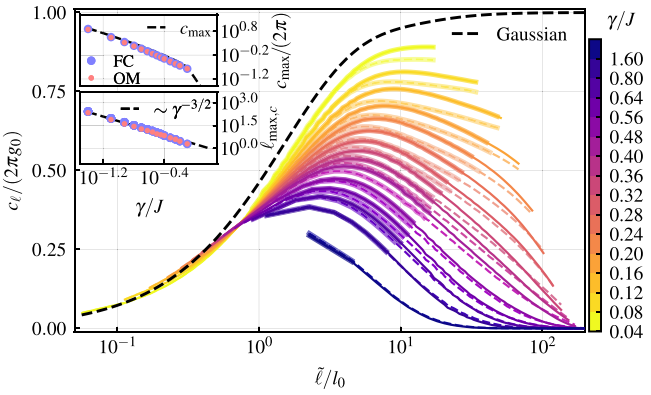


FIG. 6. Rescaled effective central charge calculated by applying Eq. (128) to the data shown in Fig. 5 for fermion counting (solid lines) and generalized occupation measurements (colored dashed lines). For $\gamma \ll J$, the data approach the Gaussian result (black dashed line). Upper inset: scaling of the maximum of the central charge $c_{\max}$ for fermion counting (blue circles) and occupation measurements (red circles) compared to the prediction obtained by inserting Eq. (126) into Eq. (125) (black dashed line). Lower inset: scaling of the position of the maximum $\ell_{\max,c}$ of the central charge. The data agree with the predicted scaling $\sim \gamma^{-3/2}$, Eq. (126).

C. Mutual information and conformal invariance

The scaling of the entanglement entropy (24) with subsystem size is the key property distinguishing different measurement-induced phases. More refined measures of entanglement such as the bi- and tripartite mutual information have proven useful for locating critical points and characterizing critical phases. In particular, these quantities carry signatures of conformal invariance.

The bipartite mutual information of two disjoint subsystems A and C, separated by a third subsystem B, is defined as

$$I_2 = S_A + S_C - S_{A\cup C}, \tag{129}$$

and provides a measure for the correlations between subsystems A and C [118]. In studies of measurement-induced transitions in quantum circuits, for subsystems of sizes $\ell_A = \ell_C = L/8$ and $\ell_B = 3L/8$, the bipartite mutual information has been found to decay exponentially with system size L in both area-law and volume-law phases [3,5]. At the critical point, I_2 exhibits a peak that remains finite in the thermodynamic limit. Likewise, the tripartite mutual information, defined as

$$I_3 = S_A + S_B + S_C + S_{A\cup B\cup C} - S_{A\cup B} - S_{B\cup C} - S_{A\cup C}, \tag{130}$$

remains finite at the critical point [7,9,11]. In the area-law phase, I_3 vanishes, and it has an extensive negative value in the volume-law phase.

Apart from being indicators of measurement-induced phase transitions, the interest in the bi- and tripartite mutual information is due to the existence of analytical predictions for these quantities for 1D CFTs. These predictions are expected to apply at critical points and in critical phases [29]. In CFTs, I_2 and I_3 depend only on the cross ratio [119–121]

$$x = \frac{\ell_A \ell_C}{\ell_{A\cup B}\ell_{B\cup C}} \tag{131}$$

and are given by

$$I_2 = \frac{c}{3}\ln\left(\frac{1}{1-x}\right) + \mathcal{G}(x), \qquad I_3 = \mathcal{G}(x), \tag{132}$$

where c is the central charge of the CFT and $\mathcal{G}(x)$ is a universal function that depends on the full operator content of the theory. For finite systems with periodic boundary conditions, the subsystem sizes ℓ_A, ℓ_C, $\ell_{A\cup B}$, and $\ell_{B\cup C}$ should be replaced by the corresponding chord lengths.

1. Analytical predictions

Proceeding as described in Sec. VIII B for the entanglement entropy, we can obtain analytical predictions for the mutual information (129). For subsystems of sizes $\ell_A = \ell_C = \ell$ and $\ell_B = \ell'$ with $\ell, \ell' \gg l_0 \gg 1$, we find that

$$\frac{I_2}{2\pi g_0/3} \sim \ln\left(\frac{1}{1-x}\right)\left[1 - \frac{\ln(\ell/l_0)}{4\pi\beta g_0}\right] - \frac{14(3-x)x^2 l_0^2}{(1-x)^2\ell^2}. \tag{133}$$

For fixed cross ratio x and considered as a function of ℓ, the bipartite mutual information exhibits a maximum at

$$\ell_{\max,I_2} = 2\sqrt{14\pi\beta(3-x)}\ln\left(\frac{1}{1-x}\right)^{-1/2}\frac{x}{|1-x|}l_0^{3/2}, \tag{134}$$

which scales with the measurement rate as $\ell_{\max,I_2} \sim \gamma^{-3/2}$, in analogy to the position of the maximum of the effective central charge given in Eq. (126).

On the same order of approximation that we have used to obtain predictions for the entanglement entropy and the bipartite mutual information, the tripartite mutual information vanishes. Indeed, generalizing Eq. (104) to $C^{(2)}_{A,B} = \sum_{l\in A, l'\in B} C_{l-l'}$ such that $C^{(2)}_A = C^{(2)}_{A,A}$, and using the fact that the density correlation function (90) is symmetric under the exchange of l and l', we obtain $C^{(2)}_{A\cup B,A\cup B} = C^{(2)}_A + C^{(2)}_B + 2C^{(2)}_{A,B}$ for any two disjoint subsystems A and B. Then, keeping only the contribution from the second cumulant in Eq. (25), we find that $I_3 = 0$, indicating that the leading contribution to the tripartite mutual information comes from the fourth cumulant. However, the

fourth cumulant vanishes in a Gaussian theory. In fact, the numerical results for I_3 presented below show qualitatively different behavior for fermion counting and generalized occupation measurements. Explaining these differences analytically would require going beyond not only Gaussian theory but even the long-wavelength effective field theory developed in Sec. VII, which is identical for both types of measurement.

2. Numerics

Figure 7 shows the bipartite mutual information for $\ell_A = \ell_C = \ell$ and $\ell_B \approx 3\ell$ chosen such that the cross ratio (131) is $x \approx 1/16$ for all values of $\ell \in \{1, \ldots, L/8\}$. The variations of $\ell_B/\ell \approx 3$ result in slight discontinuities in the data. Combining the finite-size phase diagram sketched in Fig. 2(c) with the known behavior of I_2 across measurement-induced phase transitions [3,5], we expect the bipartite mutual information to be finite only within the critical range, and to decay toward zero for both $\tilde{\ell} \ll l_0$ and $\tilde{\ell} \gg l_c$. This expectation is confirmed in Fig. 7, where we find the mutual information to reach a maximum at $\ell_{\max,I_2} \sim \gamma^{-3/2}$, within the critical range and in good agreement with the scaling predicted by Eq. (134). We note that agreement between the numerical results for $\gamma \ll J$ and the results obtained from Gaussian theory is worse for the bipartite mutual information than for the entanglement entropy shown in Fig. 5. As we have confirmed numerically, this discrepancy can be traced back to contributions from cumulants of higher than second order in Eq. (25), which we neglect in the Gaussian results, and which are more important for the mutual information.

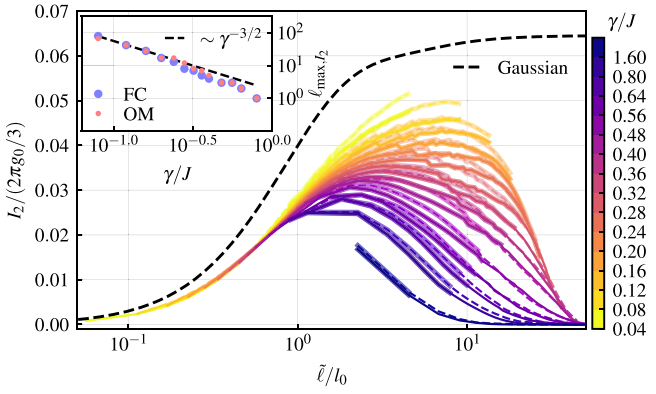


FIG. 7. Rescaled bipartite mutual information for fermion counting (solid lines) and generalized occupation measurements (colored dashed lines) for subsystem sizes $\ell_A = \ell_C = \ell$ and $\ell_B \approx 3\ell$ (see the lower inset) chosen to approximately fix the cross ratio (131) to $x \approx 1/16$, with deviations $< 1\%$. The Gaussian approximation is shown for comparison (black dashed line). Upper inset: scaling of the position of the maximum of the bipartite mutual information $\ell_{\max,I_2}$ for fermion counting (blue circles) and occupation measurements (red circles), approaching the theoretical prediction (134) for $\gamma \ll J$ (black dashed line). The considered subsystems are sketched in the lower left corner for periodic boundary conditions.

The tripartite mutual information is shown in Fig. 8 for the same choice of subsystems as in Fig. 7. On short scales $\tilde{\ell} \lesssim l_0$, the tripartite mutual information behaves as expected in a volume-law phase, growing extensively to negative values for both fermion counting (solid lines) and occupation measurements (dashed lines). The minimum value of I_3 is reached at $\ell_{\min,I_3} \sim \gamma^{-1}$, close to the lower boundary of the critical phase at $l_0 \sim \gamma^{-1}$. Notably, on scales $\tilde{\ell} \gtrsim l_0$ beyond the volume-law regime, the tripartite mutual information shows qualitatively different behavior for fermion counting and generalized occupation measurements. For fermion counting, I_3 remains negative, and approaches $I_3 \to 0$ from below for $\tilde{\ell} \to \infty$, as expected in an area-law phase. In contrast, for generalized occupation measurements, I_3 crosses to positive values and eventually approaches zero from above. These findings confirm that the tripartite mutual information probes behavior that is not captured by the long-wavelength effective field theory developed in Sec. VII, as discussed above.

So far, we have considered the bi- and tripartite mutual information for fixed cross ratio x and as a function of subsystem size ℓ. We now turn to a more stringent test of conformal invariance within the critical range. As we have discussed in Sec. VIII B, on scales $\ell \gtrsim l_0$, Gaussian theory predicts logarithmic growth of the entanglement entropy with a central charge $c = 2\pi g_0$. However, due the renormalization of g_0 induced by strong fluctuations of massless replicon modes, the range of approximately logarithmic growth is actually bounded by $\ell \lesssim l_c$, and the value of the central charge, given by the maximum value $c_{\max}$ of c_ℓ, is reduced as compared to the Gaussian result. These insights

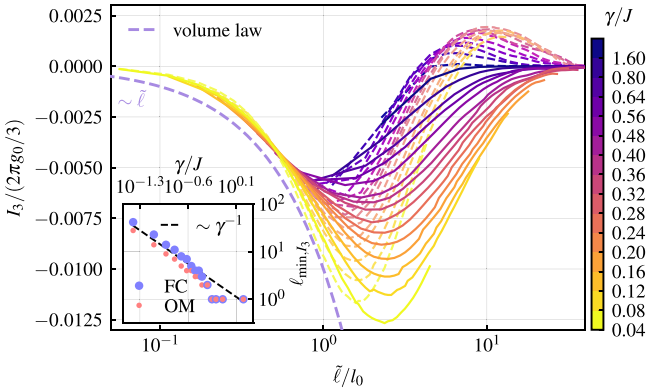


FIG. 8. Rescaled tripartite mutual information for fermion counting (solid lines) and generalized occupation measurements (colored dashed lines) for the same choice of subsystems as in Fig. 7. Volume-law behavior of about $\tilde{\ell}$ is shown for comparison (purple dashed line). Inset: the position of the minimum of the tripartite mutual information $\ell_{\min,I_3}$ scales as $\sim \gamma^{-1}$ (black dashed line) both for fermion counting (blue circles) and occupation measurements (red circles).

serve as a guideline in searching for signatures of emergent conformal symmetry in I_2 and I_3.

For a CFT, it follows from Eq. (132) that the difference $I_2 - I_3$ is fully determined by the central charge and the cross ratio,

$$I_2 - I_3 = \frac{c}{3} \ln\left(\frac{1}{1-x}\right). \tag{135}$$

This difference is shown for fermion counting in Fig. 9. We have obtained similar results for generalized occupation measurements, but do not show them for the sake of brevity. A moderate value of $\gamma/J = 0.2$ is chosen here to best illustrate deviations from conformal invariance at both short and large scales. Each curve corresponds to a fixed value of $\ell_A = \ell_C = \ell$, while $\ell_B = \ell'$ is varied to sample different values of the cross ratio x, Eq. (131). We find good agreement with the CFT prediction (135) for values $\tilde{\ell}' \in [a l_0, l_c]$ within the critical range and when the central charge c in Eq. (135) is set to the maximum value $c_{\max}$ of the effective central charge c_ℓ shown in Fig. 6. The factor $a = 8$ is introduced such that the lower bound agrees with the onset of algebraic scaling on scales $\tilde{l} \gg l_0$ in Fig. 4. These results provide strong evidence for emergent conformal invariance within the critical range.

It should be noted that, for the data shown in Fig. 9, I_3 is typically several orders of magnitude smaller than I_2. Therefore, the picture does not change when I_2 is considered instead of $I_2 - I_3$. The collapse of I_2 as a function of the cross ratio for continuous measurements of occupation numbers described by a quantum state diffusion equation has been shown in Ref. [29] for a selection of subsystems. However, only the systematic analysis of the dependence on subsystem size presented above, which avoids an undersampling of subsystem sizes outside of the critical range, has allowed us to demonstrate that there is agreement with the CFT expectation only within the critical range and for $c = c_{\max}$.

Finally, we apply the same analysis to the tripartite mutual information. We have argued in Sec. VIII B that logarithmic growth of the entanglement entropy within the critical range is described by Gaussian theory with perturbative corrections due the nonlinearity of the sigma model manifold. This level of the theoretical description should, therefore, capture all signatures of emergent conformal invariance. However, as shown above, the tripartite mutual information vanishes in Gaussian theory, and cannot be obtained from the NLSM. These observations suggest that $\mathcal{G}(x) = 0$ in Eq. (132), and that nonzero values of I_3 can be attributed to nonuniversal fluctuations on short scales. Indeed, we do not observe a collapse of I_3 plotted as a function of the cross ratio in Fig. 10. As we have already seen in Fig. 8, the tripartite mutual information exhibits

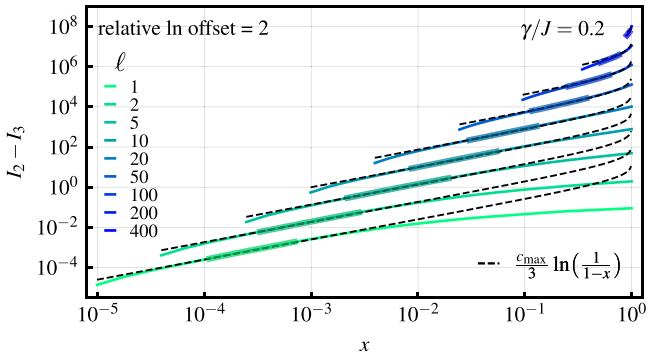


FIG. 9. Difference between bi- and tripartite mutual information for fermion counting with $\gamma/J = 0.2$ (colored lines). The subsystem size $\ell_A = \ell_C = \ell$ is fixed for each curve according to the legend, while $\ell_B = \ell'$ is varied to sample different values of the cross ratio x. For better visibility, each curve with $\ell > 1$ is shifted by a factor of e^2 relative to the curve with the next smaller value of ℓ, as indicated in the top center. The CFT prediction (black dashed line) coincides with the data when ℓ' is within the critical range (thicker colored lines). Violations of conformal invariance occur both on short scales $\tilde{\ell}' \lesssim a l_0$ (large values of x) and large scales $\tilde{\ell}' \gtrsim l_c$ (small values of x), where the factor $a = 8$ is introduced such that the lower bound agrees with the onset of algebraic scaling observed in Fig. 4.

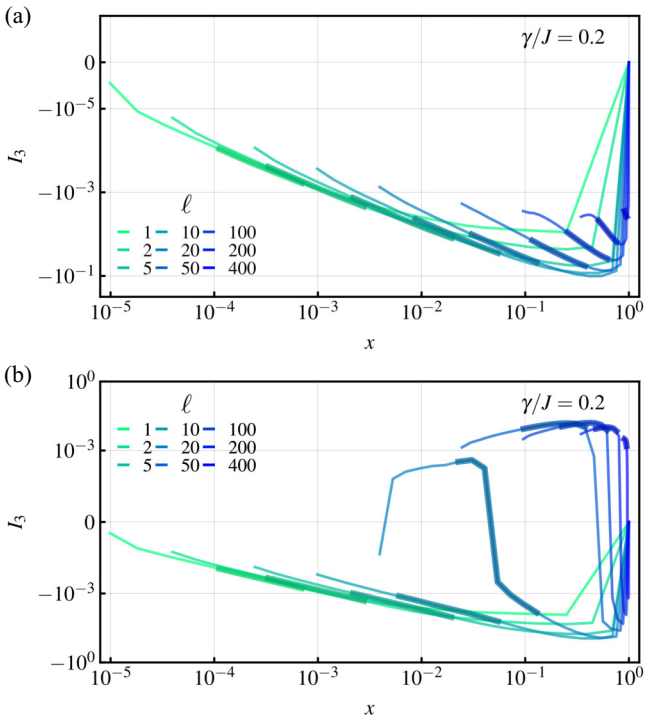


FIG. 10. Tripartite mutual information as a function of the cross ratio x for (a) fermion counting and (b) occupation measurements on a symmetric logarithmic scale and with $\gamma/J = 0.2$. In contrast to $I_2 - I_3$ shown in Fig. 9, the tripartite mutual information I_3 shows qualitatively different behavior for fermion counting and occupation measurements, and does not collapse to a single function of the cross ratio within the critical range.

qualitatively different behavior for fermion counting and occupation measurements, with I_3 assuming only negative values for fermion counting, but changing sign for occupation measurements.

IX. CONCLUSIONS AND OUTLOOK

We have presented an in-depth comparative study of two 1D models of free fermions subjected to different types of generalized measurement processes: monitored loss and gain or fermion counting on the one hand, and generalized measurements of local occupation numbers on the other hand. A high rate of fermion counts signals fast fluctuations of the quantum state of the fermionic many-body system. In contrast, generalized or projective measurements of occupation numbers lead to a freezing of the dynamics. Despite this striking difference, the dynamics of both models have important similarities in the frequent-measurement limit: emergent classicality and a suppression of coherent dynamics, which are hallmarks of the quantum Zeno effect for occupation measurements and which we attribute to a generalized Zeno effect for fermion counting. These similarities explain heuristically why both models exhibit close to identical results in various observables in the steady state, including density correlations, the entanglement entropy, and the bipartite mutual information. There are qualitative differences only in the tripartite mutual information.

Combining analytical insights from replica Keldysh field theory with numerical results from simulations of quantum jump trajectories, we have provided strong evidence for the absence of a measurement-induced entanglement transition in both models. In particular, we have shown that characteristic signatures of a critical phase can be observed only within a well-defined and finite range of length scales. Crucially, the upper boundary $l_c \sim \gamma^{-2}$ of this critical range is only algebraically large in the measurement rate, and, therefore, observable in numerics.

Formally, these properties can be understood to result from the universal long-wavelength description in terms of an NLSM that applies to both models. We have clarified the origin of the underlying SU(R) symmetry, and provided a physical explanation for the occurrence of this symmetry in terms of (i) conservation of the total number of particles in the system and auxiliary reservoirs and (ii) preservation of the purity of the quantum state of the system. Our work thus settles the question about the requirements to observe a measurement-induced entanglement transition in 1D free fermions.

Furthermore, our work opens up several interesting directions for future research. While there is no measurement-induced phase transition in the considered models in one dimension, such a transition does occur in higher dimensions [43,48]. It will be interesting to study the impact of the breaking of particle-number conservation by fermion counting on the dynamical critical behavior. A classification of *dynamical* criticality based on symmetries and conservation laws—in analogy to the classification of dynamical criticality in thermodynamic equilibrium [122]—is an interesting prospect. However, exploring this possibility analytically by studying, for example, two-time correlation functions such as $\overline{\langle \hat{A}(t)\rangle\langle \hat{B}(t')\rangle}$ will require a nontrivial extension of the replica Keldysh formalism.

From a more formal perspective, the stochastic Schrödinger equation (3) can be regarded as an unraveling of a quantum master equation that is recovered by taking the average over the stochastic increments $\mathrm{d}N_{\alpha,l}(t)$. While here we have considered cases for which the stationary state of the unconditional dynamics described by the master equation is trivial, this is generically not the case, and jump operators can be chosen so as to prepare a state of interest. For example, consider a 1D fermionic chain that is connected to particle reservoirs only at its ends and in such a way that a finite current is driven through the system. An unraveling of the corresponding master equation represents an interesting setup to study the interplay of transport and entanglement dynamics on the level of individual quantum trajectories. However, such an unraveling can, in general, not be formulated as a random generalized measurement as we have done here, and the derivation of a replica Keldysh field theory described in Sec. V has to be modified. Based on such an extension of the formalism, a further interesting perspective is to investigate quantum jump unravelings of quadratic fermionic Liouvillians belonging to different symmetry classes [123–126]. The resulting replica Keldysh field theories and NLSMs will shed further light on the connections between the dynamics of continuously monitored quantum systems in d spatial dimensions and the physics of Anderson localization in $d+1$ dimensions [115].

Finally, let us discuss implications of our work beyond noninteracting fermions. As we have already mentioned, our results show that charge sharpening, which has recently been discussed in random quantum circuits [17,18,21,68] and interacting fermionic systems [53,54], can occur even in the absence of charge conservation: for free-fermionic systems, Eq. (25) relates the entanglement entropy to the variance of the subsystem charge, that is, the second cumulant of the subsystem particle number; in particular, area-law scaling of the entanglement entropy, which we have found to be induced by fermion counting, implies that the system is in a charge-sharp phase [21]. It is an interesting prospect for future studies to explore charge sharpening in interacting fermionic systems and random quantum circuits with broken charge conservation.

ACKNOWLEDGMENTS

E.S. and L.S. acknowledge support from the Austrian Science Fund (FWF) through the projects 10.55776/P33741

and 10.55776/COE1, and from the European Union - NextGenerationEU.

DATA AVAILABILITY

The data that support the findings of this article are openly available [127].

APPENDIX A: MINIMAL PHYSICAL MODELS AND THEIR DESCRIPTION THROUGH A STOCHASTIC SCHRÖDINGER EQUATION

In this appendix, we outline the derivation of the stochastic Schrödinger equation (3) for minimal physical models of fermion counting and generalized occupation measurements. These models are inspired by theoretical descriptions of continuous measurements in mesoscopic electronics [76].

1. Fermion counting

We consider the setup of a quantum dot coupled to two reservoirs described in Sec. III A [76]. The quantum dot corresponds to a single fermionic lattice site, with annihilation and creation operators $\hat{\psi}$ and $\hat{\psi}^\dagger$, respectively, and Hamiltonian

$$\hat{H}_0 = \omega_0 \hat{\psi}^\dagger \hat{\psi}. \tag{A1}$$

We denote the reservoir annihilation and creation operators by $\hat{b}_{\alpha,k}$ and $\hat{b}^\dagger_{\alpha,k}$, where $\alpha = -$ for the reservoir that acts as the drain, $\alpha = +$ for the reservoir that acts as the source, and k is a discrete index that labels the reservoir states. The Hamiltonians of the reservoir states with energies $\omega_{\alpha,k}$ read

$$\hat{H}_\alpha = \sum_k \omega_{\alpha,k} \hat{b}^\dagger_{\alpha,k} \hat{b}_{\alpha,k}, \tag{A2}$$

and the reservoirs are coupled to the quantum dot by

$$\hat{H}_{\text{coup}} = \mathrm{i} \sum_{\alpha,k} (T_{\alpha,k} \hat{\psi}^\dagger \hat{b}_{\alpha,k} - T^*_{\alpha,k} \hat{b}^\dagger_{\alpha,k} \hat{\psi}) \tag{A3}$$

with tunneling coefficients $T_{\alpha,k}$. Both reservoirs are assumed to be in thermodynamic equilibrium at a low temperature, with chemical potentials chosen such that the reservoir states at energy ω_0 are empty in the drain and occupied in the source. We model this scenario by assuming the dot and reservoirs to be in the pure state $|\Psi(0)\rangle = |\psi(0), 0_-, 1_+\rangle$ at time $t = 0$, with 0_- and 1_+ denoting empty and occupied states of the drain and source, respectively.

Our goal is to derive a stochastic Schrödinger equation describing the dynamics of the quantum dot. As a first step, we move to an interaction frame with respect to the bath Hamiltonians (A2) and integrate the Schrödinger equation for state $|\Psi(t)\rangle$ of the dot and reservoirs in small time steps Δt. In Born and Markov approximations, the increment of the wave function, $\Delta|\Psi(t)\rangle = |\Psi(t+\Delta t)\rangle - |\Psi(t)\rangle$, is given by [74]

$$\Delta|\Psi(t)\rangle = [-\mathrm{i}\hat{H}_{\text{eff}}\Delta t + \sqrt{2}\hat{L}_- \Delta\hat{B}^\dagger_-(t) + \sqrt{2}\hat{L}_+ \Delta\hat{B}_+(t)]|\Psi(t)\rangle. \tag{A4}$$

The effective Hamiltonian reads

$$\hat{H}_{\text{eff}} = \hat{H}_0 - \mathrm{i} \sum_{\alpha=\pm} \hat{L}^\dagger_\alpha \hat{L}_\alpha, \tag{A5}$$

where $\hat{L}_- = \sqrt{\gamma_-/2}\,\hat{\psi}$ and $\hat{L}_+ = \sqrt{\gamma_+/2}\,\hat{\psi}^\dagger$ are the jump operators defined in Eq. (4) for a single lattice site. Furthermore, in Eq. (A4), we have introduced quantum Itô increments,

$$\Delta\hat{B}_\alpha(t) = \sqrt{\frac{2}{\gamma_\alpha}} \int_t^{t+\Delta t} \mathrm{d}t' \sum_k T_{\alpha,k} \hat{b}_{\alpha,k} \mathrm{e}^{-\mathrm{i}\omega_{\alpha,k}t'}, \tag{A6}$$

which obey the anticommutation relations

$$\{\Delta\hat{B}_\alpha(t), \Delta\hat{B}^\dagger_\alpha(t')\} = \Delta t\, \delta_{t,t'}, \tag{A7}$$

where $\delta_{t,t'}$ is the Kronecker delta for discrete times t and t'. The operators $\Delta\hat{B}_\alpha(t)$ and $\Delta\hat{B}^\dagger_\alpha(t)$ destroy and create fermions in the drain and source at a given time t, as opposed to the operators $\hat{b}_{\alpha,k}$ and $\hat{b}_{\alpha,k}$, which are associated with a frequency $\omega_{\alpha,k}$. Finally, the loss and gain rates appearing in Eq. (A4) are defined as $\gamma_\alpha = 2\pi\rho_\pm(\omega_0)\,|T_\pm(\omega_0)|$, where $\rho_\alpha(\omega_0)$ and $T_\alpha(\omega_0)$ are the density of states and tunneling amplitudes at the energy of the dot, which are introduced upon taking the continuum limit such that $\sum_k \to \int_0^\infty \mathrm{d}\omega\, \rho_\alpha(\omega)$ and $T_{\alpha,k} \to T_\alpha(\omega)$ [76].

The operators $\hat{L}_-\Delta\hat{B}^\dagger_-(t)$ and $\hat{L}_+\Delta\hat{B}_+(t)$ in Eq. (A4) describe the transfer of a fermion from the quantum dot to the drain and from the source to the dot, respectively. Since the Itô increments anticommute at different times, a fermion that has been transferred from the dot to the drain at time t cannot be transferred back at a later time t'. Formally, state $\Delta\hat{B}^\dagger_-(t)|0_-\rangle$ is annihilated by $\Delta\hat{B}_-(t')$. An analogous argument applies to the transfer of fermions from the source to the dot. Therefore, in Eq. (A4), the operators $\Delta\hat{B}_-(t)$ and $\Delta\hat{B}^\dagger_+(t)$ do not occur.

In analogy to photon counting in quantum optics, fermion counting is implemented by measuring the number operators,

$$\hat{N}_\alpha(t) = \frac{\Delta\hat{B}^\dagger_\alpha(t)}{\sqrt{\Delta t}} \frac{\Delta\hat{B}_\alpha(t)}{\sqrt{\Delta t}}, \tag{A8}$$

at each time step, with possible measurement outcomes $N_\alpha(t) = 0, 1$. To provide a physical interpretation of these

measurements, we may again take inspiration from mesoscopic electronics [76]. In this context, we can imagine the reservoirs as being connected via Ohmic contacts to an external circuit, such that a fermion in the drain is quickly absorbed in the circuit, and a fermion transferred from the source to the quantum dot is quickly replenished. These processes lead to measurable current spikes in the external circuit. The presence or absence of such spikes at time t can thus be interpreted as a projective measurements of the occupation numbers $\hat{N}_\alpha(t)$.

To describe the statistics of the measurement outcomes and the change of the state of the quantum dot for a given outcome, it is convenient to rewrite Eq. (A4) in the form

$$|\Psi(t+\Delta t)\rangle = \left[\hat{M}_0 + \hat{M}_- \frac{\Delta\hat{B}_-^\dagger(t)}{\sqrt{\Delta t}} + \hat{M}_+ \frac{\Delta\hat{B}_+(t)}{\sqrt{\Delta t}}\right]|\Psi(t)\rangle, \tag{A9}$$

where the measurement operators are defined as

$$\hat{M}_0 = 1 - \mathrm{i}\hat{H}_{\mathrm{eff}}\Delta t, \quad \hat{M}_- = \sqrt{2\Delta t}\,\hat{L}_-, \quad \hat{M}_+ = \sqrt{2\Delta t}\,\hat{L}_+. \tag{A10}$$

A measurement of the number operators, Eq. (A8), performed on state $|\Psi(t+\Delta t)\rangle$, Eq. (A9), yields $N_-(t)=0$ and $N_+(t)=1$ with probability

$$p_0(t) = \langle\psi(t)|\hat{M}_0^\dagger\hat{M}_0|\psi(t)\rangle. \tag{A11}$$

After a measurement with this outcome, the state of the quantum dot is given by

$$\begin{aligned}|\psi(t+\Delta t)\rangle &= \frac{\hat{M}_0|\psi(t)\rangle}{\sqrt{p_0(t)}} \\ &= \left[1 - \mathrm{i}\hat{H}_{\mathrm{eff}}\Delta t + \sum_{\alpha=\pm}\tilde{p}_\alpha(t)\Delta t\right]|\psi(t)\rangle,\end{aligned} \tag{A12}$$

where we have expanded the denominator up to order Δt, and where, as in Eq. (5), we have defined

$$\tilde{p}_\alpha(t) = \langle\psi(t)|\hat{L}_\alpha^\dagger\hat{L}_\alpha|\psi(t)\rangle. \tag{A13}$$

The measurement outcome above and the change of the state in Eq. (A12) correspond to the case that no quantum jump has occurred during the time step, and the states of the drain and source remain unchanged. In contrast, for $N_-(t)=1$ and $N_+(t)=1$, one fermion has been transferred from the quantum dot to the drain. This happens with probability $p_-(t) = 2\tilde{p}_-(t)\Delta t$, and the state after the measurement is

$$|\psi(t+\Delta t)\rangle = \frac{\hat{M}_-|\psi(t)\rangle}{\sqrt{p_-(t)}} = \frac{\hat{L}_-|\psi(t)\rangle}{\sqrt{\tilde{p}_-(t)}}. \tag{A14}$$

For $N_-(t)=0$ and $N_+(t)=0$, a fermion has been transferred from the source to the dot, which happens with probability $p_+(t) = 2\tilde{p}_+(t)\Delta t$. Then, the state after the measurement is

$$|\psi(t+\Delta t)\rangle = \frac{\hat{M}_+|\psi(t)\rangle}{\sqrt{p_+(t)}} = \frac{\hat{L}_+|\psi(t)\rangle}{\sqrt{\tilde{p}_+(t)}}. \tag{A15}$$

Performing measurements of the number operators (A8) in each time step results in stochastic dynamics of the wave function of the quantum dot, conditional to the measurement outcomes. To formulate these dynamics as an evolution equation, we define stochastic increments $\Delta N_\alpha(t) = 0, 1$ that count the number of fermions that are transferred from the dot to the drain and from the source to the dot during the step from t to $t+\Delta t$. Neglecting terms of order $\Delta N_\alpha(t)\Delta t$ [76], we can thus write the increment of the wave function as

$$\begin{aligned}\Delta|\psi(t)\rangle = \Bigg\{&\left[-\mathrm{i}\hat{H}_{\mathrm{eff}} + \sum_{\alpha=\pm}\tilde{p}_\alpha(t)\right]\Delta t \\ &+ \sum_{\alpha=\pm}\left[\frac{\hat{L}_\alpha}{\sqrt{\tilde{p}_\alpha(t)}} - 1\right]\Delta N_\alpha(t)\Bigg\}|\psi(t)\rangle.\end{aligned} \tag{A16}$$

In the limit of infinitesimal time steps, $\Delta t \to \mathrm{d}t$, the stochastic increments $\Delta N_\alpha(t) \to \mathrm{d}N_\alpha(t)$ describe a Poisson point process with the properties specified in Sec. III A [128], and the evolution of the quantum dot is then described by the stochastic Schrödinger equation (3) with $L=1$ and where we omit the contribution from $\hat{H}_0$, Eq. (A1), which leads to a global phase factor for each trajectory.

2. Generalized occupation measurements

Measurements of the occupation of a quantum dot can be implemented by modifying the above setup as outlined in Sec. III A: instead of tunneling from the reservoirs to the dot as described by Eq. (A3), we consider tunneling directly from the source to the drain that is, however, possible only when the dot is occupied [76],

$$\hat{H}_{\mathrm{coup}} = \mathrm{i}\sum_{k,q}\hat{\psi}^\dagger\hat{\psi}(\chi\hat{b}_{-,k}^\dagger\hat{b}_{+,q} - \chi^*\hat{b}_{+,q}^\dagger\hat{b}_{-,k}). \tag{A17}$$

This coupling Hamiltonian, with a mode-independent tunneling rate χ, is a simplified version of a setup that has been realized in mesoscopic devices, for example, in Ref. [81].

As above, we integrate the Schrödinger equation for the dot and reservoirs in small time steps, leading to

$$\Delta|\Psi(t)\rangle = [-\mathrm{i}\hat{H}_{\mathrm{eff}}\Delta t + \sqrt{2}\hat{L}\Delta\hat{B}(t)]|\Psi(t)\rangle, \tag{A18}$$

where $\hat{n} = \hat{\psi}^\dagger\hat{\psi}$ and $\hat{L} = \sqrt{\gamma}\,\hat{n}$. The measurement rate is $\gamma = 2\pi\rho_-(\omega_0)\rho_+(\omega_0)\,|\chi|^2\,(\mu_+ - \mu_-)$, where the μ_α are

the chemical potentials of the reservoirs, and the effective Hamiltonian is given by

$$\hat{H}_{\text{eff}} = \hat{H}_0 - \mathrm{i}\hat{L}^\dagger\hat{L}. \tag{A19}$$

We have again introduced quantum Itô increments,

$$\Delta\hat{B}(t) = \sqrt{\frac{\gamma}{2}}\chi^* \int_t^{t+\Delta t} \mathrm{d}t' \sum_{k,q} \hat{b}^\dagger_{-,k}\hat{b}_{+,q}\mathrm{e}^{-\mathrm{i}(\omega_{+,q}-\omega_{-,k})t'}, \tag{A20}$$

which obey canonical anticommutation relations,

$$\{\Delta\hat{B}(t), \Delta\hat{B}^\dagger(t')\} = \Delta t\,\delta_{t,t'}. \tag{A21}$$

From here on, the derivation of the stochastic Schrödinger equation describing the dynamics of the quantum dot is analogous to that for fermion counting outlined above.

APPENDIX B: IMPLEMENTATION OF GENERALIZED MEASUREMENTS

The generalized measurements described by Eqs. (15) and (16) can be implemented through projective measurements, performed on auxiliary degrees of freedom, as explained in the following.

1. Fermion counting

As in Appendix A, we consider first a single fermionic site or quantum dot, coupled to two reservoirs, designated as the drain and source. However, the reservoirs comprise a single state each, and not a continuum of states as above. Our goal is to implement a generalized measurement on the quantum dot with measurement operators $\hat{M}_- = \hat{\psi}$ and $\hat{M}_+ = \hat{\psi}^\dagger$. Before the measurement, the drain is empty, the source is filled, and the quantum dot is in an arbitrary superposition state,

$$|\Psi\rangle = (c_0 + c_1\hat{\psi}^\dagger)\hat{b}^\dagger_+|0\rangle, \tag{B1}$$

where $|0\rangle$ is the vacuum state of the dot, drain, and source. To implement the measurement, we first entangle the quantum dot with the reservoirs by applying two gates sequentially. The first gate, $\hat{U}_-$, transfers a fermion from the dot to the drain,

$$\hat{U}_- = \mathrm{e}^{-\mathrm{i}\hat{V}_-}, \qquad \hat{V}_- = \frac{\mathrm{i}\pi}{2}(\hat{\psi}^\dagger\hat{b}_- - \hat{b}^\dagger_-\hat{\psi}). \tag{B2}$$

The second gate, $\hat{U}_+$, fills the dot from the source. To avoid a fermion being transferred from the source to the drain through the application of $\hat{U}_+\hat{U}_-$, the action of the second gate is conditioned on the drain being empty,

$$\hat{U}_+ = \mathrm{e}^{-\mathrm{i}\hat{V}_+}, \qquad \hat{V}_+ = \frac{\mathrm{i}\pi}{2}(1 - \hat{b}^\dagger_-\hat{b}_-)(\hat{\psi}^\dagger\hat{b}_+ - \hat{b}^\dagger_+\hat{\psi}). \tag{B3}$$

Applying these gates to the state in Eq. (B1) leads to

$$\hat{U}_+\hat{U}_-|\Psi\rangle = (c_0\hat{\psi}^\dagger - c_1\hat{b}^\dagger_-\hat{b}^\dagger_+)|0\rangle. \tag{B4}$$

Now we perform a projective measurement of the occupation of the reservoirs, $\hat{N}_b = \frac{1}{2}\sum_{\alpha=\pm}\hat{n}_\alpha$, with possible outcomes 0 and 1. For outcome 0, the nonnormalized state after the measurement is

$$(1 - \hat{N}_b)\hat{U}_+\hat{U}_-|\Psi\rangle = c_0\hat{\psi}^\dagger|0\rangle = \hat{\psi}^\dagger\hat{b}_+|\Psi\rangle. \tag{B5}$$

The norm of this state is the probability for this outcome to occur, $p_0 = |c_0|^2 = \langle\Psi|\hat{\psi}^\dagger\hat{\psi}|\Psi\rangle$. For outcome 1, the nonnormalized state after the measurement is

$$\hat{N}_b\hat{U}_+\hat{U}_-|\Psi\rangle = -c_1\hat{b}^\dagger_-\hat{b}^\dagger_+|0\rangle = \hat{\psi}\hat{b}^\dagger_-|\Psi\rangle \tag{B6}$$

with probability $p_1 = |c_1|^2 = \langle\Psi|\hat{\psi}\hat{\psi}^\dagger|\Psi\rangle$. In both cases, through the measurement, the entangled state in Eq. (B4) collapses, and the dot and reservoirs become disentangled. The reservoirs can then be reinitialized for the next measurement, and we may consider the effect of the measurement process on the dot alone. As desired, the states after the measurement in Eqs. (B5) and (B6) as well as the corresponding probabilities are equivalent to a generalized measurement with the measurement operators $\hat{M}_\pm$ given above.

It remains to generalize this measurement process to an extended lattice system. This is achieved straightforwardly by first selecting a lattice site $l \in \{1, \ldots, L\}$ with uniform probability $1/L$ and then carrying out the generalized measurement at this lattice site as described above. This is equivalent to the generalized measurement with measurement operators given in Eq. (15), where the $1/\sqrt{L}$ factors and the corresponding $1/L$ factors in the probabilities in Eq. (8) can be interpreted as resulting from randomly picking a lattice site.

2. Generalized occupation measurements

The effect of a generalized measurement described by Eq. (16) on a single quantum dot is trivial. Therefore, we consider the general case of N particles on L lattice sites, coupled to L drain states with annihilation operators $\hat{b}_{-,l}$, but only a single source mode with annihilation operator $\hat{b}_+$. Note that this is different from the derivation of the stochastic Schrödinger equation discussed in Appendix A 2 and the sketch in Fig. 1. The initial state

is a superposition of states with N fermions on sites $l_1, \ldots, l_N \in \{1, \ldots, L\}$, with respective amplitudes $\psi_{l_1,\ldots,l_N}$:

$$|\Psi\rangle = \sum_{l_1<\cdots<l_N} \psi_{l_1,\ldots,l_N} \left(\prod_{n=1}^{N} \hat{\psi}^\dagger_{l_n} \right) \hat{b}^\dagger_+ |0\rangle. \tag{B7}$$

There is a single fermion in the source mode, while the drain states are empty. As above, to implement the measurement, we first entangle the system with the reservoirs. We apply a unitary gate that transfers the fermion from the source to the drain state at sites l, conditioned on the corresponding sites in the system being occupied:

$$\hat{U} = \mathrm{e}^{-\mathrm{i}\hat{V}}, \qquad \hat{V} = \frac{\mathrm{i}\pi}{2\sqrt{N}} \sum_{l=1}^{L} \hat{n}_l \, (\hat{b}^\dagger_{-,l} \hat{b}_+ - \hat{b}^\dagger_+ \hat{b}_{-,l}). \tag{B8}$$

Consequently, in each term in the sum in Eq. (B7), the reservoir fermion ends up in an equal superposition of sites l_n that are occupied in the system,

$$\hat{U}|\Psi\rangle = \frac{1}{\sqrt{N}} \sum_{l_1<\cdots<l_N} \psi_{l_1,\ldots,l_N} \left(\prod_{n=1}^{N} \hat{\psi}^\dagger_{l_n} \right) \sum_{n=1}^{N} \hat{b}^\dagger_{-,l_n} |0\rangle. \tag{B9}$$

Next, we perform a projective measurement of the position of the fermion in the drain, described by the operator $\hat{X}_- = \sum_{l=1}^{L} l \hat{b}^\dagger_{-,l} \hat{b}_{-,l}$. Possible outcomes of this measurement are $l \in \{1, \ldots, L\}$. For result l, the state after the measurement is

$$\begin{aligned} &\hat{b}^\dagger_{-,l} \hat{b}_{-,l} \hat{U}|\Psi\rangle \\ &\quad = \frac{1}{\sqrt{N}} \sum_{l_1<\cdots<l_N} \delta_{l\in\{l_1,\ldots,l_N\}} \psi_{l_1,\ldots,l_N} \left(\prod_{n=1}^{N} \hat{\psi}^\dagger_{l_n} \right) \hat{b}^\dagger_{-,l} |0\rangle \\ &\quad = \frac{1}{\sqrt{N}} \hat{n}_l \hat{b}^\dagger_{-,l} \hat{b}_+ |\Psi\rangle, \end{aligned} \tag{B10}$$

where the factor $\delta_{l\in\{l_1,\ldots,l_N\}}$ indicates that only those terms should be retained in the sum over occupied sites $l_1, \ldots, l_N$, for which l is occupied. The probability for outcome l, given by the norm of the state, evaluates to $p_l = \langle\Psi|\hat{n}_l|\Psi\rangle/N$. Focusing again on the effect of the measurement on the system, we see that it can equivalently be described as a generalized measurement with measurement operators given in Eq. (16).

APPENDIX C: TELEGRAPH-REDUCED AUTOCORRELATION FUNCTION

The telegraph-reduced autocorrelation function (18) can be calculated analytically in the limit $\gamma \gg J$. For simplicity of notation, we assume that the evolution has already reached a stationary state at $t' = 0$. A closed equation of motion can be obtained for the correlation function defined as

$$Q_{l_1,l_2,l_3}(t) = \overline{q_{l_1,l_2,l_3}(t) z_{l_3}(0)}, \qquad q_{l_1,l_2,l_3}(t) = z_{l_1,l_2}(t) s_{l_3}(t), \tag{C1}$$

where

$$z_{l,l'}(t) = 2D_{l,l'}(t) - 1, \quad z_l(t) = z_{l,l}(t), \quad s_l(t) = (-1)^{N_l(t)}, \tag{C2}$$

with the single-particle density matrix defined in Eq. (13), and

$$N_l(t) = \int_0^t \mathrm{d}N_l(t'), \qquad \mathrm{d}N_l(t) = \sum_{\alpha=\pm} \mathrm{d}N_{\alpha,l}(t). \tag{C3}$$

The telegraph-reduced autocorrelation function (18) is obtained by setting $l_1 = l_2 = l_3$ in Eq. (C1), $Q(t) = Q_{l,l,l}(t)$. To obtain the evolution equation of $Q_{l_1,l_2,l_3}(t)$, we first consider the stochastic increment in a single trajectory,

$$\begin{aligned} &\mathrm{d}q_{l_1,l_2,l_3}(t) \\ &\quad = \mathrm{d}z_{l_1,l_2}(t) s_{l_3}(t) + z_{l_1,l_2}(t) \mathrm{d}s_{l_3}(t) + \mathrm{d}z_{l_1,l_2}(t) \mathrm{d}s_{l_3}(t). \end{aligned} \tag{C4}$$

The product of two increments in the last term yields a nonvanishing contribution: for Poisson processes, $\mathrm{d}t\mathrm{d}N_{\alpha,l}(t) = 0$, but $\mathrm{d}N_{\alpha,l}(t)\mathrm{d}N_{\alpha',l'}(t) = \delta_{\alpha,\alpha'}\delta_{l,l'}\mathrm{d}N_{\alpha,l}(t)$ is nonzero [76]. To obtain the increment $\mathrm{d}z_{l,l'}(t)$, we first rewrite the stochastic Schrödinger equation (3) as a stochastic master equation for the conditional state $\hat{\rho}(t) = |\psi(t)\rangle\langle\psi(t)|$. Then, using Wick's theorem, the latter can be recast as an equation for the single-particle density matrix, which leads to

$$\begin{aligned} \mathrm{d}z_{l,l'}(t) = -\mathrm{i}[H, z(t)]_{l,l'} \mathrm{d}t - 2 \sum_{m=1}^{L} \Bigg[&\frac{D_{l,m}(t) D_{m,l'}(t)}{D_{m,m}(t)} \mathrm{d}N_{-,m}(t) \\ &- \frac{[\delta_{l,m} - D_{l,m}(t)][\delta_{m,l'} - D_{m,l'}(t)]}{1 - D_{m,m}(t)} \mathrm{d}N_{+,m}(t) \Bigg] \end{aligned} \tag{C5}$$

with H defined in Eq. (47). We insert this result into Eq. (C4), along with the expression for $\mathrm{d}s_l(t)$ that follows from

$$s_l(t + \mathrm{d}t) = s_l(t)[1 - 2\mathrm{d}N_l(t)] = s_l(t) + \mathrm{d}s_l(t). \tag{C6}$$

Thus, with the averages of the Poisson increments $\mathrm{d}N_{\alpha,l}(t)$ given in Sec. III, we obtain

$$\frac{\mathrm{d}Q_{l,l,l}(t)}{\mathrm{d}t} = 2J \, \mathrm{Im}[Q_{l,l+1,l}(t) + Q_{l,l-1,1}(t)]. \tag{C7}$$

The equation of motion for $Q_{l_1,l_2,l_3}(t)$ with unequal indices has an additional contribution proportional to γ; for example,

$$\frac{\mathrm{d}Q_{l,l\pm1,l}}{\mathrm{d}t} = \mathrm{i}J[Q_{l+1,l\pm1,l}(t) + Q_{l-1,l\pm1,l}(t) - Q_{l,l\pm1-1,l}(t) - Q_{l,l\pm1+1,l}(t)] - 2\gamma Q_{l,l\pm1,l}. \tag{C8}$$

Our goal is to solve these coupled equations of motion perturbatively in $J \ll \gamma$. To zeroth order, from Eq. (C7), we obtain $Q(t) = Q_{l,l,l}(t) = \text{const}$—by construction, $Q(t)$ does not decay in the absence of coherent hopping. The decay of $Q_{l,l,l}(t)$ is due to the coupling to $Q_{l,l\pm1,l}(t)$ at first order in J. More generally, the commutator with H in Eq. (C5) couples $Q_{l,l,l}(t)$ to $Q_{l_1,l_2,l_3}(t)$ at order $|l_1 - l_3| + |l_2 - l_3|$. Therefore, the leading correction to the zeroth-order result is obtained by setting the right-hand side of Eq. (C8) to zero, keeping only contributions involving $Q_{l,l,l}(t)$ and $Q_{l,l\pm1,l}(t)$, which leads to

$$Q_{l,l\pm1,l}(t) = -\frac{\mathrm{i}J}{2\gamma}Q(t). \tag{C9}$$

Inserting this into Eq. (C7), and using $Q(0) = 1$, we obtain $Q(t) = \mathrm{e}^{-2\nu t}$ with $\nu = J^2/\gamma$, as claimed in the main text.

APPENDIX D: REGULARIZATION, CAUSALITY STRUCTURE, AND NORMALIZATION IN KELDYSH FIELD THEORY

Here, we address points (i) and (ii) listed below Eq. (55). Furthermore, we discuss the causality structure and normalization of the Keldysh partition function in the replica limit.

1. Regularization of the Keldysh action

(i) In the construction of the Keldysh functional integral, in Eq. (38), time evolution from t_0 to t is split into N time steps of duration $\Delta t = (t - t_0)/N$. At each discrete time $t_n = t_0 + \Delta t n$, a resolution of the identity in terms of coherent states, $|\pm\psi_{\pm,n}\rangle = \exp\{\pm\sum_{r=1}^{R}\sum_{l=1}^{L}\psi_{\pm,r,l,n}\hat{\psi}^{\dagger}_{r,l}\}|0\rangle$, where $|0\rangle$ is the vacuum state, is inserted. If a measurement is performed between times t_n and t_{n+1}, we thus obtain a matrix element of the measurement operator between the coherent states $|\psi_{\pm,n}\rangle$ and $|\psi_{\pm,n+1}\rangle$. For generalized occupation measurements with measurement operators given in Eq. (16), the matrix elements on the forward and backward branches contain the factors

$$\begin{aligned}&\langle\psi_{+,n+1}|\hat{n}_{r,l}|\psi_{+,n}\rangle = \psi^{*}_{+,r,l,n+1}\psi_{+,r,l,n}\langle\psi_{+,n+1}|\psi_{+,n}\rangle,\\ &\langle-\psi_{-,n}|\hat{n}_{r,l}|-\psi_{-,n+1}\rangle\\ &\quad = \psi^{*}_{-,r,l,n}\psi_{-,r,n+1,l}\langle-\psi_{-,n}|-\psi_{-,n+1}\rangle,\end{aligned} \tag{D1}$$

where the fields that represent the operators $\hat{n}_{r,l}$ are one discrete time step apart. However, as shown in Ref. [38], in the functional integral, we can replace

$$\begin{aligned}\psi^{*}_{+,r,l,n+1}\psi_{+,r,l,n} &\to \psi^{*}_{+,r,l,n}\psi_{+,r,l,n} + 1,\\ \psi^{*}_{-,r,l,n}\psi_{-,r,l,n+1} &\to \psi^{*}_{-,r,l,n}\psi_{-,r,l,n} + 1,\end{aligned} \tag{D2}$$

where now the fields are evaluated at equal times. This is a prerequisite for introducing fermionic bilinears at equal times as new variables. The vertex in Eq. (54) is thus modified as

$$V[\psi^{*},\psi] = \frac{1}{n}(\psi^{*}_{+}\psi_{+}+1)(\psi^{*}_{-}\psi_{-}+1). \tag{D3}$$

For fermion counting, with the linear measurement operators in Eq. (15), this issue does not arise.

(ii) In the discrete-time formulation of the theory, Green's function is defined as $\mathrm{i}G_{n,n'} = \langle\psi_n\psi^{\dagger}_{n'}\rangle$ [107]. Working in the basis introduced through the Larkin-Ovchinnikov rotation (56), the continuous-time limit is given by

$$G(t,t') = \lim_{n,n',N\to\infty}\left(G_{n,n'} + \frac{\mathrm{i}}{2}\delta_{n,n'}\sigma_x\right), \tag{D4}$$

where the limit is taken such that $t_n \to t$ and $t_{n'} \to t'$. In the last term, we leave the identity matrices in replica and lattice space implicit. The shift $\mathrm{i}\delta_{n,n'}\sigma_x/2$ on the right-hand side leads to the continuous-time Green function at equal times being given by the symmetrized limit as in Eq. (55),

$$G(t,t) = \tfrac{1}{2}[G(t,t+0^{+}) + G(t,t-0^{+})]. \tag{D5}$$

In turn, this implies that the Keldysh Green's function is continuous at $t = t'$, and that the anti-Keldysh component of Green's function vanishes at all times—which is not the case for the discrete-time Green function $G_{n,n'}$ that has a nonvanishing anti-Keldysh component at $n = n'$ [107].

For most applications of Keldysh field theory, the shift on the right-hand side of Eq. (D4) is irrelevant and can be omitted. However, here we have to take it into account to ensure normalization of the Keldysh partition function, as discussed below. The shift can be incorporated into the action by switching to a regularization in which the free discrete-time Green function is $G^{(\mathrm{reg})}_{n,n'} = G_{n,n'} + \mathrm{i}\delta_{n,n'}\sigma_x/2$ [42]. Changing the regularization is achieved through the

relation

$$Z_R(t) = \int \frac{\mathrm{D}[\psi^*,\psi]}{\mathrm{Det}(-\mathrm{i}G_0^{-1})} \times \exp\left\{\mathrm{i}\left(\psi^\dagger G_0^{-1}\psi + \gamma\int \mathrm{d}^2\mathbf{x}\,\mathcal{L}_M[\psi_l^*,\psi_l]\right)\right\} = \int \frac{\mathrm{D}[\psi^*,\psi]}{\mathrm{Det}(-\mathrm{i}G_0^{(\mathrm{reg})-1})} \times \exp\left\{\mathrm{i}\left(\psi^\dagger G_0^{(\mathrm{reg})-1}\psi + \gamma\int \mathrm{d}^2\mathbf{x}\,\mathcal{L}_M^{(\mathrm{reg})}[\psi_l^*,\psi_l]\right)\right\}, \tag{D6}$$

where we make the determinants that are usually absorbed in the integration measure explicit [107]. The regularized measurement Lagrangian can be constructed order by order in an expansion in γ. To first order, $\mathcal{L}_M^{(\mathrm{reg})}$ is obtained by adding the sum over all partial contractions, where each contraction is $\langle\psi_n\psi_{n'}^\dagger\rangle = \delta_{n,n'}\sigma_x/2$, to the original measurement Lagrangian $\mathcal{L}_M$. Since these contractions are diagonal in replica space, they can be added to each factor of the product over replicas in Eq. (52), that is, to the vertices (53) and (D3). As stated in the main text, the vertices for fermion counting do not change under the regularization. The regularized vertex for occupation measurements is given in Eq. (58).

2. Causality structure and normalization of the Keldysh partition function

For closed quantum systems undergoing unitary dynamics without measurements, the Keldysh partition function is normalized to unity, $Z(t) = \mathrm{tr}[\hat\rho(t)] = 1$, as follows from the normalization of the density matrix $\hat\rho(t)$. However, the replica Keldysh partition function $Z_R(t)$ is defined in Eq. (38) in terms of R copies of the nonnormalized density matrix $\hat D(t)$. In the replica limit $R \to 1$, the completeness relation of measurement operators implies again that $Z_R(t) \to 1$. For $R > 1$, on the other hand, the replica Keldysh partition function is not normalized. This is because the products of measurement operators over r replicas, which occur in $\bigotimes_{r=1}^R \hat D_r(t)$, do not obey a completeness relation.

In Keldysh field theory for closed systems, the normalization of the partition function is reflected in the causality structure of the action, in particular, in the property that the action vanishes for $\psi_+ = \psi_-$ and $\psi_+^* = \psi_-^*$ [106–109]. To see this, we consider a system with Hamiltonian $\hat H$. The Keldysh partition function is $Z(t) = \int \mathrm{D}[\psi^*,\psi]\mathrm{e}^{\mathrm{i}S}$ where $S = \int_{t_0}^t \mathrm{d}t'\mathcal{L}[\psi^*,\psi]$, and with the Lagrangian

$$\mathcal{L}[\psi^*,\psi] = \sum_{\sigma=\pm}\sigma\left(\psi_\sigma^\dagger\partial_t\psi_\sigma - H[\psi_\sigma^*,\psi_\sigma]\right). \tag{D7}$$

From $Z(t) = \mathrm{tr}[\hat\rho(t)] = 1$, it follows that

$$\partial_t Z = \mathrm{i}\langle\mathcal{L}[\psi^*,\psi]\rangle = \mathrm{i}\sum_{\sigma=\pm}\sigma\langle\psi_\sigma^\dagger\partial_t\psi_\sigma - H[\psi_\sigma^*,\psi_\sigma]\rangle = 0. \tag{D8}$$

Upon taking the sum over $\sigma = \pm$, both terms in the average vanish individually. Indeed, the cyclic property of the trace implies that the expectation value of any operator $\hat O$ at time t can be evaluated equivalently on the forward and on the backward branch of the Keldysh contour, and, therefore,

$$\langle\mathcal{L}[\psi^*,\psi]\rangle = \left\langle\mathcal{L}[\psi^*,\psi]\big|_{\psi_+=\psi_-,\psi_+^*=\psi_-^*}\right\rangle. \tag{D9}$$

Then, $\langle\mathcal{L}[\psi^*,\psi]\rangle = 0$ follows for the Lagrangian of a closed system in Eq. (D7) from the causality structure,

$$\mathcal{L}[\psi^*,\psi]\big|_{\psi_+=\psi_-,\psi_+^*=\psi_-^*} = 0. \tag{D10}$$

This shows that the causality structure of the action guarantees the normalization of the Keldysh partition function.

As mentioned in Sec. V D, the term $\psi_2^*\psi_1$ in the regularized vertex for occupation measurements, Eq. (58), violates the usual causality structure. Inverting the Larkin-Ovchinnikov rotation (56) shows that this term couples the forward and backward branches. The above argument based on the cyclic property of the trace does, in general, not apply, and Eqs. (D9) and (D10) do not hold for such terms. To see that the partition function is normalized even though the action does not obey the usual causality structure, one should note that, according to Eq. (D8), normalization is ensured when the expectation value of the Lagrangian vanishes. We now confirm that this condition is met.

The free evolution described by the first term in the Keldysh action in Eq. (51) obeys the causality structure for any value of R, and, therefore, we only need to consider the measurement Lagrangian (52). For $R = 1$, we thus require

$$\langle\mathrm{i}\mathcal{L}_M[\psi^*,\psi]\rangle = \sum_{n=\pm}\langle V_n[\psi^*,\psi]\rangle - 1 = 0. \tag{D11}$$

We first check this condition for fermion counting. Using the form of the vertices given in Eq. (57), we obtain

$$\langle\mathrm{i}\mathcal{L}_M[\psi_l^*,\psi_l]\rangle = \mathrm{i}[G_{l,l}^R(t,t) - G_{l,l}^A(t,t)] - 1. \tag{D12}$$

To evaluate Green's functions at equal times, we express them through fermionic field operators [106]:

$$\mathrm{i}G^{R}_{l,l'}(t,t') = \langle \psi_{1,l}(t)\psi^{*}_{1,l'}(t')\rangle = \theta(t-t')\langle\{\hat{\psi}_l(t), \hat{\psi}^{\dagger}_{l'}(t')\}\rangle,$$
$$\mathrm{i}G^{A}_{l,l'}(t,t') = \langle \psi_{2,l}(t)\psi^{*}_{2,l'}(t')\rangle = -\theta(t'-t)\langle\{\hat{\psi}_l(t), \hat{\psi}^{\dagger}_{l'}(t')\}\rangle,$$
$$\mathrm{i}G^{K}_{l,l'}(t,t') = \langle \psi_{1,l}(t)\psi^{*}_{2,l'}(t')\rangle = \langle[\hat{\psi}_l(t), \hat{\psi}^{\dagger}_{l'}(t')]\rangle,$$

with two-time averages defined as in Eq. (20). The values of Green's functions in the symmetrized limit of equal times, Eq. (D5), follow directly from fermionic anticommutation relations and the expectation value $\langle \hat{n}_l\rangle_{\mathrm{ss}}$ in the unconditional steady state. According to Sec. III A, $\langle \hat{n}_l\rangle_{\mathrm{ss}} = n$ for occupation measurements, with $n = 1/2$ for fermion counting with equal rates of loss and gain. We thus obtain

$$\mathrm{i}G^{R/A}_{l,l'}(t,t) = \pm\tfrac{1}{2}\delta_{l,l'}, \quad \mathrm{i}G^{K}_{l,l'}(t,t) = (1-2n)\delta_{l,l'}. \tag{D13}$$

Inserting these values into Eq. (D12) yields $\langle \mathrm{i}\mathcal{L}_M[\psi^{*}_l, \psi_l]\rangle = 0$, confirming that the Keldysh partition function is normalized.

Finally, we check Eq. (D11) for occupation measurements. Since the regularized vertex (58) is quartic, the expectation value in Eq. (D11) cannot be evaluated exactly. At lowest order in γ, we can use Wick's theorem to obtain

$$\langle \mathrm{i}\mathcal{L}_M[\psi^{*}_l, \psi_l]\rangle = \frac{1}{n}\left[\frac{1}{4} - \frac{\mathrm{i}}{2}G^{K}_{l,l}(t,t) + G^{R}_{l,l}(t,t)G^{A}_{l,l}(t,t)\right] - 1, \tag{D14}$$

where now Green's functions are those of the system without measurements. However, Eq. (D13) still applies, and we again find that $\langle \mathrm{i}\mathcal{L}_M[\psi^{*}_l, \psi_l]\rangle = 0$.

APPENDIX E: THE SYMMETRY UNDERLYING THE NLSM

The SU(R) symmetry underlying the NLSM is introduced in Sec. V C as a strong symmetry of the time-evolution superoperator. Its representation in Keldysh field theory is discussed in Sec. V E. In the following, we first present the derivation of the symmetry in the operator formalism, which leads to condition (i) for the symmetry to occur given in Sec. V C. Then, we demonstrate the symmetry for the measurement Lagrangian for fermion counting, Eq. (61). Finally, we discuss modifications of the theory for inefficient detection, which lead to a breaking of the symmetry. We thus also show that condition (ii) is necessary.

1. Derivation in the operator formalism

We want to show that condition (i) formulated in Sec. V C implies Eq. (44). In the R-fold replicated time-evolution operator, $\prod_{r=1}^{R}\hat{V}_r(t)$, each factor $\hat{V}_r(t)$ is of the form given in Eq. (33), and comprises both coherent dynamics and measurements. We thus proceed in two steps. First we discuss under which conditions the transformation $\hat{G}_\Phi$ defined in Eq. (42) is a symmetry of the Hamiltonian that generates the coherent dynamics. Second we show that applying $\hat{G}_\Phi$ to the measurement operators leads to the phase factor in Eq. (44).

For generality, we consider coherent evolution generated by a generic quadratic Hamiltonian. Then, $\prod_{r=1}^{R}\hat{V}_r(t)$ contains an R-replica Hamiltonian of the form

$$\hat{H}_R = \sum_{r=1}^{R}\sum_{l,l'=1}^{L}(-J_{l,l'}\hat{\psi}^{\dagger}_{r,l}\hat{\psi}_{r,l'} + \Delta_{l,l'}\hat{\psi}_{r,l}\hat{\psi}_{r,l'} + \mathrm{H.c.}). \tag{E1}$$

Using Eq. (43), one can immediately see that particle-number-conserving terms in the Hamiltonian are symmetric under $\hat{G}_\Phi$. In contrast, pairing terms are not symmetric. Such pairing terms are contained in the Majorana model of Ref. [45].

We next consider measurements. As above, for the sake of generality, we allow more generic types of measurement operators than those considered in the main text. Our only requirement is contained in condition (i) in Sec. V C: we assume that at all times, each replica is in a pure Gaussian state with a fixed number of particles. Note that these properties are also preserved by coherent evolution generated by a particle-number-conserving quadratic Hamiltonian. Such states are Slater determinants, as given for R replicas in Eq. (41). The above requirement is thus satisfied if each measurement operator maps an N-particle Slater determinant to an $(N+\Delta N)$-particle Slater determinant, where the integer ΔN may depend on the measurement operator. For the operators in Eq. (16) that describe generalized measurements of occupation measurements, $\Delta N = 0$, whereas for fermion counting with measurement operators given in Eq. (15), $\Delta N = -1$ and $\Delta N = +1$ for the measurement operators $\hat{M}_{-,l}$ and $\hat{M}_{+,l}$, respectively.

Consider now a generic measurement operator $\hat{M}$ that satisfies this requirement. We want to infer how $\prod_{r=1}^{R}\hat{M}_r$ transforms under $\hat{G}_\Phi$. In fact, for our purposes, it is sufficient to determine the transformation of the restriction of $\prod_{r=1}^{R}\hat{M}_r$ to the space spanned by R-replica Slater determinants that are symmetric under permutations of replicas as given in Eq. (41). This is because, by construction of the replica formalism in Sec. V B, the initial R-replica state is symmetric under permutations of replicas, and this property is conserved due to the product structure of the time-evolution operator, $\prod_{r=1}^{R}\hat{V}_r(t)$. Combined with the above assumptions on preservation of Gaussianity and a fixed number of particles in each replica, we see that $\prod_{r=1}^{R}\hat{M}_r$ maps permutation-symmetric R-replica N-particle Slater determinants to permutation-symmetric R-replica $(N+\Delta N)$-particle Slater determinants.

As a preliminary step, we consider the transformation of the product of field operators over the replica index,

$$\hat{G}_\Phi^\dagger\Big(\prod_{r=1}^R \hat{\psi}_{r,l}\Big)\hat{G}_\Phi = \prod_{r=1}^R\sum_{r'=1}^R (G_\Phi)_{r,r'}\hat{\psi}_{r',l} = \sum_{r'_1,\dots,r'_R=1}^R \prod_{r=1}^R (G_\Phi)_{r,r'_r}\hat{\psi}_{r'_r,l}. \tag{E2}$$

The product in the last equality can be split into two independent products. A further simplification is due to fermionic statistics: the product $\prod_{r=1}^R \hat{\psi}_{r'_r,l}$ is nonzero only if all replica indices r'_r are different, that is, if $r'_r = \sigma_r$, where $\sigma \in S_R$ is an element of the symmetric group of permutations of R elements. Then, upon rearranging the product we obtain $\prod_{r=1}^R \hat{\psi}_{\sigma_r,l} = \mathrm{sgn}(\sigma)\prod_{r=1}^R \hat{\psi}_{r,l}$. We thus find that

$$\begin{aligned}\hat{G}_\Phi^\dagger\Big(\prod_{r=1}^R \hat{\psi}_{r,l}\Big)\hat{G}_\Phi &= \sum_{\sigma\in S_R}\mathrm{sgn}(\sigma)\Big(\prod_{r=1}^R (G_\Phi)_{r,\sigma_r}\Big)\Big(\prod_{r=1}^R \hat{\psi}_{r,l}\Big)\\ &= \det(G_\Phi)\prod_{r=1}^R \hat{\psi}_{r,l}\\ &= \mathrm{e}^{\mathrm{i}\,\mathrm{tr}_R(\Phi)/2}\prod_{r=1}^R \hat{\psi}_{r,l},\end{aligned} \tag{E3}$$

which shows that the product of field operators is invariant under transformation $\hat{G}_\Phi$ if $\mathrm{tr}_R(\Phi) = 0$. Otherwise, the product acquires a phase factor.

We next consider the action of $\hat{G}_\Phi$ on a permutation-symmetric R-replica N-particle Slater determinant as given in Eq. (41). With the above results, we can straightforwardly deduce the action of $\hat{G}_\Phi^\dagger$ on this state:

$$\begin{aligned}\hat{G}_\Phi^\dagger|\psi_{R,N}\rangle &= s_{N,R}\prod_{n=1}^N\prod_{r=1}^R\sum_{l=1}^L \psi_{l,n}\hat{G}_\Phi^\dagger\hat{\psi}_{r,l}^\dagger\hat{G}_\Phi|0\rangle\\ &= s_{N,R}\prod_{n=1}^N\prod_{r=1}^R\sum_{r'=1}^R (G_\Phi)^*_{r,r'}\sum_{l=1}^L \psi_{l,n}\hat{\psi}_{r,l}^\dagger|0\rangle\\ &= \mathrm{e}^{-\mathrm{i}N\,\mathrm{tr}_R(\Phi)/2}|\psi_{R,N}\rangle.\end{aligned} \tag{E4}$$

In the first equality, we have used the fact that $\hat{G}_\Phi^\dagger|0\rangle = |0\rangle$, and the fact that exchanging the order of products over r and n in Eq. (41) leads merely to a sign factor $s_{N,R} = (-1)^{N(N-1)R(R-1)/4}$; in the second equality, we have employed Eq. (43); finally, proceeding as in Eq. (E3) establishes the third equality.

As explained above, we may focus on the restriction of $\prod_{r=1}^R \hat{M}_r$ to a map from R-replica N-particle Slater determinants $|\psi_{R,N}\rangle$, Eq. (41), to the same type of state but with $N + \Delta N$ particles. Under this restriction and with Eq. (E4), we find that

$$\hat{G}_\Phi^\dagger\Big(\prod_{r=1}^R \hat{M}_r\Big)\hat{G}_\Phi = \mathrm{e}^{-\mathrm{i}\Delta N\,\mathrm{tr}_R(\Phi)/2}\prod_{r=1}^R \hat{M}_r. \tag{E5}$$

Combining this result with our observation that a particle-number-conserving Hamiltonian is symmetric under $\hat{G}_\Phi$ establishes Eq. (44). In the latter, ΔN is the total change of the number of particles, accumulated over all measurements contained in Eq. (33).

2. Symmetry of the measurement Lagrangian under $\mathcal{R}_\Phi$

To show that rotations of the form $\mathcal{R}_\Phi$ are a symmetry of the measurement Lagrangian for fermion counting, Eq. (61), we first perform two auxiliary calculations. We define the adjoint action of a matrix A on a matrix B as $\mathcal{A}_A B = [A, B]$. Then,

$$\begin{aligned}\mathcal{R}_\Phi^{-1}\tau_\pm\mathcal{R}_\Phi &= \sum_{n=0}^\infty \frac{(-\mathrm{i})^n}{n!}\mathcal{A}^n_{\Phi\sigma_x/2}\tau_\pm = \sum_{n=0}^\infty \frac{(\mp\mathrm{i}\Phi)^n}{n!}\tau_\pm\\ &= \tau_\pm \mathrm{e}^{\mp\mathrm{i}\Phi},\end{aligned} \tag{E6}$$

where we have used the fact that $\tau_\pm$ is invariant—up to a change of sign—under multiplication by σ_x from both the left and the right, $\sigma_x\tau_\pm = \pm\tau_\pm$ and $\tau_\pm\sigma_x = \mp\tau_\pm$, which can be combined to $\mathcal{A}_{\sigma_x}\tau_\pm = \pm 2\tau_\pm$. Next, for a matrix A in the Keldysh and replica spaces, we consider

$$\begin{aligned}\mathrm{tr}_K(\mathcal{R}_\Phi\tau_\pm A\mathcal{R}_\Phi^{-1}) &= \sum_{n=0}^\infty \frac{\mathrm{i}^n}{n!}\mathrm{tr}_K(\mathcal{A}^n_{\Phi\sigma_x/2}\tau_\pm A)\\ &= \sum_{n=0}^\infty \frac{\mathrm{i}^n}{n!}\mathcal{A}^n_{\Phi/2}\,\mathrm{tr}_K(\sigma_x^n\tau_\pm A)\\ &= \sum_{n=0}^\infty \frac{(\pm\mathrm{i})^n}{n!}\mathcal{A}^n_{\Phi/2}\,\mathrm{tr}_K(\tau_\pm A)\\ &= \mathrm{e}^{\pm\mathrm{i}\Phi/2}\,\mathrm{tr}_K(\tau_\pm A)\mathrm{e}^{\mp\mathrm{i}\Phi/2}.\end{aligned} \tag{E7}$$

These two results and $\det_R(\mathrm{e}^{\mp\mathrm{i}\Phi}) = \mathrm{e}^{\mp\mathrm{i}\,\mathrm{tr}_R(\Phi)} = 1$ lead to

$$\begin{aligned}\det_R[\mathrm{tr}_K(\tau_\pm\mathcal{R}_\Phi\mathcal{G}\mathcal{R}_\Phi^{-1})] &= \det_R[\mathrm{tr}_K(\mathcal{R}_\Phi\tau_\pm\mathrm{e}^{\mp\mathrm{i}\Phi}\mathcal{G}\mathcal{R}_\Phi^{-1})]\\ &= \det_R[\mathrm{e}^{\pm\mathrm{i}\Phi/2}\,\mathrm{tr}_K(\tau_\pm\mathrm{e}^{\mp\mathrm{i}\Phi}\mathcal{G})\mathrm{e}^{\mp\mathrm{i}\Phi/2}]\\ &= \det_R(\mathrm{e}^{\mp\mathrm{i}\Phi})\det_R[\mathrm{tr}_K(\tau_\pm\mathcal{G})]\\ &= \det_R[\mathrm{tr}_K(\tau_\pm\mathcal{G})],\end{aligned} \tag{E8}$$

showing that the transformation $\mathcal{G} \mapsto \mathcal{R}_\Phi\mathcal{G}\mathcal{R}_\Phi^{-1}$ is indeed a symmetry of Eq. (61) for $R > 1$.

The above derivation relies on $\tau_\pm$ being invariant under multiplication by σ_x. This invariance does not apply to multiplication by σ_y or σ_z. Therefore, rotations with σ_x replaced by σ_y or σ_z are not symmetries of the measurement Lagrangian.

3. Breaking of the symmetry due to inefficient detection

Finally, we elaborate on condition (ii) in Sec. V E that the outcomes of all measurements have to be recorded. To prove the necessity of imposing this condition, we demonstrate the breaking of the symmetry due to inefficient detection. As discussed, for example, in Ref. [76], inefficient detection can be modeled by averaging over a finite fraction of the measurement outcomes. Here, we focus on fully inefficient detection, as described by the unconditional dynamics of R replicas.

But, for the moment, let us disregard measurements and focus on the Hamiltonian dynamics of an isolated system. The total system is subdivided into two parts, the system of interest and a reservoir. Conservation of the total number of particles is reflected, via the Noether theorem, in a global continuous U(1) symmetry of the Hamiltonian. When we integrate out the reservoir to obtain a description of the system alone, the U(1) symmetry of the total system becomes a strong or a weak U(1) symmetry of the system dynamics if particles cannot or can be exchanged between the system and reservoir, respectively [108,109]. The former case is realized in the unconditional dynamics obtained by averaging over the outcomes of occupation measurements; the latter case applies to the unconditional dynamics under fermion counting. For a single replica, the relevant phase rotation symmetries are $\psi_\pm \mapsto e^{i\phi_\pm}\psi_\pm$. The strong symmetry is equivalent to invariance of the Keldysh action under this transformation for arbitrary choices of ϕ_+ and ϕ_-. For the weak symmetry, invariance of the action is required only for $\phi_+ = \phi_-$. Let us now consider the unconditional dynamics of R replicas under fermion counting. This is described by a contribution to the Keldysh action of the form given in Eq. (52), but with a sum instead of a product over replicas, that is, $\sum_{r=1}^{R}(\psi_{+,r}\psi^*_{-,r} + \psi^*_{+,r}\psi_{-,r}) = \psi^\dagger_+\psi_- - \psi^\dagger_-\psi_+$. Evidently, this term is symmetric under transformation (70) with $\Phi_+ = \Phi_-$, which generalizes the weak U(1) symmetry associated with conservation of the number of particles in the total system to R replicas. However, the strong SU(R) symmetry underlying the NLSM, given by Eq. (70) with arbitrary $\Phi_\pm$, is broken. The breaking of the latter symmetry can also be understood in the operator formalism, where the unconditional dynamics is described by Liouvillian (21), or on the level of quantum states: in the unconditional dynamics, an initially pure state with N particles evolves into an incoherent mixture of states with different numbers of particles [104,105]. However, as shown above, the strong SU(R) symmetry requires the system to be in a pure state with a fixed number of particles at all times.

These considerations show that the conservation of the total number of particles in the system and reservoirs is not sufficient to guarantee the existence of a strong SU(R) symmetry. An additional necessary requirement is that each exchange of particles between the system and reservoirs has to be detected, such that the system remains in a pure state.

APPENDIX F: FLUCTUATION EXPANSION OF THE KELDYSH ACTION

To obtain the variation of the Keldysh action with respect to $\mathcal{G}$ and thereby find the saddle-point manifolds described by Eqs. (78) and (79), and to derive the action that governs the Gaussian theory discussed in Sec. VI, we perform an expansion of the Keldysh action around its saddle points.

1. Fluctuation expansion of the measurement Lagrangian for fermion counting

The existence of a manifold of saddle points rather than just a single isolated saddle point is a direct consequence of the symmetries of the action. Therefore, to establish the full manifold, it is sufficient to show that a single point on the manifold is indeed a saddle point. For the manifold described by Eqs. (76) and (78), a convenient choice is given by $Q = \sigma_z$, where we omit the identity 1_R in replica space for brevity. We parametrize fluctuations around this configuration as $\mathcal{G} = -i(\sigma_z + \delta Q_\mathcal{G})/2$. Inserting this expression into Eq. (61), we obtain

$$i\mathcal{L}_M = \frac{1}{2^R}\sum_{\alpha=\pm}\det{}_R[1 - i\,\mathrm{tr}_K(\tau_\alpha \delta Q_\mathcal{G})] - 1. \tag{F1}$$

By expanding the determinant using

$$\det(1+\epsilon X) = 1 + \epsilon\,\mathrm{tr}(X) - \frac{\epsilon^2}{2}[\mathrm{tr}(X^2) - \mathrm{tr}(X)^2] + O(\epsilon^3), \tag{F2}$$

we find that, to zeroth and first orders in $\delta Q_\mathcal{G}$,

$$i\mathcal{L}^{(0)}_M = \frac{1}{2^{R-1}} - 1, \qquad i\mathcal{L}^{(1)}_M = \frac{1}{2^R}\,\mathrm{tr}(\sigma_z \delta Q_\mathcal{G}). \tag{F3}$$

There are two contributions of second order. The first one is

$$\begin{aligned} \mathrm{i}\mathcal{L}_M^{(2,1)} &= \frac{1}{2^{R+1}} \sum_{\alpha=\pm} \mathrm{tr}_R[\mathrm{tr}_K(\tau_\alpha \delta Q_\mathcal{G})^2] \\ &= -\frac{1}{2^{R+2}} \sum_{r,r'=1}^{R} [\mathrm{tr}_K(\sigma_z \delta Q_{\mathcal{G},r,r'})\, \mathrm{tr}_K(\sigma_z \delta Q_{\mathcal{G},r',r}) \\ &\quad - \mathrm{tr}_K(\sigma_y \delta Q_{\mathcal{G},r,r'})\, \mathrm{tr}_K(\sigma_y \delta Q_{\mathcal{G},r',r})]. \end{aligned} \tag{F4}$$

For fixed replica indices r and r', $\delta Q_{\mathcal{G},r,r'}$ is a 2×2 matrix in Keldysh space. To simplify Eq. (F4), we can therefore use the following relation between determinants and traces of 2×2 matrices A and B:

$$\det(A+B) = \det(A) + \det(B) + \mathrm{tr}(A)\,\mathrm{tr}(B) - \mathrm{tr}(AB). \tag{F5}$$

This allows us to express the products of traces in Eq. (F4) as

$$\begin{aligned} &\mathrm{tr}_K(\sigma_z \delta Q_{\mathcal{G},r,r'})\, \mathrm{tr}_K(\sigma_z \delta Q_{\mathcal{G},r',r}) \\ &\quad = \mathrm{tr}_K(\sigma_z \delta Q_{\mathcal{G},r,r'} \sigma_z \delta Q_{\mathcal{G},r',r}) - \det{}_K(\delta Q_{\mathcal{G},r,r'} + \delta Q_{\mathcal{G},r',r}) \\ &\qquad + \det{}_K(\delta Q_{\mathcal{G},r,r'}) + \det{}_K(\delta Q_{\mathcal{G},r',r}), \end{aligned} \tag{F6}$$

and analogously for the terms involving σ_y. The terms that contain $\det_K$ cancel in the difference between terms involving σ_z and σ_y in Eq. (F4). We thus obtain

$$\mathrm{i}\mathcal{L}_M^{(2,1)} = -\frac{1}{2^{R+2}} \mathrm{tr}[(\sigma_z \delta Q_\mathcal{G})^2 - (\sigma_y \delta Q_\mathcal{G})^2]. \tag{F7}$$

The second contribution of second order reads

$$\begin{aligned} \mathrm{i}\mathcal{L}_M^{(2,2)} &= -\frac{1}{2^{R+1}} \sum_{\alpha=\pm} \mathrm{tr}_R[\mathrm{tr}_K(\tau_\alpha \delta Q_\mathcal{G})]^2 \\ &= \frac{1}{2^{R+2}} [\mathrm{tr}(\sigma_z \delta Q_\mathcal{G})^2 - \mathrm{tr}(\sigma_y \delta Q_\mathcal{G})^2]. \end{aligned} \tag{F8}$$

Using the first-order contribution in Eq. (F3), we can derive the saddle-point equation $\delta S/\delta \mathcal{G} = \mathrm{i}2(\delta S/\delta Q_\mathcal{G}) = 0$, leading to $\Sigma = \gamma Q/2^{R-1}$ with $Q = \sigma_z$ as expected.

2. Fluctuation expansion of the measurement Lagrangian for occupation measurements

To obtain the saddle-point manifold and derive the Gaussian theory of Sec. VI, it is sufficient to expand the measurement Lagrangian in fluctuations around a particular saddle point, which can be chosen as $Q = \Lambda$ for occupation measurements. However, the derivation of the NLSM for occupation measurements requires an expansion around Q_0 given in Eq. (109), which reduces to $Q_0 = \Lambda$ for $\mathcal{R}_\phi = \mathcal{R}_\theta = 1$. From Λ given in Eq. (77), Q_0 inherits the properties $Q_0^2 = 1$, $\mathrm{tr}_K(Q_0) = 0$, and $\det_K(Q_0) = -1$. Inserting $\mathcal{G} = -\mathrm{i}(Q_0 + \delta Q_\mathcal{G})/2$ into Eq. (62), we obtain

$$\begin{aligned} \mathrm{i}\mathcal{L}_M = \frac{1}{(4n)^R} \{ &\det[1 - \sigma_x(Q_0 + \delta Q_\mathcal{G})] \\ &+ \mathrm{tr}_K(\sigma_x \delta Q_\mathcal{G}) + 2R(1 - 2\rho_0)\} - 1, \end{aligned} \tag{F9}$$

where ρ_0 is defined in Eq. (115). A more convenient form for the expansion of the determinant in $\delta Q_\mathcal{G}$ is given by

$$\begin{aligned} &\det[1 - \sigma_x(Q_0 + \delta Q_\mathcal{G})] \\ &\quad = [-\det{}_K(\sigma_x - Q_0)]^R \det[1 - (\sigma_x - Q_0)^{-1} \delta Q_\mathcal{G}]. \end{aligned} \tag{F10}$$

To calculate the inverse $(\sigma_x - Q_0)^{-1}$, we use the following relation, which is valid for any invertible 2×2 matrix A:

$$A^{-1} = \frac{1}{\det(A)} [\mathrm{tr}(A) - A]. \tag{F11}$$

Furthermore, using Eq. (F5), we obtain $\det_K(\sigma_x - Q_0) = -4\rho_0$. We thus find that

$$\begin{aligned} &\frac{1}{(4n)^R} \det[1 - \sigma_x(Q_0 + \delta Q_\mathcal{G})] \\ &\quad = \frac{\rho_0^R}{n^R} \det\left(1 + \frac{Q_0 - \sigma_x}{4\rho_0} \delta Q_\mathcal{G}\right). \end{aligned} \tag{F12}$$

Then, employing Eq. (F2) to expand $\mathrm{i}\mathcal{L}_M$ to second order in $\delta Q_\mathcal{G}$, we obtain

$$\mathrm{i}\mathcal{L}_M^{(0)} = \frac{\rho_0^R}{n^R} + \frac{2R}{(4n)^R}(1 - 2\rho_0) - 1, \tag{F13a}$$

$$\mathrm{i}\mathcal{L}_M^{(1)} = \frac{\rho_0^{R-1}}{4n^R} \mathrm{tr}[(Q_0 - \sigma_x)\delta Q_\mathcal{G}] + \frac{1}{(4n)^R} \mathrm{tr}(\sigma_x \delta Q_\mathcal{G}), \tag{F13b}$$

$$\mathrm{i}\mathcal{L}_M^{(2,1)} = -\frac{\rho_0^{R-2}}{32n^R} \mathrm{tr}\{[(Q_0 - \sigma_x)\delta Q_\mathcal{G}]^2\}, \tag{F13c}$$

$$\mathrm{i}\mathcal{L}_M^{(2,2)} = \frac{\rho_0^{R-2}}{32n^R} \mathrm{tr}[(Q_0 - \sigma_x)\delta Q_\mathcal{G}]^2. \tag{F13d}$$

To show that $Q = \Lambda$ is a saddle point, we can replace Q_0 by Λ in the expansion above, leading to $\rho_0 = n$. Then, the solution to $\delta S/\delta \mathcal{G} = 0$ is given by

$$\Sigma = \frac{\gamma}{2n} \left\{ \Lambda - \left[1 - \frac{1}{(4n)^{R-1}} \right] \sigma_x \right\}. \tag{F14}$$

The Pauli matrix σ_x in Keldysh space corresponds to a nonvanishing anti-Keldysh component of the self-energy and thus violates the usual causality structure. However, in the replica limit $R \to 1$, the coefficient of σ_x vanishes, and we recover the expected causal result $\Sigma = \gamma Q/(2n)$ with $Q = \Lambda$.

3. Expansion of the full action

Next, we expand the action (67) in fluctuations around the particular saddle points given by Eqs. (78) and (79) with $\mathcal{R}_\Phi = \mathcal{R}_\phi = 1$. For simplicity, we set $R = 1$ in all numerical factors. Then, fluctuations around the saddle points can be parametrized as $\Sigma = \gamma(\Lambda + \delta Q_\Sigma)/(2n)$, where $n = 1/2$ for fermion counting or occupation measurements at half filling.

The saddle-point self-energy $\Sigma = \gamma\Lambda/(2n)$ obeys the familiar causality structure of propagators in Keldysh field theory. Therefore, at the saddle point, $\mathrm{Tr}[\ln(G^{-1})] = 0$ and $\mathrm{Tr}(\mathcal{G}\Sigma) = 0$ [107]. For fermion counting with $A = 0$ in Eq. (67), this implies that $\mathrm{i}S_0^{(0)} = 0$. Furthermore, according to Eq. (F3), $\mathrm{i}\mathcal{L}_M^{(0)} = 0$ also, so that the Keldysh action vanishes at the saddle point, in agreement with the expected normalization $Z_R(t) = 1$ of the Keldysh partition function in the replica limit $R \to 1$. For occupation measurements, matrix A in Eq. (66) involves an anti-Keldysh component, leading to a nonvanishing contribution

$$\mathrm{i}S_0^{(0)} = \mathrm{i}\,\mathrm{Tr}(GA) = -\frac{\gamma LT}{2n}(1-2n), \tag{F15}$$

where we have set $G = \Lambda$, L is the system size, and $T = t - t_0$ is the total evolution time. However, this contribution is canceled by the measurement action: from Eq. (F13a), with $\rho_0 = n$ at the saddle point $Q_0 = \Lambda$, we obtain

$$\mathrm{i}\gamma S_M^{(0)} = \mathrm{i}\gamma \int \mathrm{d}^2\mathbf{x}\,\mathcal{L}_M^{(0)} = \frac{\gamma LT}{2n}(1-2n), \tag{F16}$$

such that $\mathrm{i}(S_0^{(0)} + \mathrm{i}\gamma S_M^{(0)}) = 0$.

In an expansion around a saddle point, there is no contribution of first order. To second order in δQ_Σ, we find that

$$\mathrm{i}S_0^{(2)} = \frac{1}{4\tau_0}\,\mathrm{Tr}\left(\frac{1}{2\tau_0} G\delta Q_\Sigma G\delta Q_\Sigma - \delta Q_\Sigma \delta Q_\mathcal{G}\right), \tag{F17}$$

where $\tau_0 = n/\gamma$. The dressed Green function in momentum space is defined as

$$\begin{aligned} G_q(\omega) &= [\omega - \xi_q + \mathrm{i}\Lambda/(2\tau_0)]^{-1} \\ &= \tfrac{1}{2}G_q^R(\omega)(1+\Lambda) + \tfrac{1}{2}G_q^A(\omega)(1-\Lambda), \end{aligned} \tag{F18}$$

where $\xi_q = -2J\cos(q)$ and retarded G^R and advanced G^A Green's functions are given by

$$G_q^{R/A}(\omega) = \frac{1}{\omega - \xi_q \pm \mathrm{i}/(2\tau_0)}. \tag{F19}$$

Indeed, as stated in the main text in Eq. (82), only the diffusion block $\mathcal{B}_l(t) = G_l^R(t)G_{-l}^A(-t)$ contributes to Eq. (F17).

APPENDIX G: DERIVATION OF THE NLSM

As explained in Sec. VII, the parametrization in Eqs. (107) and (109) is chosen such that the symmetries of the action that are broken spontaneously by the saddle point $Q = \Lambda$ and thus give rise to Goldstone modes appear explicitly. For fermion counting, these are rotations of the form $\mathcal{R}_\Phi$, Eq. (108); for generalized occupation measurements, rotations of the form $\mathcal{R}_\phi$, Eq. (110), are also a symmetry of the action. The NLSM describes fluctuations of the corresponding massless Goldstone modes, and is obtained by integrating out the massive fluctuations described by Θ, θ, and, for fermion counting, ϕ.

To derive the NLSM, we first take the spatial continuum limit, in which matrix H defined in Eq. (47) is replaced by a differential operator containing derivatives with respect to a continuous spatial coordinate x. Inserting Eq. (106) into action (67) and performing an expansion in spatial and temporal derivatives yields a Lagrangian of the form [107]

$$\mathrm{i}\mathcal{L}_0[Q] = \mathrm{tr}\left[\frac{1}{2}\Lambda\mathcal{R}^{-1}\partial_t\mathcal{R} - \frac{\nu}{8}(\partial_x Q)^2\right] - \frac{\gamma}{2n}(1-2n), \tag{G1}$$

where $\nu = 2nJ^2/\gamma$. In the term $\mathrm{i}\,\mathrm{Tr}(GA)$ in Eq. (67), we have neglected derivatives of $\mathcal{R}$, which would be multiplied by an additional small parameter $A \sim \gamma$. Rotations of the form $\mathcal{R}_\Phi$, Eq. (108), being a symmetry of the action and, in particular, commuting with A, drop out of $\mathrm{i}\,\mathrm{Tr}(GA)$. Then, expanding $\mathrm{i}\,\mathrm{Tr}(GA)$ in the massive mode Θ leads to terms of second order in γ, which should be dropped on our order of approximation. The same reasoning can be repeated for the rotations given in Eq. (110). Consequently, in Eq. (G1) we have replaced the term $\mathrm{i}\,\mathrm{Tr}(GA)$ by its value on the saddle point given in (F15).

The expansion of the derivative terms in Eq. (G1) in Θ is detailed in Ref. [42] and yields

$$\begin{aligned} \mathrm{i}\mathcal{L}_0[Q] = \mathrm{tr}&\left[\frac{1}{2}\Lambda\mathcal{R}_0^{-1}\partial_t\mathcal{R}_0 - \frac{\nu}{8}(\partial_x Q_0)^2\right] \\ &+ \frac{1}{4}\,\mathrm{tr}_K(Q_0\sigma_z)\,\mathrm{tr}_R[\Theta U^{-1/2}(\partial_t U)U^{-1/2}] \\ &- \nu\rho_0(1-\rho_0)\,\mathrm{tr}_R[(\partial_x U^{-1})(\partial_x U)] - \frac{\gamma}{2n}(1-2n), \end{aligned} \tag{G2}$$

where $\mathcal{R}_0 = \mathcal{R}_\phi\mathcal{R}_\theta$, $U = \mathrm{e}^{\mathrm{i}\Phi}$, and ρ_0 is defined in Eq. (115).

We focus now for the moment on the replica-symmetric sector of the theory, setting $R = 1$. Since θ is a massive mode for both fermion counting and occupation measurements, we expand $\mathcal{L}_0$ to second order in θ. Furthermore, we drop terms that contain $\partial_t\theta$ and $\partial_t\phi$ and no other fields. Such terms contribute to the action only at the initial and

final time. However, these contributions vanish. We thus find that, with $f = 1 - 2n$,

$$\begin{aligned} \mathrm{i}\mathcal{L}_0[Q_0] = &-\frac{\mathrm{i}}{4}(2+f\theta)\theta\partial_t\phi \\ &-\frac{\nu}{4}\{[1-f^2+2f\theta-(1-f^2)\theta^2](\partial_x\phi)^2 \\ &\quad -\mathrm{i}2f(f-\theta)(\partial_x\phi)(\partial_x\theta) \\ &\quad +(1+f^2)(\partial_x\theta)^2\} - \frac{f\gamma}{2n}. \end{aligned} \tag{G3}$$

Returning to $R > 1$, we next consider the contribution from the measurement Lagrangian, given in Eqs. (61) and (62) for fermion counting and occupation measurements, respectively, where we insert Eq. (106). The parametrization of rotations in Eq. (107) is chosen such that $\mathcal{R}_\Phi$, being a symmetry of the Lagrangian for both models, drops out. For fermion counting, $\mathcal{R}_\Phi$ is the only symmetry. Therefore, we can expand Q to second order in the massive modes Θ, ϕ, and θ,

$$\mathcal{R}_\Theta Q_0 \mathcal{R}_\Theta^{-1} = \sigma_z + \delta Q, \tag{G4}$$

where

$$\delta Q = \phi\sigma_y - \theta\sigma_x - \frac{\theta^2}{2}\sigma_z - \frac{\phi^2}{2}\sigma_z - \frac{\Theta^2}{2}\sigma_z - \Theta(\sigma_x + \sigma_z\theta). \tag{G5}$$

Then, using Eqs. (F3), (F7), and (F8), we obtain

$$\mathrm{i}\mathcal{L}_M[Q] = -\tfrac{1}{2}[\mathrm{tr}_R(\Theta^2) + \theta^2 + \phi^2], \tag{G6}$$

where we have set $R = 1$ in all numerical factors, such that $\mathcal{L}_M^{(0)}$, given in Eq. (F3), vanishes.

For occupation measurements, $\mathcal{R}_\phi$ is also a symmetry. Therefore, we cannot expand Q in ϕ as we did for fermion counting, and Eqs. (G4) and (G5) have to be replaced by

$$\mathcal{R}_\Theta Q_0 \mathcal{R}_\Theta^{-1} = Q_0 + \delta Q, \tag{G7}$$

where

$$\delta Q = \frac{\mathrm{i}}{2}\Theta[\sigma_y, Q_0] - \frac{\Theta^2}{4}(Q_0 - \sigma_y Q_0 \sigma_y). \tag{G8}$$

Inserting Eq. (G7) into Eqs. (F13) we obtain an expansion of the measurement Lagrangian in Θ,

$$\mathrm{i}\mathcal{L}_M = \frac{f}{2n} - \frac{1}{32n\rho_0}\,\mathrm{tr}_K(\sigma_z Q_0)^2\,\mathrm{tr}_R(\Theta^2). \tag{G9}$$

To find the replica-symmetric Lagrangian for fermion counting, we can simplify Eq. (G3) further by setting $f = 0$, performing an expansion to second order in both ϕ and θ, and omitting the last term that stems from $\mathrm{i}\,\mathrm{tr}(GA)$. Then, combining Eq. (G3) with Eq. (G6) yields Eq. (111). For occupation measurements, combining Eq. (G3) with Eq. (G9) we obtain Eq. (112). In the replicon sector described by the modes Φ and Θ, integration over Θ leads to Eq. (113) for both models.

APPENDIX H: MODIFIED NLSM FOR PARTICLE-HOLE SYMMETRIC HAMILTONIANS

Through the gauge transformation $\hat{\psi}_l \mapsto \mathrm{i}^l\hat{\psi}_l$, the hopping matrix H in Eq. (47) becomes purely imaginary, and obeys the PHS condition $H = -H^\intercal$. As we discuss here, PHS modifies the target manifold of the NLSM [19,52,54]. We summarize only the key steps in the derivation of the modified NLSM. Details of the derivation will be presented elsewhere.

We begin by explicitly symmetrizing the action with respect to PHS. Consider first the Hamiltonian contribution to action (46). After the above gauge transformation and the Larkin-Ovchinnikov rotation (56), this contribution can be written as

$$\begin{aligned} \psi^\dagger H\psi &= \tfrac{1}{2}\psi^\dagger(H - H^\intercal)\psi \\ &= \tfrac{1}{2}(\psi^\dagger H\psi + \psi^\intercal H\psi^*) = \bar{\Psi}H\Psi, \end{aligned} \tag{H1}$$

where we have introduced the vectors of fields,

$$\Psi = \frac{1}{\sqrt{2}}\begin{pmatrix}\psi \\ \mathrm{i}\sigma_y\psi^*\end{pmatrix}, \quad \bar{\Psi} = \frac{1}{\sqrt{2}}[\psi^\dagger, \psi(-\mathrm{i}\sigma_y)] = \Psi^\intercal\mathcal{C}. \tag{H2}$$

For fixed lattice site index l, the vectors $\Psi_l(t)$ and $\bar{\Psi}_l(t)$ have $4R$ components in the combined Keldysh, charge-conjugation, and replica space. The charge-conjugation matrix is defined as $\mathcal{C} = \sigma_y \otimes \sigma_y$, where the first and second factors of σ_y act in the Keldysh and charge-conjugation spaces, respectively, and the identity in replica space is left implicit.

The matrices $\pm\mathrm{i}\sigma_y$ in Eq. (H2) are not required to symmetrize the Hamiltonian contribution to the action. However, for these definitions of Ψ and $\bar{\Psi}$, the measurement vertices in Eqs. (57) and (58) also take forms that do not have any structure in charge-conjugation space and are thus manifestly particle-hole symmetric: for fermion counting, we obtain

$$V_\pm[\bar{\Psi}, \Psi] = \mathrm{i}\bar{\Psi}\tau_\pm\Psi \tag{H3}$$

with matrices $\tau_\pm$, which are defined below Eq. (61), acting in Keldysh space; for generalized occupation measurements, we can write the measurement vertex in the

exponentiated form

$$V[\bar{\Psi},\Psi]=\frac{1}{4n}e^{2\bar{\Psi}\sigma_x\Psi}, \tag{H4}$$

again with matrix σ_x acting in Keldysh space.

As for broken PHS, the next step is to perform a generalized Hubbard-Stratonovich transformation. However, Eq. (60) has to be modified to an integration over Hermitian $4R\times 4R$ matrices $\mathcal{G}$ and Σ that obey the condition $\mathcal{G}=-\mathcal{C}\mathcal{G}^{\intercal}\mathcal{C}$, which follows from $\mathcal{G}=-i\Psi\bar{\Psi}$ and Eq. (H2). The measurement Lagrangian for fermion counting in Eq. (61) is thus replaced by

$$i\mathcal{L}_M=\sum_{\alpha=\pm}e^{\beta\,\mathrm{tr}_{CR}\{\ln[\mathrm{tr}_K(\tau_\alpha\mathcal{G}/\beta)]\}}-1, \tag{H5}$$

where $\beta=1/2$. Here and in the following, the corresponding expressions for broken PHS are recovered by setting $\beta=1$. The measurement Lagrangian for occupation measurements (62) becomes

$$i\mathcal{L}_M=\frac{1}{n^R}e^{\beta\,\mathrm{tr}[\ln(1/2-i\sigma_x\mathcal{G}/\beta)]}+\frac{i}{2^{2R-1}n^R}\mathrm{tr}(\sigma_x\mathcal{G})-1. \tag{H6}$$

Finally, action (67) also acquires a factor of $\beta=1/2$,

$$iS_0[\mathcal{G},\Sigma]=\mathrm{Tr}\{\beta[\ln(G^{-1})+iGA]-i\mathcal{G}\Sigma\}, \tag{H7}$$

where $A=0$ for fermion counting; for occupation measurements, A is defined in Eq. (66).

Next, we consider the saddle points of the particle-hole symmetrized action. Equation (76) becomes $\mathcal{G}=-i\beta Q/2$; in contrast, the self-energy can still be expressed through Q as in Eqs. (78) and (79). Note, however, that the replica-symmetric saddle point, $Q=Q_0\otimes 1_R$, is now determined by a 4×4 matrix Q_0 in the Keldysh and charge-conjugation spaces:

$$Q_0=\begin{pmatrix}\Lambda & 0\\ 0 & -\sigma_y\Lambda^{\intercal}\sigma_y\end{pmatrix} \tag{H8}$$

with Λ given in Eq. (77).

The target manifold of the NLSM can now be determined in three steps. (i) Identify the group G of transformations $Q\mapsto\mathcal{R}Q\mathcal{R}^{-1}$ that preserve Hermiticity as well as the generalized skew-symmetry condition $Q=-\mathcal{C}Q^{\intercal}\mathcal{C}$, and are symmetries of the action. In Keldysh space, these transformations are

$$\mathcal{R}=M\begin{pmatrix}\mathcal{V} & 0\\ 0 & \sigma_y\mathcal{V}^*\sigma_y\end{pmatrix}M, \tag{H9}$$

where $M=(1/\sqrt{2})\left(\begin{smallmatrix}1 & 1\\ 1 & -1\end{smallmatrix}\right)$ is the matrix form of the Larkin-Ovchinnikov rotation (56). For fermion counting, matrices $\mathcal{V}$ are in $G=\mathrm{SU}(2R)$; for occupation measurements, conservation of the number of particles results in an enlarged symmetry group $G=\mathrm{U}(2R)=\mathrm{U}(1)\rtimes\mathrm{SU}(R)$. (ii) Identify the subgroup $H\subset G$ of transformations that leave the saddle point Q_0 invariant. This is the case for matrices $\mathcal{V}$ that obey the condition $\mathcal{V}^{\intercal}\sigma_y\mathcal{V}=\sigma_y$ and thus form the compact symplectic group $H=\mathrm{Sp}(R)$. (iii) The target manifold of the NLSM is G/H. Focusing on the replicon sector of the theory, the target manifold of the NLSM for both fermion counting and generalized occupation measurements is thus $\mathrm{SU}(2R)/\mathrm{Sp}(R)$. Crucially, also in the presence of PHS, the target manifold of the replicon NLSM is not modified for fermion counting as compared to models with a conserved number of particles [52,54]. Particle-number conservation affects only the replica-symmetric sector: the U(1) NLSM becomes massive when particle-number conservation is broken by fermion counting.

[1] B. Misra and E. C. G. Sudarshan, The Zeno's paradox in quantum theory, J. Math. Phys. **18**, 756 (1977).

[2] Y. Li, X. Chen, and M. P. A. Fisher, Quantum Zeno effect and the many-body entanglement transition, Phys. Rev. B **98**, 205136 (2018).

[3] B. Skinner, J. Ruhman, and A. Nahum, Measurement-induced phase transitions in the dynamics of entanglement, Phys. Rev. X **9**, 031009 (2019).

[4] M. Szyniszewski, Entanglement transition from variable-strength weak measurements, Phys. Rev. B **100**, 064204 (2019).

[5] Y. Li, X. Chen, and M. P. A. Fisher, Measurement-driven entanglement transition in hybrid quantum circuits, Phys. Rev. B **100**, 134306 (2019).

[6] Y. Bao, Theory of the phase transition in random unitary circuits with measurements, Phys. Rev. B **101**, 104301 (2020).

[7] M. J. Gullans and D. A. Huse, Dynamical purification phase transition induced by quantum measurements, Phys. Rev. X **10**, 041020 (2020).

[8] X. Turkeshi, R. Fazio, and M. Dalmonte, Measurement-induced criticality in (2 + 1)-dimensional hybrid quantum circuits, Phys. Rev. B **102**, 014315 (2020).

[9] A. Zabalo, M. J. Gullans, J. H. Wilson, S. Gopalakrishnan, D. A. Huse, and J. H. Pixley, Critical properties of the measurement-induced transition in random quantum circuits, Phys. Rev. B **101**, 060301 (2020).

[10] Y. Bao, S. Choi, and E. Altman, Symmetry enriched phases of quantum circuits, Ann. Phys. (N. Y.). **435**, 168618 (2021).

[11] M. Ippoliti, M. J. Gullans, S. Gopalakrishnan, D. A. Huse, and V. Khemani, Entanglement phase transitions in measurement-only dynamics, Phys. Rev. X **11**, 011030 (2021).

[12] A. Nahum, Measurement and entanglement phase transitions in all-to-all quantum circuits, on quantum trees, and in Landau-Ginsburg theory, PRX Quantum **2**, 010352 (2021).

[13] A. Lavasani, Y. Alavirad, and M. Barkeshli, Measurement-induced topological entanglement transitions in symmetric random quantum circuits, Nat. Phys. **17**, 342 (2021).

[14] P. Sierant, M. Schirò, M. Lewenstein, and X. Turkeshi, Measurement-induced phase transitions in $(d+1)$-dimensional stabilizer circuits, Phys. Rev. B **106**, 214316 (2022).

[15] A. Zabalo, M. J. Gullans, J. H. Wilson, R. Vasseur, A. W. W. Ludwig, S. Gopalakrishnan, D. A. Huse, and J. H. Pixley, Operator scaling dimensions and multifractality at measurement-induced transitions, Phys. Rev. Lett. **128**, 050602 (2022).

[16] X. Yu and X.-L. Qi, Measurement-induced entanglement phase transition in random bilocal circuits, arXiv:2201.12704.

[17] U. Agrawal, A. Zabalo, K. Chen, J. H. Wilson, A. C. Potter, J. H. Pixley, S. Gopalakrishnan, and R. Vasseur, Entanglement and charge-sharpening transitions in U(1) symmetric monitored quantum circuits, Phys. Rev. X **12**, 41002 (2022).

[18] F. Barratt, U. Agrawal, S. Gopalakrishnan, D. A. Huse, R. Vasseur, and A. C. Potter, Field theory of charge sharpening in symmetric monitored quantum circuits, Phys. Rev. Lett. **129**, 120604 (2022).

[19] C.-M. Jian, B. Bauer, A. Keselman, and A. W. W. Ludwig, Criticality and entanglement in nonunitary quantum circuits and tensor networks of noninteracting fermions, Phys. Rev. B **106**, 134206 (2022).

[20] C.-M. Jian, H. Shapourian, B. Bauer, and A. W. W. Ludwig, Measurement-induced entanglement transitions in quantum circuits of non-interacting fermions: Born-rule versus forced measurements, arXiv:2302.09094.

[21] H. Oshima and Y. Fuji, Charge fluctuation and charge-resolved entanglement in a monitored quantum circuit with $U(1)$ symmetry, Phys. Rev. B **107**, 014308 (2023).

[22] S. P. Kelly, U. Poschinger, F. Schmidt-Kaler, M. P. A. Fisher, and J. Marino, Coherence requirements for quantum communication from hybrid circuit dynamics, SciPost Physics **15**, 250 (2023).

[23] Z. Weinstein, S. P. Kelly, J. Marino, and E. Altman, Scrambling transition in a radiative random unitary circuit, Phys. Rev. Lett. **131**, 220404 (2023).

[24] S. P. Kelly and J. Marino, Entanglement transitions induced by quantum-data collection, Phys. Rev. A **111**, L010402 (2025).

[25] S. P. Kelly and J. Marino, Generalizing measurement-induced phase transitions to information exchange symmetry breaking, Phys. Rev. A **111**, 012425 (2025).

[26] X. Cao, A. Tilloy, and A. De Luca, Entanglement in a fermion chain under continuous monitoring, SciPost Phys. **7**, 024 (2019).

[27] X. Chen, Emergent conformal symmetry in nonunitary random dynamics of free fermions, Phys. Rev. Res. **2**, 033017 (2020).

[28] A. Nahum, Entanglement and dynamics of diffusion-annihilation processes with Majorana defects, Phys. Rev. Res. **2**, 023288 (2020).

[29] O. Alberton, M. Buchhold, and S. Diehl, Entanglement transition in a monitored free-fermion chain: from extended criticality to area law, Phys. Rev. Lett. **126**, 170602 (2021).

[30] Q. Tang, Quantum criticality in the nonunitary dynamics of $(2+1)$-dimensional free fermions, Phys. Rev. B **103**, 174303 (2021).

[31] M. Buchhold, Y. Minoguchi, A. Altland, and S. Diehl, Effective theory for the measurement-induced phase transition of Dirac fermions, Phys. Rev. X **11**, 041004 (2021).

[32] M. Van Regemortel, Z.-P. Cian, A. Seif, H. Dehghani, and M. Hafezi, Entanglement entropy scaling transition under competing monitoring protocols, Phys. Rev. Lett. **126**, 123604 (2021).

[33] M. Coppola, E. Tirrito, D. Karevski, and M. Collura, Growth of entanglement entropy under local projective measurements, Phys. Rev. B **105**, 094303 (2022).

[34] F. Carollo and V. Alba, Entangled multiplets and unusual spreading of quantum correlations in a continuously monitored tight-binding chain, Phys. Rev. B **106**, L220304 (2022).

[35] B. Ladewig, S. Diehl, and M. Buchhold, Monitored open fermion dynamics: Exploring the interplay of measurement, decoherence, and free Hamiltonian evolution, Phys. Rev. Res. **4**, 033001 (2022).

[36] M. Buchhold, T. Müller, and S. Diehl, Revealing measurement-induced phase transitions by pre-selection, arXiv:2208.10506.

[37] X. Turkeshi, Enhanced entanglement negativity in boundary-driven monitored fermionic chains, Phys. Rev. B **106**, 024304 (2022).

[38] Q. Yang, Y. Zuo, and D. E. Liu, Keldysh nonlinear sigma model for a free-fermion gas under continuous measurements, Phys. Rev. Res. **5**, 033174 (2023).

[39] M. Szyniszewski, O. Lunt, and A. Pal, Disordered monitored free fermions, Phys. Rev. B **108**, 165126 (2023).

[40] H. Lóio, A. De Luca, J. De Nardis, and X. Turkeshi, Purification timescales in monitored fermions, Phys. Rev. B **108**, L020306 (2023).

[41] Y. Le Gal, X. Turkeshi, and M. Schirò, Volume-to-area law entanglement transition in a non-Hermitian free fermionic chain, SciPost Phys. **14**, 138 (2023).

[42] I. Poboiko, P. Pöpperl, I. V. Gornyi, and A. D. Mirlin, Theory of free fermions under random projective measurements, Phys. Rev. X **13**, 041046 (2023).

[43] I. Poboiko, I. V. Gornyi, and A. D. Mirlin, Measurement-induced phase transition for free fermions above one dimension, Phys. Rev. Lett. **132**, 110403 (2024).

[44] G. Kells, D. Meidan, and A. Romito, Topological transitions in weakly monitored free fermions, SciPost Phys. **14**, 031 (2023).

[45] M. Fava, L. Piroli, T. Swann, D. Bernard, and A. Nahum, Nonlinear sigma models for monitored dynamics of free fermions, Phys. Rev. X **13**, 041045 (2023).

[46] J. Merritt, Entanglement transitions with free fermions, Phys. Rev. B **107**, 064303 (2023).

[47] K. Klocke, Majorana loop models for measurement-only quantum circuits, Phys. Rev. X **13**, 041028 (2023).

[48] K. Chahine and M. Buchhold, Entanglement phases, localization, and multifractality of monitored free fermions in two dimensions, Phys. Rev. B **110**, 054313 (2024).

[49] M. Eissler, I. Lesanovsky, and F. Carollo, Unraveling-induced entanglement phase transition in diffusive trajectories of continuously monitored noninteracting fermionic systems, Phys. Rev. A **111**, 022205 (2025).

[50] L. Lumia, E. Tirrito, R. Fazio, and M. Collura, Measurement-induced transitions beyond Gaussianity: A single particle description, Phys. Rev. Res. **6**, 023176 (2024).

[51] M. Tsitsishvili, D. Poletti, M. Dalmonte, and G. Chiriacò, Measurement induced transitions in non-Markovian free fermion ladders, SciPost Phys. Core **7**, 011 (2024).

[52] M. Fava, L. Piroli, D. Bernard, and A. Nahum, Monitored fermions with conserved $U(1)$ charge, Phys. Rev. Res. **6**, 043246 (2024).

[53] H. Guo, M. S. Foster, C.-M. Jian, and A. W. W. Ludwig, Field theory of monitored, interacting fermion dynamics with charge conservation, arXiv:2410.07317.

[54] I. Poboiko, P. Pöpperl, I. V. Gornyi, and A. D. Mirlin, Measurement-induced transitions for interacting fermions, Phys. Rev. B **111**, 024204 (2025).

[55] Y. Fuji, Measurement-induced quantum criticality under continuous monitoring, Phys. Rev. B **102**, 054302 (2020).

[56] S. Goto and I. Danshita, Measurement-induced transitions of the entanglement scaling law in ultracold gases with controllable dissipation, Phys. Rev. A **102**, 033316 (2020).

[57] Q. Tang, Measurement-induced phase transition: A case study in the nonintegrable model by density-matrix renormalization group calculations, Phys. Rev. Research **2**, 013022 (2020).

[58] E. V. H. Doggen, Generalized quantum measurements with matrix product states: Entanglement phase transition and clusterization, Phys. Rev. Res. **4**, 023146 (2022).

[59] Y. Minoguchi, P. Rabl, and M. Buchhold, Continuous Gaussian measurements of the free boson CFT: A model for exactly solvable and detectable measurement-induced dynamics, SciPost Phys. **12**, 009 (2022).

[60] N. Lang, Entanglement transition in the projective transverse field Ising model, Phys. Rev. B **102**, 094204 (2020).

[61] D. Rossini, Measurement-induced dynamics of many-body systems at quantum criticality, Phys. Rev. B **102**, 035119 (2020).

[62] T. Botzung, S. Diehl, and M. Müller, Engineered dissipation induced entanglement transition in quantum spin chains: from logarithmic growth to area law, Phys. Rev. B **104**, 184422 (2021).

[63] X. Turkeshi, Measurement-induced entanglement transitions in the quantum Ising chain: from infinite to zero clicks, Phys. Rev. B **103**, 224210 (2021).

[64] Z. Weinstein, Nonlocality and entanglement in measured critical quantum Ising chains, Phys. Rev. B **107**, 245132 (2023).

[65] Z. Yang, Entanglement in a one-dimensional critical state after measurements, Phys. Rev. B **108**, 165120 (2023).

[66] E. Tirrito, A. Santini, R. Fazio, and M. Collura, Full counting statistics as probe of measurement-induced transitions in the quantum Ising chain, SciPost Phys. **15**, 096 (2023).

[67] C. Noel, P. Niroula, D. Zhu, A. Risinger, L. Egan, D. Biswas, M. Cetina, A. V. Gorshkov, M. J. Gullans, D. A. Huse, and C. Monroe, Measurement-induced quantum phases realized in a trapped-ion quantum computer, Nat. Phys. **18**, 760 (2022).

[68] U. Agrawal, J. Lopez-Piqueres, R. Vasseur, S. Gopalakrishnan, and A. C. Potter, Observing quantum measurement collapse as a learnability phase transition, Phys. Rev. X **14**, 041012 (2024).

[69] Google Quantum AI and Collaborators, Measurement-induced entanglement and teleportation on a noisy quantum processor, Nature **622**, 481 (2023).

[70] J. M. Koh, S.-N. Sun, M. Motta, and A. J. Minnich, Measurement-induced entanglement phase transition on a superconducting quantum processor with mid-circuit readout, Nat. Phys. **19**, 1314 (2023).

[71] H. Kamakari, J. Sun, Y. Li, J. J. Thio, T. P. Gujarati, M. P. Fisher, M. Motta, and A. J. Minnich, Experimental demonstration of scalable cross-entropy benchmarking to detect measurement-induced phase transitions on a superconducting quantum processor, Phys. Rev. Lett. **134**, 120401 (2025).

[72] M. A. Nielsen and I. L. Chuang, *Quantum Computation and Quantum Information* (Cambridge University Press, Cambridge, 2012), 10th ed.

[73] C. Gardiner and P. Zoller, *The Quantum World of Ultra-Cold Atoms and Light Book I: Foundations of Quantum Optics* (Imperial College Press, London, 2014), Vol. 2.

[74] C. Gardiner and P. Zoller, *The Quantum World of Ultra-Cold Atoms and Light Book II: The Physics of Quantum-Optical Devices* (Imperial College Press, London, 2015), Vol. 4.

[75] K. Jacobs and D. A. Steck, A straightforward introduction to continuous quantum measurement, Contemp. Phys. **47**, 279 (2006).

[76] H. M. Wiseman and G. J. Milburn, *Quantum Measurement and Control* (Cambridge University Press, Cambridge, 2009), 1st ed.

[77] P. Di Francesco, P. Mathieu, and D. Sénéchal, *Conformal Field Theory*, Graduate Texts in Contemporary Physics (Springer New York, New York, NY, 1997).

[78] C. Gardiner, *Stochastic Methods* (Springer Berlin, Heidelberg, Berlin, Heidelberg, 2009), 4th ed.

[79] P. Calabrese and J. Cardy, Entanglement entropy and conformal field theory, J. Phys. A Math. Theor. **42**, 504005 (2009).

[80] A. J. Daley, Quantum trajectories and open many-body quantum systems, Adv. Phys. **63**, 77 (2014).

[81] S. Gustavsson, R. Leturcq, M. Studer, I. Shorubalko, T. Ihn, K. Ensslin, D. C. Driscoll, and A. C. Gossard, Electron counting in quantum dots, Surf. Sci. Rep. **64**, 191 (2009).

[82] E. Starchl and L. M. Sieberer, Relaxation to a parity-time symmetric generalized Gibbs ensemble after a quantum quench in a driven-dissipative Kitaev chain, Phys. Rev. Lett. **129**, 220602 (2022).

[83] E. Starchl and L. M. Sieberer, Quantum quenches in driven-dissipative quadratic fermionic systems with parity-time symmetry, Phys. Rev. Res. **6**, 013016 (2024).

[84] D. S. Abrams and S. Lloyd, Simulation of many-body fermi systems on a universal quantum computer, Phys. Rev. Lett. **79**, 2586 (1997).

[85] G. Ortiz, J. E. Gubernatis, E. Knill, and R. Laflamme, Quantum algorithms for fermionic simulations, Phys. Rev. A **64**, 022319 (2001).

[86] S. B. Bravyi and A. Y. Kitaev, Fermionic quantum computation, Ann. Phys. (N. Y). **298**, 210 (2002).

[87] R. C. Ball, Fermions without fermion fields, Phys. Rev. Lett. **95**, 176407 (2005).

[88] F. Verstraete and J. I. Cirac, Mapping local Hamiltonians of fermions to local Hamiltonians of spins, J. Stat. Mech. Theory Exp. **2005**, P09012 (2005).

[89] J. D. Whitfield, J. Biamonte, and A. Aspuru-Guzik, Simulation of electronic structure Hamiltonians using quantum computers, Mol. Phys. **109**, 735 (2011).

[90] R. Barends *et al.*, Digital quantum simulation of fermionic models with a superconducting circuit, Nat. Commun. **6**, 7654 (2015).

[91] J. D. Whitfield, V. Havlíček, and M. Troyer, Local spin operators for fermion simulations, Phys. Rev. A **94**, 030301 (2016).

[92] D. González-Cuadra, D. Bluvstein, M. Kalinowski, R. Kaubruegger, N. Maskara, P. Naldesi, T. V. Zache, A. M. Kaufman, M. D. Lukin, H. Pichler, B. Vermersch, J. Ye, and P. Zoller, Fermionic quantum processing with programmable neutral atom arrays, Proc. Natl. Acad. Sci. **120**, 1 (2023).

[93] D. Bernard, T. Jin, and O. Shpielberg, Transport in quantum chains under strong monitoring, EPL (Europhysics Lett.) **121**, 60006 (2018).

[94] T. Chou, K. Mallick, and R. K. P. Zia, Non-equilibrium statistical mechanics: from a paradigmatic model to biological transport, Rep. Prog. Phys. **74**, 116601 (2011).

[95] K. Mallick, The exclusion process: A paradigm for non-equilibrium behaviour, Phys. A Stat. Mech. Appl. **418**, 17 (2015).

[96] D. T. Gillespie, Stochastic simulation of chemical kinetics, Annu. Rev. Phys. Chem. **58**, 35 (2007), pMID: 17037977.

[97] G. L. Daquila and U. C. Täuber, Slow relaxation and aging kinetics for the driven lattice gas, Phys. Rev. E **83**, 051107 (2011).

[98] I. Klich and L. Levitov, Quantum noise as an entanglement meter, Phys. Rev. Lett. **102**, 100502 (2009).

[99] H. F. Song, C. Flindt, S. Rachel, I. Klich, and K. Le Hur, Entanglement entropy from charge statistics: Exact relations for noninteracting many-body systems, Phys. Rev. B **83**, 161408 (2011).

[100] H. F. Song, S. Rachel, C. Flindt, I. Klich, N. Laflorencie, and K. Le Hur, Bipartite fluctuations as a probe of many-body entanglement, Phys. Rev. B **85**, 035409 (2012).

[101] K. H. Thomas and C. Flindt, Entanglement entropy in dynamic quantum-coherent conductors, Phys. Rev. B **91**, 125406 (2015).

[102] I. S. Burmistrov, K. S. Tikhonov, and I. V. Gornyi, Entanglement entropy and particle number cumulants of disordered fermions, Ann. Phys. (N. Y). **383**, 140 (2017).

[103] Strictly speaking, the tensor product of fermionic Fock spaces is not well defined. However, one can give meaning to such a tensor product by first mapping the fermionic Fock spaces to bosonic ones through a Jordan-Wigner transformation, then forming the tensor product of the bosonic spaces, and finally reintroducing fermionic operators in the product space [45].

[104] B. Buča and T. Prosen, A note on symmetry reductions of the Lindblad equation: Transport in constrained open spin chains, New J. Phys. **14**, 073007 (2012).

[105] V. V. Albert and L. Jiang, Symmetries and conserved quantities in Lindblad master equations, Phys. Rev. A **89**, 022118 (2014).

[106] A. Altland and B. D. Simons, *Condensed Matter Field Theory* (Cambridge University Press, Cambridge, 2010), 2nd ed.

[107] A. Kamenev, *Field Theory of Non-Equilibrium Systems* (Cambridge University Press, Cambridge, 2023), 2nd ed.

[108] L. M. Sieberer, M. Buchhold, and S. Diehl, Keldysh field theory for driven open quantum systems, Rep. Prog. Phys. **79**, 096001 (2016).

[109] L. M. Sieberer, M. Buchhold, J. Marino, and S. Diehl, Universality in driven open quantum matter, Rev. Mod. Phys. **97**, 025004 (2025).

[110] One might wonder whether the replica Keldysh action agrees in the limit $R \to 1$ with the Keldysh action corresponding to the master equation that is obtained by averaging the stochastic Schrödinger equation (3) over the increments $\mathrm{d}N_{\alpha,l}(t)$. For occupation measurements, this is not the case. In the derivation of the replica Keldysh action, we have used the rate of jumps in Eq. (10). This rate reduces to γ only for $N = L/2$. Moreover, this rate is calculated using the operator identity $\sum_{l=1}^{L} \hat{\psi}_l^\dagger \hat{\psi}_l = N$. In contrast, in the master equation, the rate of jumps is encoded implicitly in the anticommutator in Eq. (21), which yields additional terms in the Keldysh action.

[111] This is a purely technical issue and does not imply that the dynamics is noncausal.

[112] According to the terminology introduced in Ref. [108], invariance of the Keldysh action under phase rotations with opposite signs on the forward and backward branches is an example of a quantum symmetry. For equal signs, we speak of a classical symmetry. In the operator formalism, a classical symmetry corresponds to a weak symmetry, and the combination of classical and quantum symmetries is equivalent to a strong symmetry [104,105]. A definition of quantum symmetries that agrees with strong symmetries is adopted in Ref. [109].

[113] S. Hikami, Three-loop ß-functions of non-linear σ models on symmetric spaces, Phys. Lett. B **98**, 208 (1981).

[114] F. Wegner, Four-loop-order β-function of nonlinear σ-models in symmetric spaces, Nucl. Phys. B **316**, 663 (1989).

[115] F. Evers and A. D. Mirlin, Anderson transitions, Rev. Mod. Phys. **80**, 1355 (2008).

[116] P. Calabrese and J. Cardy, Entanglement entropy and quantum field theory, J. Stat. Mech. Theory Exp. **2004**, P06002 (2004).

[117] I. Peschel and V. Eisler, Reduced density matrices and entanglement entropy in free lattice models, J. Phys. A Math. Theor. **42**, 504003 (2009).

[118] M. M. Wolf, F. Verstraete, M. B. Hastings, and J. I. Cirac, Area laws in quantum systems: Mutual information and correlations, Phys. Rev. Lett. **100**, 070502 (2008).

[119] P. Calabrese, J. Cardy, and E. Tonni, Entanglement entropy of two disjoint intervals in conformal field theory, J. Stat. Mech. Theory Exp. **2009**, P11001 (2009).

[120] V. Marić and M. Fagotti, Universality in the tripartite information after global quenches, Phys. Rev. B **108**, L161116 (2023).

[121] V. Marić and M. Fagotti, Universality in the tripartite information after global quenches: (Generalised) quantum XY models, J. High Energy Phys. **2023**, 140 (2023).

[122] P. C. Hohenberg and B. I. Halperin, Theory of dynamic critical phenomena, Rev. Mod. Phys. **49**, 435 (1977).

[123] A. Altland, M. Fleischhauer, and S. Diehl, Symmetry classes of open fermionic quantum matter, Phys. Rev. X **11**, 021037 (2021).

[124] S. Lieu, M. McGinley, and N. R. Cooper, Tenfold way for quadratic Lindbladians, Phys. Rev. Lett. **124**, 040401 (2020).

[125] L. Sá, P. Ribeiro, and T. Prosen, Symmetry classification of many-body Lindbladians: Tenfold way and beyond, Phys. Rev. X **13**, 031019 (2023).

[126] K. Kawabata, A. Kulkarni, J. Li, T. Numasawa, and S. Ryu, Symmetry of open quantum systems: Classification of dissipative quantum chaos, PRX Quantum **4**, 030328 (2023).

[127] E. Starchl, M. H. Fischer, and L. M. Sieberer, Generalized Zeno effect and entanglement dynamics induced by fermion counting, [dataset] Universitt Innsbruck, 2025.

[128] H.-P. Breuer and F. Petruccione, *The Theory of Open Quantum Systems* (Oxford University Press, Oxford, 2007).